JOHANNES KEPLER
UNIVERSITÄT LINZ
Netzwerk für Forschung, Lehre und Praxis

Nanostructured Electrodes From Inorganic Materials for Hybrid Solar Cells

Dissertation zur Erlangung des akademischen Grades

Doctor Technicae

im *Doktoratsstudium der technischen Wissenschaften*

Angefertigt am *Linz Institute for Organic Solar Cells (LIOS)*

Eingereicht von:

Dipl. Ing. Serap Günes

unter der Betreuung von:

o. Univ. Prof. Dr. Serdar N. Sariciftci

Ass. Prof. Dr. Helmut Neugebauer

Beurteilung:

o. Univ. Prof. Dr. Serdar N. Sariciftci

o. Univ. Prof. Dr. Wolfgang Buchberger

Linz, June 2006

Eidesstattliche Erklärung

Ich erkläre an Eides statt, dass ich die vorliegende Dissertation selbständig und ohne fremde Hilfe verfasst, andere als die angegebenen Quellen und Hilfsmittel nicht benutzt bzw. Die wörtlich oder sinngemäß entommenen Stellen als solche kenntlich gemacht habe.

DI Serap Günes

Linz, April 2006

Die Vorliegende Doktorarbeit entstand zwischen September 2002 und April 2006 am Linzer Institut für Organische Solarzellen der Technisch-Naturwissenshaftlichen Fakultäat der Universität Linz unter Betreuung von Prof. Dr. N.S. Sariciftci und Dr. Helmut Neugebauer.

Abstract

Hybrid solar cells have been the subject of intensive research during the last decade. A hybrid solar cell, consisting of both organic and inorganic materials, combine the unique properties of inorganic semiconductors with the film forming properties of conjugated polymers. Inorganic semiconductors are easy accesible and most of the inorganic semiconductors can be manufactured as nanoparticles. High absorption coefficients together with the size tunability offered by inorganic semiconductor nanoparticles is advantageous. On the other hand, easy processibility and tailorable functionality of organic materials make this organic/inorganic hybrid concept more interesting and attractive.

In this thesis, different kinds of hybrid solid state devices are presented. Solid state dye sensitized solar cells using poly(3-hexylthiophene) (P3HT) and TiO_2 electrodes were fabricated and characterized. The efficiency of such devices are dependent on the penetration of P3HT into the pores of TiO_2 nanoparticles and also the compact TiO_2 underlayers. Devices showed power conversion efficiencies of 0.3 % and incident photon to current efficiency (IPCE) of 8 % at 550 nm monochromatic irridiation.

On the other hand, a novel concept, combining two solar cell concepts, a solid-state nanocrystal-sensitized solar cell and a nanocrystal/polymer blended solar cell are described. HgTe nanocrystals are demonstrated to increase the photon harvesting efficiency of hybrid solar cells over a broad spectral region between 350 nm and 1500 nm. These devices give incident photon to current efficiencies up to 10% at around 550 nm monochromatic irradiation and short circuit current densities of 2 mA/cm^2 under simulated AM 1.5 (100 mW/cm^2) illumination.

Also, hybrid solar cells consisting of $CuInS_2$ as p-type nanoporous electrodes have been demonstrated. Bilayers of nanoporous $CuInS_2$ and PCBM 1-(3-methoxycarbonyl)-propyl-1-1-phenyl-[6,6]-C_{61} with or without using a dye complex of $RuL_2(NCS)_2$/2TBA (where L= 2,2′-bipyridyl-4,4′-dicarboxylic acid; TBA= tetrabutylammonium) are fabricated and characterized. This configuration offers new possibilities in the further development of solid state hybrid solar cells. From a technological point of view the low temperature sintering is advantageous since flexible plastic foils can be used instead of glass substrate. All active components in this new solar cell configuration are solution processable, therefore allowing a large-area fabrication.

Finally, solution processed bilayer heterojunction hybrid solar cells using PbS nanoparticles and poly (3-hexylthiophene) (P3HT) have been demonstrated.

Kurzfassung

Bereits seit mehr als zehn Jahren sind Hybridsolarzellen Gegenstand intensiver Forschung. Sie bestehen aus einer Kombination organischer und anorganischer Materialien, die die einzigartigen Eigenschaften anorganischer Halbleiter mit der Fähigkeit konjugierter Polymere vereinigen dünne Filme zu bilden. Anorganische Halbleiter sind leicht zugänglich und können zumeist auch als Nanokristalle hergestellt werden. Die Vorteile dieser Nanokristalle liegen in ihren hohen Absorptionskoeffizienten und der Herstellbarkeit verschiedener Größen. Auf der anderen Seite zeichnen sich die organischen Materialien durch vorteilhafte Verarbeitbarkeit und der Möglichkeit ihre Funktionalitäten maßzuschneidern aus. Die Kombination dieser beiden Komponenten mit ihren spezifischen Eigenschaften macht dieses Hybridkonzept sehr interessant und attraktiv.

In der vorliegenden Dissertation werden verschiedene Arten von so genannten Festphasen Hybridsolarzellen vorgestellt. Zum einen sind dies Farbstoffsolarzellen, die auf einer Kombination von Poly(3-hexylthiophen) (P3HT) und TiO_2 Elektroden basieren. Die Effizienz dieser Bauelemente hängt von der Beschaffenheit der dichten TiO_2 Untergrundschicht ab bzw. wie weit P3HT in die Poren des porösen Teils der TiO_2 Elektroden eindringen kann. Typischerweise werden mit dieser Konfiguration photovoltaische Effizienzen von 0.3% unter simulierter Sonnenbestrahlung (AM1.5, 100 mW/cm²) und eine externe Quanteneffizienz von 8% bei 550 nm monochromatischer Beleuchtung erreicht.

Des Weiteren wird ein neuartiges Konzept beschrieben, bei dem Elemente zweier unterschiedlicher Solarzellentypen, zum einen Festphasen Nanokristall sensibilisierte Solarzellen und zum anderen Nanokristall/konjugiertes Polymer Mischung Solarzellen, kombiniert werden. Es konnte in diesem Zusammenhang gezeigt werden, dass durch Zugabe von HgTe Nanokristallen die Ausbeute an absorbierten Photonen in einem breiten spektralen Bereich von 350 – 1500 nm gesteigert wird. Auf diesem System basierende Solarzellen erreichen externe Quanteneffizienzen von bis zu 10% unter 550 nm Beleuchtung. Kurzschlussströme von ca. 2 mA/cm² unter simulierter Sonneneinstrahlung (AM1.5, 100 mW/cm²) können realisiert werden.

Außerdem wurden Hybridsolarzellen mit $CuInS_2$ als p-leitende Elektroden mit Poren im Nanometer Bereich demonstriert. Doppelschichten von $CuInS_2$ und 1-(3-methoxycarbonyl)-

propyl-1-phenyl-[6,6]-C61 (PCBM) mit und ohne Verwendung des Farbstoffkomplexes ($RuL_2(NCS)_2$: 2 TBA), mit L = 2,2´-Bipyridyl-4,4´-dicarbonsäure, TBA = Tetrabutylammonium) wurden hergestellt und untersucht. Dieser Aufbau eröffnet neue Möglichkeiten für die Weiterentwicklung der Festphasen Hybridsolarzelle: Die geringe Temperatur, die zum Sintern dieser Bauelemente notwendig ist, ist aus technologischer Sicht wünschenswert, um flexible Plastikfolien statt wie bisher Glassubstrate verwenden zu können. Außerdem können alle aktiven Elemente aus Lösung aufgebracht werden, was für eine großflächige Produktion von Bedeutung ist.

Als weiterer verwandter Solarzellentypus konnten aus Lösung prozessierte Hybridsolarzellen demonstriert werden, die auf einem Heteroübergang zwischen PbS Nanopartikel und P3HT Schichten basieren.

Preface

The research work presented in this thesis was carried out at the Linz Institute of Organic Solar Cells (LIOS) during the period September 2002 - April 2006.

I thank my supervisor Prof. Dr. Niyazi Serdar Sariciftci for supervising this work and for guiding me through this period and also for giving me the opportunity to be a member of his prestigious group. I also thank Assistant Professor Dr. Helmut Neugebauer for the fruitful discussions and for his strict manuscript critisms. I thank my colleagues Dr. Nenad Marjanovic, Dr. Birendra Singh and Dr. Farideh Meghdadi for their continuous supports and also to Dr. Harald Hoppe for introducing me to the AFM. I also thank present LIOS members Dr. Gilles Dennler, Dr. Le Huong Nguyen, Dip. Phys. Robert Koeppe, DI Martin Egginger, DI Anita Fuchsbauer, DI Christoph Lungenschmied, Philipp Stadler, Andreas Spiegel, Pinar Senkarabacak and former LIOS members Daniela Stoenescu, Dr. Elif Arici, Dr. Eugen Baumgartner, Dr. Antonio Cravino, Dr. Markus Scharber, DI David Mühlbacher, DI Markus Koppe, DI Christopher Kopecny, DI Hans Juergen Prall, DI Sandra Hofer, Dr. SingLi Lu.

I thank Prof. Dr. Wolfgang Heiss for fruitful discussions and support, DI Maksym Kovalenko for providing me with HgTe nanocrystals and I thank also DI Jürgen Roither for the IPCE measurements, DI Georg Pillwein for SEM characterizations. I would like to thank also Prof. Dr. Gregory Scholes and Karolina Fritz, Msc from University of Toronto for providing me with PbS nanoparticles. I thank also Sandeep Kumar for his support.

I would like to thank Gerda Kalab for her technical support. I also thank our secretaries Petra Neumaier, Erika Bradt and Birgit Paulik and also to our former secretary Gabriela Prager for their support on administrative things.

I also thank Prof. Dr. Durul Ören (Yildiz Technical University Turkey) for his continuous support on both scientific and administrative points. I thank Prof. Dr. Salih Durer (Yildiz Technical University Turkey), Prof. Dr. Esin Can Mutlu (Yildiz Technical University Turkey), Prof. Dr. Metin Subasi (Yildiz Technical University Turkey), Prof. Dr. Emel Cingi (Yildiz Technical University Turkey) for their support on administrative points.

Finally, I thank my husband Hasan Günes for his sacrifice and support during my study and I thank my parents, my grandmother and my sister for their love and support.

I dedicate this work to my husband Hasan Günes

CONTENT

Chapter 1

1. Introduction and Motivation

Among the renewable energy sources solar energy has a great importance. Sun has always been the most powerful energy source on earth. It is clean, environmentally friendly and is for free. Sunlight can be transformed into electricity using solar cells. Solar cells found applications in many different fields such as in calculators, solar lamps and even on spacecraft and satelites. Historically, conventional solar cells were built from inorganic materials such as silicon. The efficiency of such conventional solar cells made from inorganic materials reached up to 24 % [1]. However, very expensive materials and energy intensive processing techniques are required. The use of silicon crystals in the solar cells makes it expensive. Silicon crystals are moduled together manually. On the other hand, silicon purification is difficult and a lot of silicon is wasted. In addition, since the performance of silicon cells degrades as the temperature increases, the long lasting concentrated operation of silicon cells require a cooling system. A lot of effort is put on the research for new fabrication techniques.

Organic [2], hybrid [3,4] and photoelectrochemical (dye sensitized) solar cells [5] have been the alternatives for conventional silicon solar cells.

Organic solar cells mainly consist of two organic materials an electron-donating material and an electron-accepting material to make a percolating structure with interpenetrating networks [6]. The realization of the photoinduced charge transfer from the conjugated polymer to the fullerene derivatives led the development “bulk heterojunction” organic solar cells [7].

A hybrid solar cell consists of a combination of both organic and inorganic materials therefore, combines the uniqe properties of inorganic semiconductors with the film forming properties of the conjugated polymers [8]. Organic materials are inexpensive, easily processable and their functionality can be tailored by molecular design and chemical synthesis. On the other hand, inorganic semiconductors can be manufactured as nanoparticles and inorganic semiconductor nanoparticles offer the advantage of having high absorpion coefficients and size tunability. By varying the size of the nanoparticles the bandgap can be tuned therefore the absorption range can be tailored [9].

Dye sensitized solar cells (photoelectrochemical solar cells) are combination of different materials every of which performs a specific task towards the objective of conversion of sunlight into electricity. Although efficiencies of 11% are reported the technological development is still hindered due to the leakage or evaporation of the electrolyte solution [10]. The presence of an electrolyte solution in photoelectrochemical cells makes the manufacturing process difficult. Therefore, recent efforts in dye sensitized solar cell research are more focusing on replacing the electrolyte solution with a solid material to eliminate practical problems with sealing. A solid state cell exhibits a structure similar to the dye sensitized photoelectrochemical cells except for the replacement of liquid electrolyte with a p type semiconductor or "quasi solid" counterpart.

Polymeric materials as replacement for the electrolyte solution are of practical interest since they are inexpensive and can be tailored chemically to fit a wide range of technological purposes. Solid state dye sensitized solar cells using poly(3-hexylthiophene) (P3HT) based on TiO_2 electrodes have already been demonstrated, previously [11,12,13,14]. However, the efficiencies of such solar cells are still lower than that of photoelectrochemical solar cells. Initial motivation of this thesis was to realize the limiting factors in solid state dye sensitized solar cells and find approaches to overcome these limitations. In results 3.1, solid state hybrid solar cells based on TiO_2 nanoporous electrodes using poly(3-hexylthiophene) (P3HT) have been fabricated and characterized. The effect of film deposition techniques, the influence of a compact TiO_2 underlayer have been investigated.

From photon harvesting efficiency point of view, the use of inorganic nanocrystals instead of dyes in dye sensitized solar cells implies several advantages such as the tunability of the bandgap [15]. Thus, the absorption spectrum can be tuned to match the spectral distribution of sunlight so that a full spectrum solar cell can be easily fabricated. The second motivation was to replace the dye used in dye sensitized solar cells with inorganic nanocrystals to increase the photon harvesting efficiency. In results 3.2, a novel concept, combining two solar cell concepts, a solid-state nanocrystal-sensitized solar cell and a nanocrystal/polymer blended solar cell are described. HgTe nanocrystals are demonstrated to increase the photon harvesting efficiency of hybrid solar cells over a broad spectral region between 350 nm and 1500 nm.

Another interesting device is based on nanoporous electrodes prepared from size quantized nanoparticles. In results 3.3, hybrid solar cells consisting of $CuInS_2$ as p-type nanoporous

electrodes have been demonstrated. This configuration offers new possibilities in the further development of solid state hyrid solar cells.

Finally, in results 3.4, solution processed bilayer heterojunction hybrid solar cells using PbS nanoparticles and P3HT are demonstrated.

1.1. Solar Cell Concepts

1.2 Organic Solar Cells

1.2.1 Organic Photovoltaic Materials

The need to develop inexpensive renewable energy sources stimulates new approaches for production of efficient, low cost photovoltaic devices [6]. The development of organic, polymer based photovoltaic elements has introduced possibility of obtaining cheap and easy producable energy from light [16]. The superior material properties of polymers (plastics) combined with a large number of easy and cheap processing techniques has made polymer based materials present in almost every aspect of modern society. Organic materials have several advantages such as low cost synthesis and easy manufacture of thin film devices by vacuum evaporation or solution cast technologies. Organic electronic materials are conjugated molecular solids where both optical absorption and charge transport are dominated by partly delocalized π and π^* orbitals [17].The flexibility of chemical tailoring of desired properties as well as the easy and cheap processing and accessibility of conjugated polymers made them competitive and attractive [16].

Conjugated polymers, also known as conducting polymers, are distinguished by alternating single and double bonds between carbon atoms on the polymer backbone (see figure 1.1) Single bonds are referred to as σ bonds, double bonds contain a σ and a π bond. All conjugated polymers have a σ bond backbone of overlapping sp^2 hybrid orbitals. The remaining out of plane p_z orbitals on the carbon atoms overlap with neighbouring p_z orbitals to give π bonds [18].

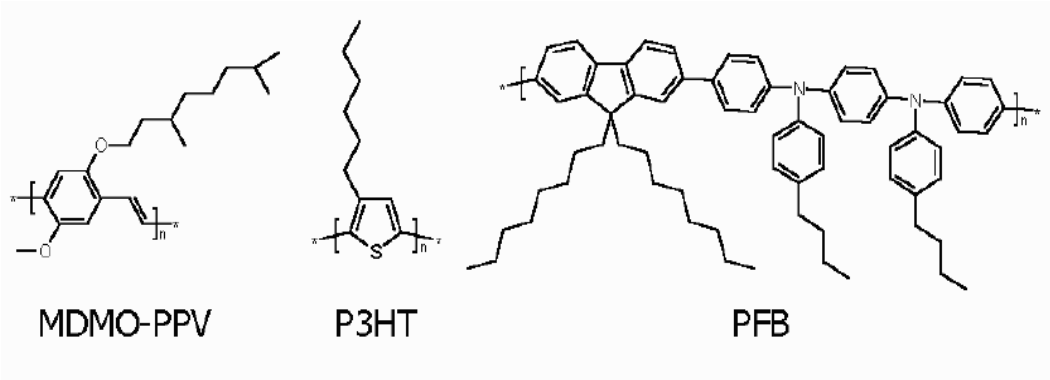

Figure 1.1 Examples of solution processable conjugated polymer semiconductors

Although the chemical structure of these materials are represented by alternating single and double bonds, in reality, the electrons that constitute the π bonds are described to be delocalized over the entire molecule.

For inorganic semiconductors, the mechanism of charge generation from incident photons is well established. For an ideal semiconductor, the electronic structure consists of a conduction band and a valence band separated by an energy gap the size of which depends upon the material. Therefore, an incident light photon can excite an electron from the valance band into the conduction band. As a consequence, a hole is remained in the valence band. Although a hole is simply an empty electronic state, it behaves as if it were an independent carrier of positive charge [19]. Conducting polymers act also as semiconductors, and their electronic properties appear to be analogous to those of inorganic semiconductors except they have no dangling bonds on the surface/interfaces due to their closed shell structure.

The π bonds are delocalized over the entire molecule, and then, the quantum mechanical overlap of p_z orbitals actually produces two orbitals, a bonding π orbital and an antibonding π^* orbital. The lower energy π-orbital produces the valence band, and the higher energy π^* orbital forms the conduction band. The difference in energy between band edges of the two levels produces the band gap that determines the optical properties of the material [18].

The charge conduction mechanism appears to be more complex for conducting polymers than for inorganic semiconductors. Organic semiconductors differ from the inorganic semiconductors in the following important aspects [17]:

1. Photogenerated excitations (excitons) are Coulombically bound and do not spontaneously dissociate into separate charges in quantitative amounts.

2. Charge transport proceeds by hopping between disorder induced localized states, rather than transport within a band which results in low mobilities.

3. The spectral range of the optical absorption is relatively narrow compared to the solar emission spectrum (figure 1.2 [20]).

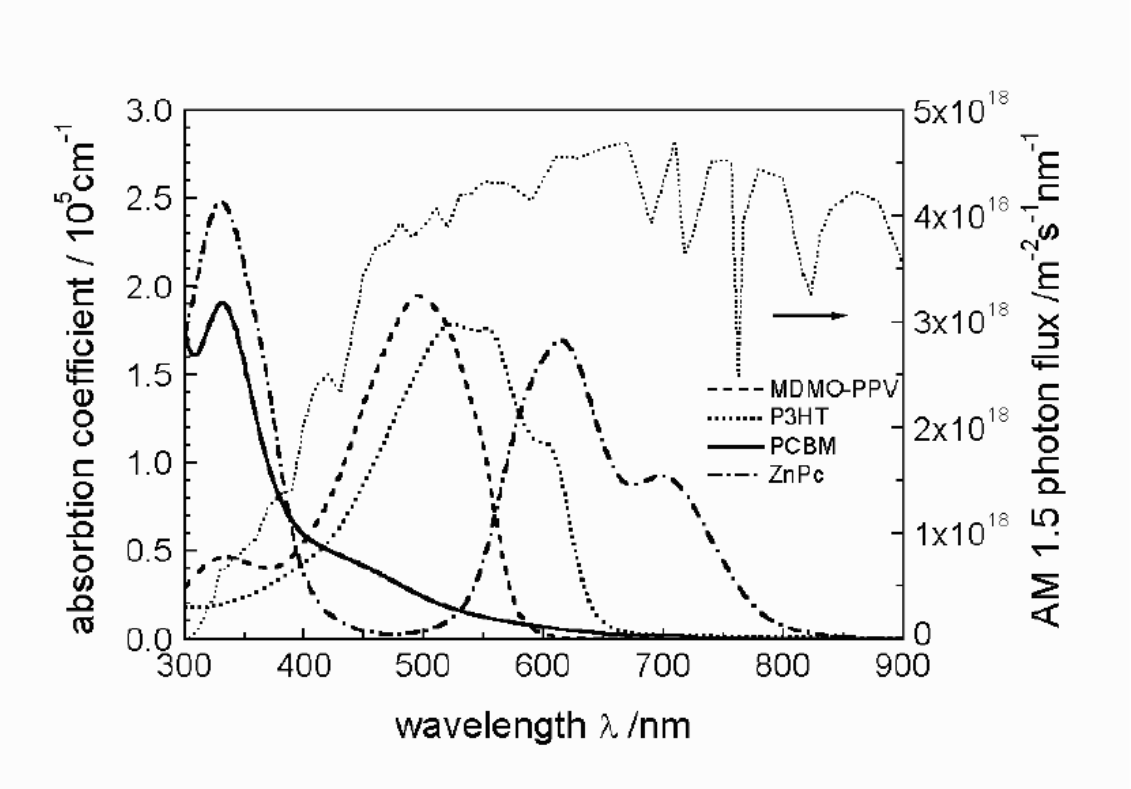

Figure 1.2 Comparison of absorption spectra of different organic materials with the solar photon flux

4. As one dimensional semiconductors, their electronic and optical properties can be highly anisotropic.

The first two features arise from the intermolecular van der Waals forces in organic solids that are weak compared to bonds in organic crystals and much weaker than the intramolecular bonds. Low mobility is aggravated by the high degree of disorder present in many organic solids. The optical excitations accessible to visible photons are usually π to π^* transitions. However, the absorption bandwidth depends on the degree of conjugation, and variable spectral sensitivity can be achieved in conjugated dye molecules [17].

1.2.2 Operation Principles of Organic Solar Cells

The typical device geometry is based on an organic material which is sandwiched between two different conducting contacts, typically indium tin oxide (ITO) and a low work function metal such as Al, Ca, or Mg (Fig. 1.3 [22]).

Metal insulator metal (MIM) tunnel diode with asymmetric work function metal electrodes, introduced by Parker for light emitting diodes [21] has been the simplest and most widely used model to explain the response of organic photovoltaic devices under illumination (See Fig 1.3). The polymer is assumed to have a negligible amount of intrinsic charge carriers and can therefore be seen as an insulator. This assumption is not sufficient under heavy illumination [22].

Figure 1.3 [22] shows a pristine polymer device under different working condions witin the MIM picture. Figure 1.3 a shows the short circuit case where no voltage is applied. There is no current flowing in the dark and the built-in electric field resulting from the difference of the metals` work functions is evenly distributed in this electric field of the respective contacts. Photogenerated holes are transported to the ITO contact whereas the electrons are transported to the Al. The driving force for charge separation is the electric field across the insulator layer. The electric field is constant over the whole layer and is provided by workfunction difference of the contacts. Figure 1.3 b shows the open circuit case, also known as “flat band condition” and, under illumination, the created charges show no preferred direction. The open circuit voltage cancels the potential difference of the contacts. The maximal observed open circuit voltage V_{oc} should be the workfunction difference between the two contacts. As there is no net driving force for the charge carriers, the current is zero [21,22].

Under forward bias, holes from the high workfunction metal and electrons from the low work function metal are injected into the organic semiconductor thin film, i.e holes are injected from ITO to the valence band whereas electrons are injected from the Al to the conduction band. The observed net current is dominated by the recombination of two charge carriers. If electrons and holes recombine radiatively, electroluminescence can be observed. Because of asymmetry of the work functions for two different metals, forward bias currents are orders of magnitude larger than reverse bias currents at low voltages. In a forward bias, a voltage, larger than the open circuit voltage is applied so that the contacts can efficiently inject charges into the semiconductor [22]. If these can recombine radiatively, the device works as a light

emitting diode (LED). The asymmetric diode behaviour results from the different injection of the two metals into the HOMO and LUMO levels, respectively, which depends on the energy barrier between them [22].

Under a negative bias, i.e. positive contact to Al and negative contact to the ITO, the diode works as photodetector [23]. Photoinduced charges are selectively transported, assisted by the external field, to the contacts, holes to the ITO and electrons to the Al. Polymer diodes are quite sensitive photodiodes.

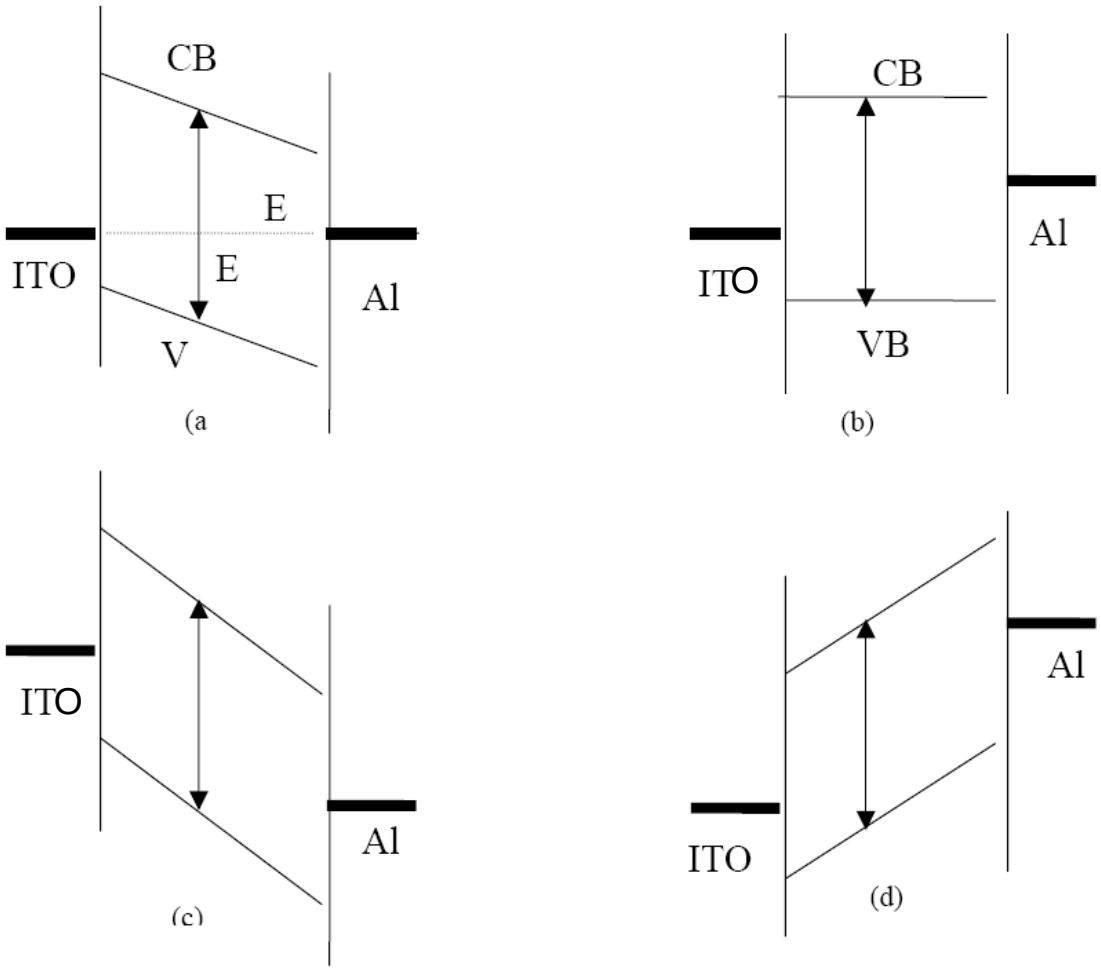

Figure 1.3 MIM picture for a polymer diode under different working conditions (a) short circuit, under illumination the holes are transported to the ITO contact, the electrons to the Al contact, (b) open circuit condition under illumination, the V_{oc} in the MIM picture is the workfunction difference between the two contacts, (c) diode under reverse bias, diode works as photodetector, and (d) diode under forward bias, diode can work as light emitting diode.

In Figure 1.4 [20] current-voltage (I-V) characteristics of a solar cell is shown in dark and under illumination. In dark, there is almost no current flowing, until the contacts start to inject heavily at forward bias for voltages larger than the open circuit voltage. Under illumination,

the current flows in the opposite direction than the injected currents. At (a) maximum generated photocurrent flows under short circuit currents, at (b) the photogenerated current is balanced at zero (flat band condition). Between (a) and (b), in the forth quadrant, the device generates power. At a certain point, denoted as maximum power point (MPP), the product between current and voltage and hence the power output is largest [20].

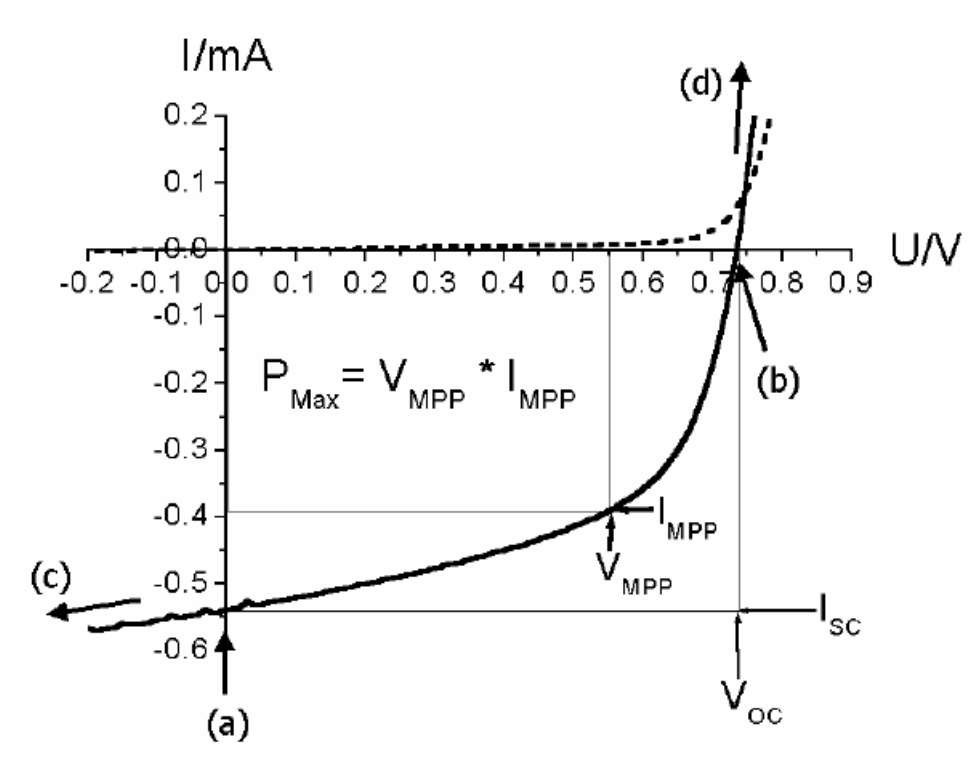

Figure 1.4 Current-voltage (I-V) curves of a solar cell (dark:dashed, illuminated: full line). The characteristic intersections with the abscissa and the ordinate are the open circuit voltage (V_{oc}) and the short circuit current (I_{sc}), respectively. The largest power output (P_{max}) is determined by the point where the product of voltage and current maximized. Division of P_{max} by the product of I_{sc} and V_{oc} yields the fill factor FF

To determine the efficiency of a solar cell, this power needs to be compared with the incident light intensity. Typically, the fill factor is calculated as:

$$FF = \frac{V_{MPP} * I_{MPP}}{V_{oc} * I_{sc}} \qquad (1.1)$$

to denote the part of the product of V_{oc} and I_{sc}, that can be used. With this, the power conversion efficiency can be written as:

$$\eta = \frac{P_{out}}{P_{in}} = \frac{I_{MPP} * V_{MPP}}{P_{in}} = \frac{FF * I_{sc} * V_{oc}}{P_{in}} \qquad (1.2)$$

Generally, the I-V characteristics of a photovoltaic device can be described by:

$$I = I_o . \left\{ \exp\left(\frac{e}{nkT} (U - I.R_s) \right) - 1 \right\} + \frac{U - I.R_s}{R_{SH}} - I_{PH} \qquad (1.3)$$

where I_o is the dark current, e the elementary charge, n the diode ideality factor, U the applied voltage, R_s the series and R_{SH} the shunt resistance and I_{PH} is the photocurrent. The corresponding equivalent circuit is depicted in Fig. 1.5 [20]. For a high FF two things are required: a) that the shunt resistance is very large in order to prevent leakage currents and b) that the series resistance is very low in order to get a sharp rise in the forward current. The series resistance simply adds up from all series resistance contributions in the device, i.e from bulk transport, from interface transfer and from transport through the contacts [20].

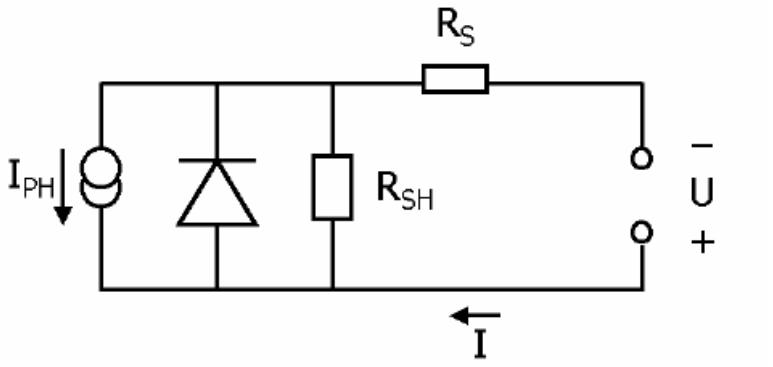

Figure 1.5 Equivalent circuit of a solar cell described by equation (1.3)

1.2.3 Types of Devices

The device architecture plays an important role in organic solar cells. As discussed previously, in organic semiconductors bound excitons are created upon photoexcitation. These excitons have to dissociate for an efficient charge transfer. Since the built-in electric fields are usually not high enough to dissociate the excitons directly, a process has to be introduced that efficiently separates the bound electron-hole pairs. The exciton dissociation is known to occur between two semiconductors such as donor-acceptor interface as well as semiconductor/metal interfaces. The following will give an insight on the most basic types of devices [20].

1.2.3.1 Single Layer Devices

The first organic solar cells were based on single organic layers sandwiched between two metal electrodes of different workfunctions. The rectifying behaviour of these devices can be explained by the MIM model (for insulators) or by the formation of a Schottky barrier (for doped materials) between the metal with the lower workfunction and the p type organic layer [20,24]. Figure 1.6 [20] shows a p type Schottky device. Close to the contact, the depletion region W, a resulting band bending from the Schottky contact is depicted. This corresponds to an electric field in which the excitons can be dissociated [20].

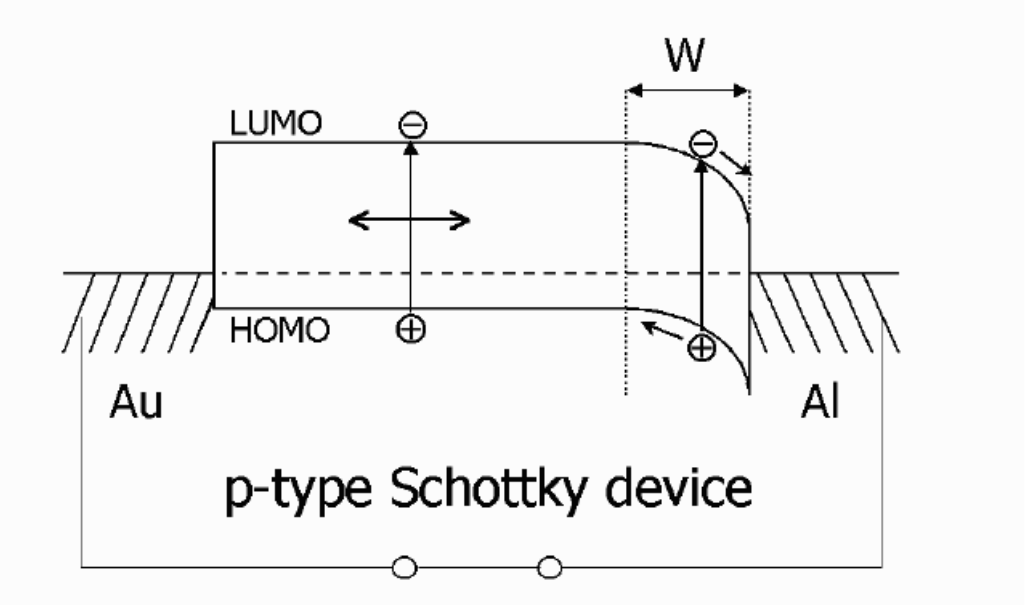

Figure 1.6 Scheme of a single layer device with a Schottky contact at the aluminium contact. Photogenerated excitons can only be dissociated in a thin depletion layer W and thus the device is exciton diffusion limited

Therefore illumination through two different semi-transparent metal contacts can lead to symbatic (propotional to the absorption coefficient) or anti-batic behaviour of the spectral photocurrent [20,25,26,27]. Since the exciton diffusion length for most organic solar cell materials is below 20 nm, only those excitons generated in a small region within $\leq$ 20 nm from the contacts contribute to the photocurrent [20]. Due to high series resistances these materials show a low fill factor and a field dependent charge carrier collection. These thin film devices can work well as photodetectors, since under a high reverse bias the electric field drives the created charges to the electrodes[20].

1.2.3.2 Bilayer Heterojunction

To overcome the limitation of photoinduced charge carrier generation a bilayer device in which a donor and an acceptor material are sequentially stacked together with a geometrical interface is introduced. At this interface the charge separation occurs [20,28,29,30,31] which is mediated by a large potential drop between donor and acceptor. The bilayer is sandwiched between two electrodes with different workfunctions matching donor HOMO and the acceptor LUMO for efficient extraction of the corresponding charge carriers [20]. For an efficient charge transfer, the LUMO and the HOMO of the donor should lie above those of the acceptor. The bilayer device structure is shown in figure 1.7 [20], neglecting all kinds of possible band bending due to energy level alignments.

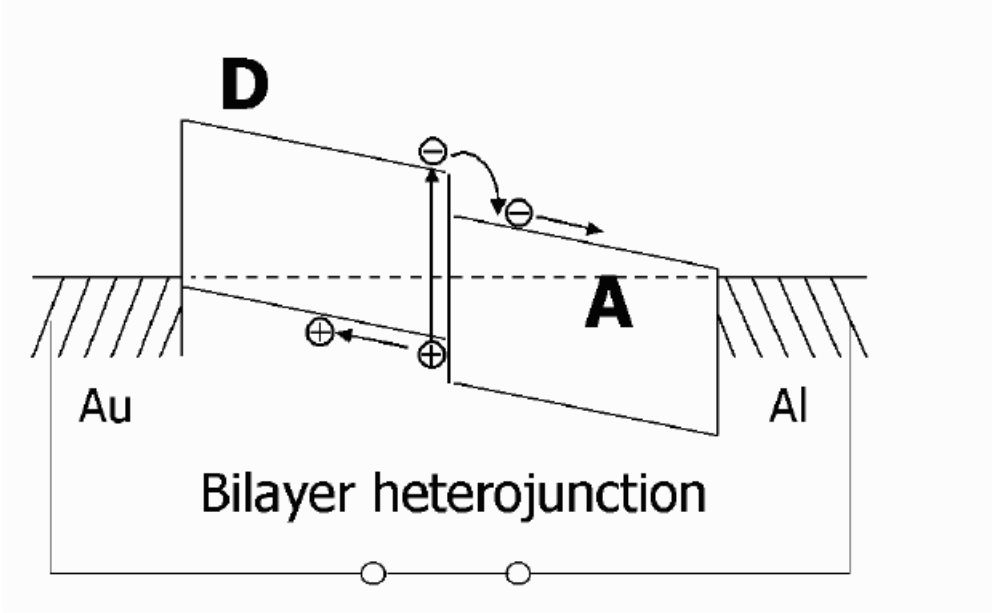

Figure 1.7 Scheme of a bilayer device. The donor (D) contacts the higher and the acceptor (A) the lower workfunction metal, to achieve good hole and electron collection respectively. Photogenerated excitons can only be dissociated in a thin layer at the interface/heterojunction and thus the device is exciton diffusion limited

While the formation of a classical p/n junction requires doped semiconductors with free charge carriers to form the electric field in the depletion region, the charge transfer in bilayer heterojunction between undoped donor and acceptor materials is due to the differences in the ionization potential and electron affinity of the adjacent materials [20]. Upon photon absorption in the donor D, the electron is excited from the HOMO to the LUMO ($S^0 \rightarrow S^1$). If now an acceptor molecule A is in close proximity, the electron may be transferred to the LUMO of A, which is energetically preferential when

$$I_{D}^{*} - A_A - U_C < O, \quad (1.4)$$

Where I_{D}^{*} is the ionization potential of the excited state (D*) of the donor, A_A the electron affinity of the acceptor and U_c the effective Coulomb interaction, respectively [6].

The release in electron energy may then be used to separate the electron and the hole from their coulomb potential. This photoinduced charge transfer (CT) only occurs under illumination, since it needs the excitation energy of the electron in the donor to reach the LUMO in the acceptor [20]. There are experimental indications [32,33,34] supported by theoretical considerations [35] of a formation of an interfacial dipole between the donor and acceptor phases, independent of illumination [20]. This can stabilize the charge separated state by a repulsive interaction between the interface and the free charges [35]. Therefore, the success of the donor/acceptor concept lies to a great extent in the relative stability of the charge separated state: the recombination rate between holes in donor and electrons in the acceptor is several orders of magnitude smaller than the forward charge transfer rate [20,36,37,38].

After the excitons are dissociated at the materials interface the electrons travel within the n type acceptor and the holes travel within the p type donor material. Hence holes and electrons are effectively separated from each other and although charge recombination is greatly reduced and it depends more on trap densities [20]. As a consequence, the photocurrent dependency on illumination intensity can be linear [26,28,29,31,39].

1.2.3.3 Bulk Heterojunction

The essence of bulk heterojunction is to blend the donor and acceptor components in a bulk volume so that each donor-acceptor interface is within a distance less than the exciton diffusion length (ca 20 nm) of each absorbing site [20].

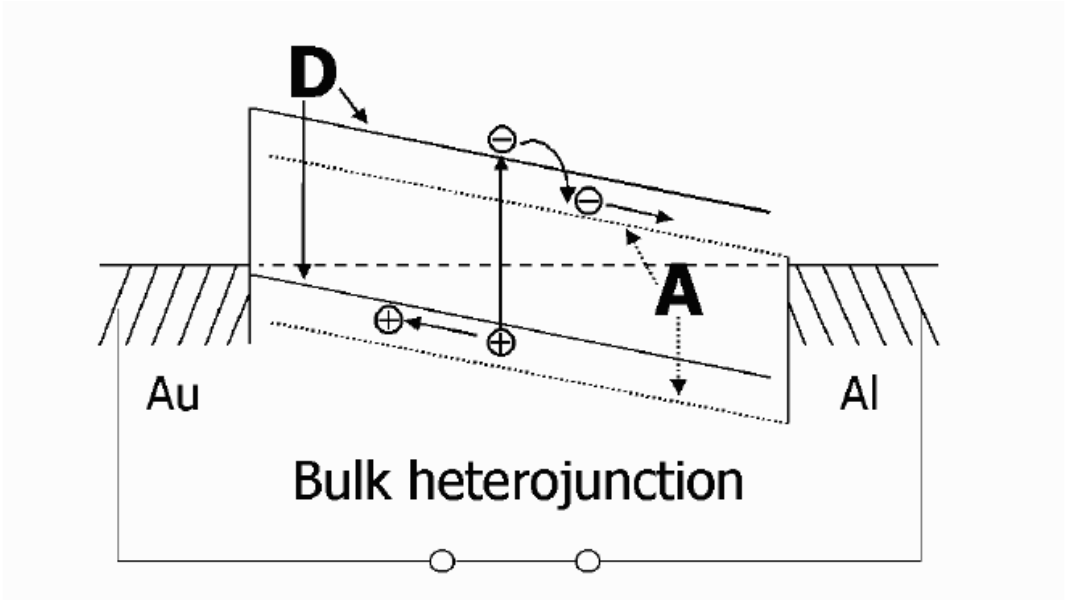

Figure 1.8 Scheme of a bulk heterojunction device. The donor (D) is blended with the acceptor (A) throughout the whole film. Thus photogenerated excitons can be dissociated into charges at any place

While in a bilayer heterojunction the donor and acceptor phase contact the anode and cathode selectively, the bulk heterojunction requires percolated pathways for the hole and electron transporting phases to the contacts (see Fig 1.8 [20]). In other words, the donor and acceptor phase have to form a bicontinious and interpenetrating network. Therefore, the bulk heterojunction devices are much more sensitive to the morphology in the blend [20]. Such an idealized cartoon picture of interpenetrating network of nanophases is shown in Figure 1.9 [40].

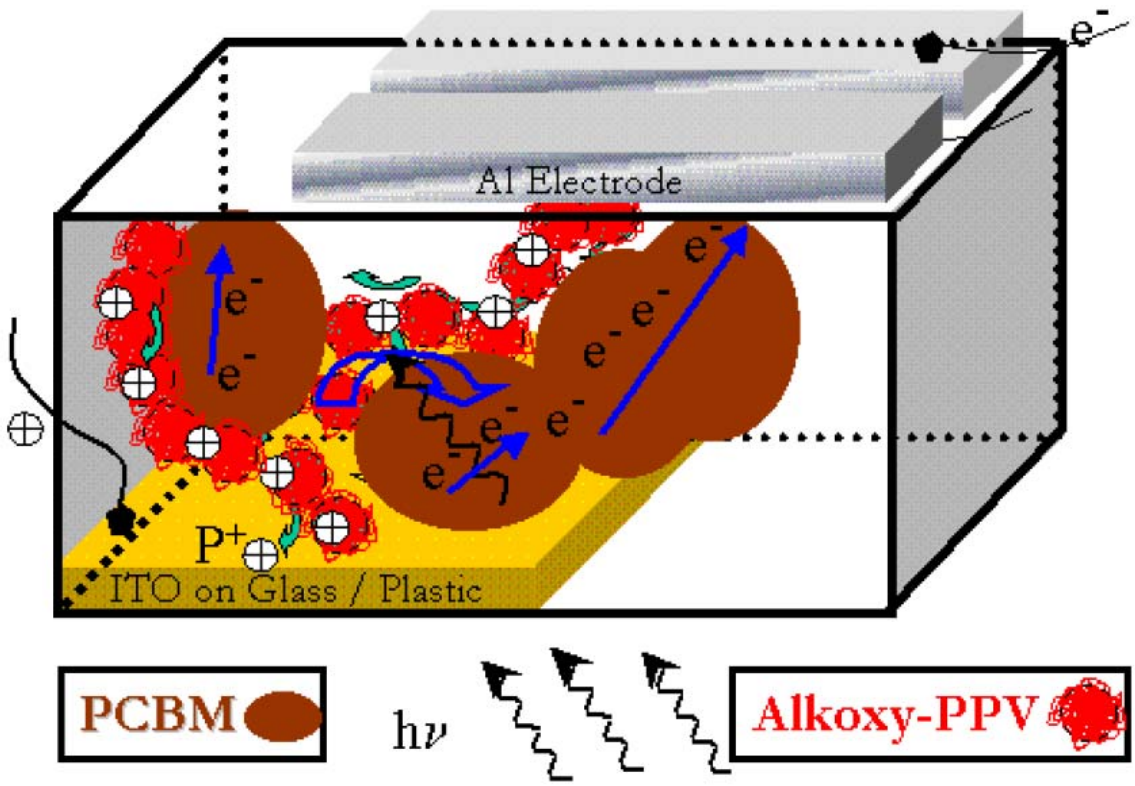

Figure 1.9 Donor and acceptor materials may be blended together to yield a dispersed heterojunction. If the length scale of blend is similar to the exciton diffusion length, then the probability that an exciton will reach the interface and dissociate is high. For efficient photocurrent collection, each material must provide a continuous path for the transport of separated charges to the contacts. Isolated domains can trap charges, causing recombination

1.2.3.4 Diffuse Bilayer Heterojunction

Another device architecture, which is conceptually in between the bilayer and the bulk heterojunction device is a diffuse bilayer heterojunction device. Therefore, it can combine the advantages of both concepts, an enlarged donor acceptor interface and a spatially uninterrupted pathway for the opposite charge carriers to their corresponding electrode [20]. The diffuse interface is achieved in different ways: If processed from solution, two thin films can be pressed together in a lamination procedure applying moderate pressure and elevated temperatures [20,41]. Another way to achieve a diffuse interface is to spincast the second layer from a solvent that partially dissolves the underlying layer [20,42,43]. Finally, also the controlled interdiffusion between an acceptor fullerene and donor polymer by annealing of a bilayer device [20,44] results in an intermixed interfacial region.

1.3 Hybrid Solar Cell Concepts

Since the operation of solid state dye sensitized solar cells mimics that of photoelectrochemical solar cells based on nanoporous TiO_2 electrodes it would be beneficial to describe first how a photoelectrochemical solar cell based on nanoporous TiO_2 electrode works although it is not a hybrid solar cell.

1.3.1 Photoelectrochemical Solar Cells Based on Nanoporous TiO_2 Electrodes

Dye sensitized solar cells (DSSC) or "Grätzel cells" are combination of several different materials such as optically transparent electrodes, semiconductor nanoparticles, coordination compounds as absorbing dyes, inorganic salts, solvents and metallic catalysts every of which performs a specific task toward the overall objective of harvesting solar light and transforming it into electricity [45]. A schematic presentation of the operation principles of DSSC is given in Figure 1.10 [45]. At the heart of the system is a mesoscopic semiconductor oxide film, which is placed in contact with an electrolyte solution containing a redox couple. The material of choice has been TiO_2 (anatase), although alternative wide bandgap oxides such as ZnO and Nb_2O_5 have also been investigated. Attached to the surface of the nanocrystalline film is a monolayer of the sensitizer. Photoexcitation of the latter results in the injection of an electron into the conduction band of the oxide. The original state of the dye is subsequently restored by electron donation from the electrolyte, usually an organic solvent containing redox system, such as the iodide/triiodide couple. The regeneration of the sensitizer by iodide intercepts the recapture of the conduction band electron by the oxidized dye. The iodide is regenerated, in turn, by the reduction of triiodine at the counter electrode, with the circuit being completed via electron migration through the external load [5].

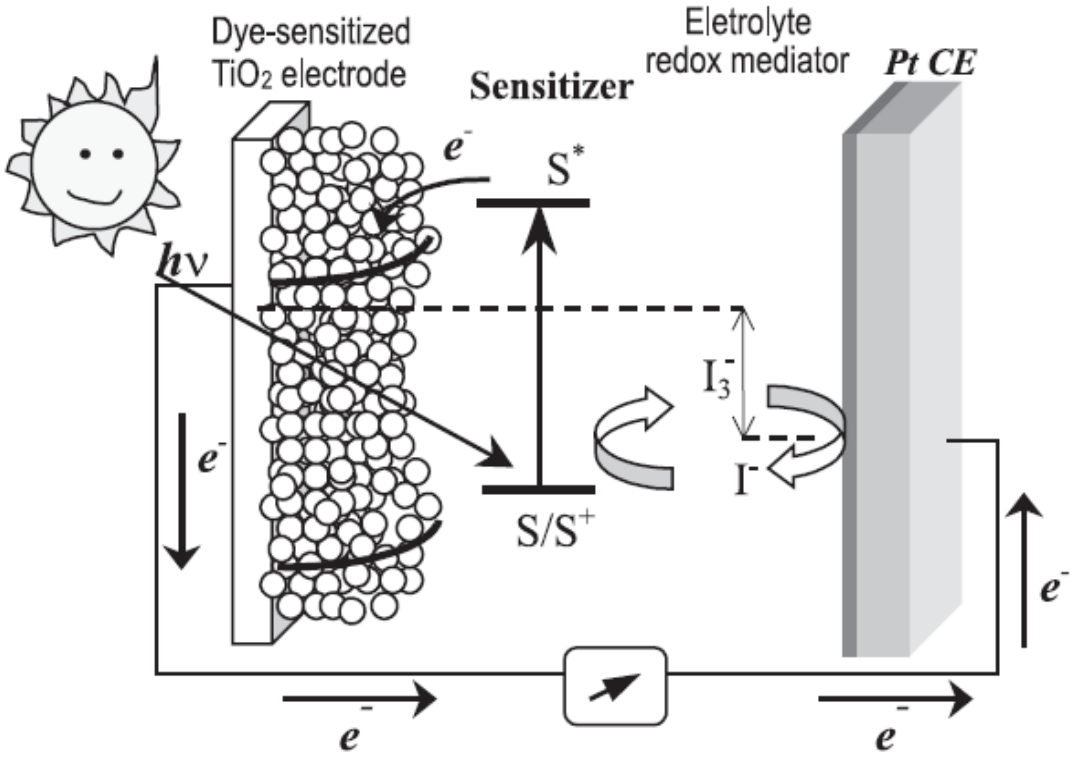

Figure 1.10 Operation principle of a dye sensitized solar cell

The voltage generated under illumination corresponds to the difference between the Fermi level of the electron in the semiconductor oxide and the redox potential of the electrolyte. Overall, the device in principle generates electric power from light without suffering any permanent chemical transformation [5].

1.3.1.1 Nanocrystalline Film Morphology

A photovoltaic conversion system based on light harvesting by a molecular absorber attached to a wide bandgap semiconductor surface faces two problems [46]:

1. A monolayer of dye on a flat surface absorbs at most a few percent of light because it occupies an area that is much larger than its optical cross section. Therefore it can only harvest a negligibly small fraction of the incoming light.

2. Compact oxide semiconductor films need to be n-doped to conduct electrons.

Therefore it is dentrimental to enlarge the interface between oxide semiconductor phase and the sensitizing dye. This is successfully achieved by introducing a nanoparticle based electrode construction which enhances the photoactive interface by orders of magnitude [5].

1.3.1.2 The Choice of The Sensitizer (Light Absorption)

While the high efficiency of the dye sensitized solar cells arises from a collective effect of numerous physical-chemical nanoscale properties, the key issue is the principle of dye sensitization of large band-gap semiconductor electrodes. In the dye sensitized solar cells this is accomplished by coating the internal surfaces of porous TiO_2 electrode with special dye molecules tuned to absorb the incoming photons [47].

The actual sensitization effect can be seen in figure 1.11 [46] as a shift of the incident photon to current efficiency (IPCE) curve of the naked TiO_2 to higher wavelengths when coated with the dye. The current efficiency of the cell is related to the 'height' of the IPCE curve, which depends on the charge separation and charge collection efficiencies [47].

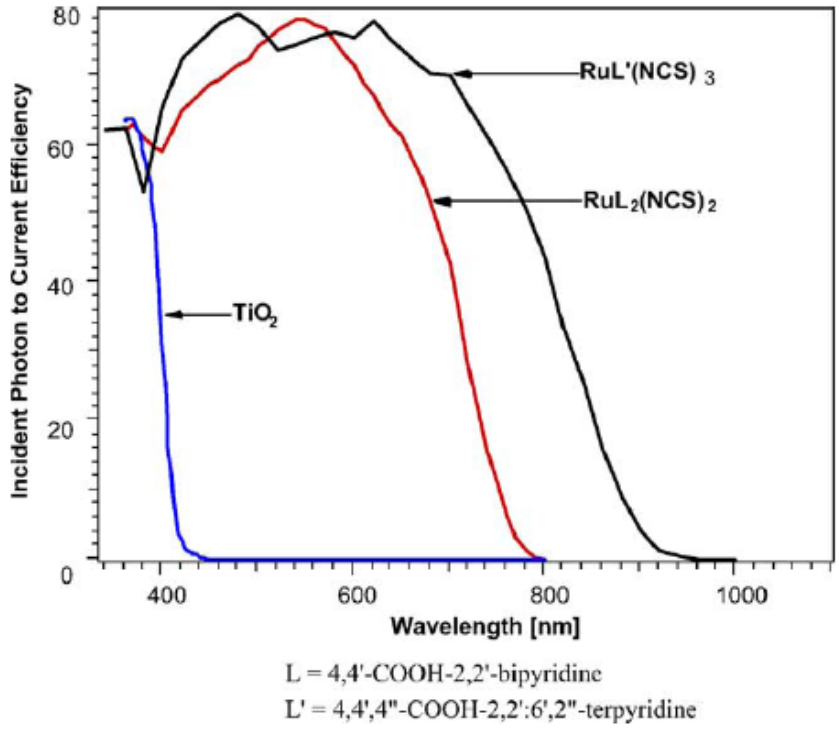

Figure 1.11 Sensitization effect can be seen as the shift of incident photon to current efficiency curves to higher wavelengths when coated with dye as compared with that of naked TiO_2

The ideal sensitizer for a single junction solar cell converting global AM 1.5 sunlight to electricity should fullfill the following requirements [5,46,48]:

1. It should absorb all light below a threshold wavelength as much as possible.

2. It must also carry attachment groups such as carboxylate or phosponate to firmly graft it to the semiconductor oxide surface.

3. Upon excitation it should inject electrons into the conduction band of the oxide with a quantum yield of unity.

4. The energy level of the excited state should be well matched to the lower band edge of the conduction band of the oxide to minimize energetic losses during the electron transfer reaction (see Fig. 1.12 [5]).

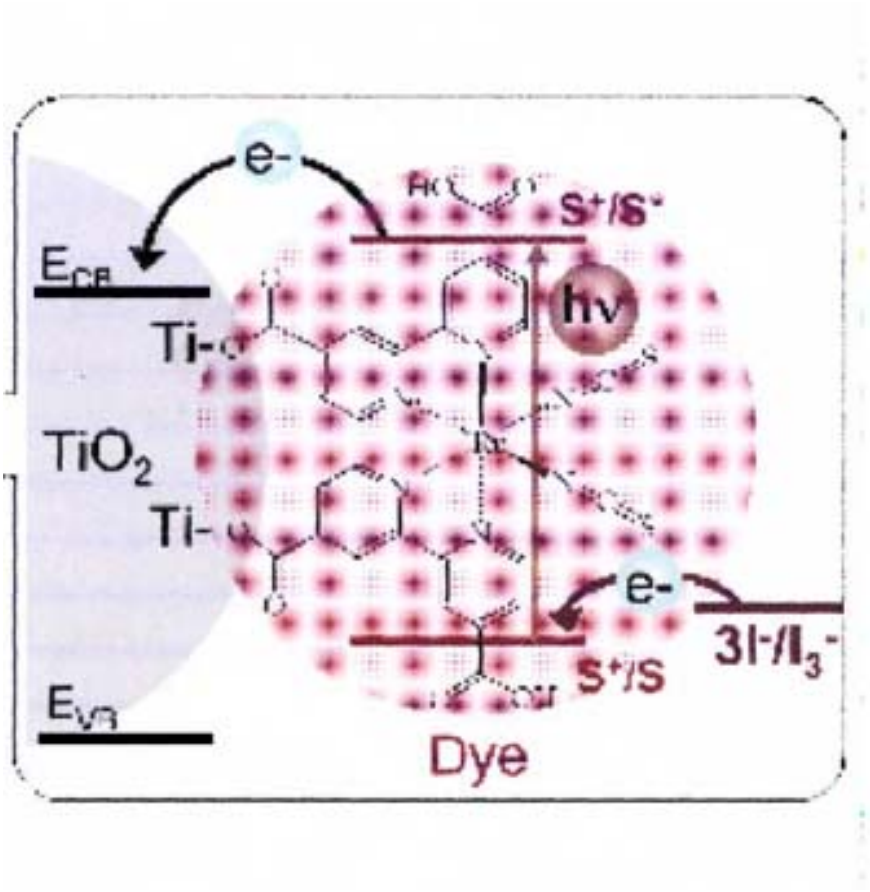

Figure 1.12 Energy level alignment of dye sensitized solar cells

5. Its redox potential should be sufficiently positive that can be regenerated via electron donation from redox electrolyte.

6. It should be stable for the exposure to natural light.

Many different compounds have been investigated for semiconductor sensitization, such as porphyrins [49,50,51], phthalocyanines [52,53,54], transition metal complexes [55,56], coumarin [57] and transition metal complexes have been the best so far.

Metal complex sensitizers usually have anchoring ligands (see fig 1.13 [48]). Anchoring ligands are responsible for the complex adsorption onto the semiconductor surface and are also chromophoric groups. Ancillary ligands are not directly attached onto the semiconductor surface and can be used for tuning the overall properties of the complexes [48].

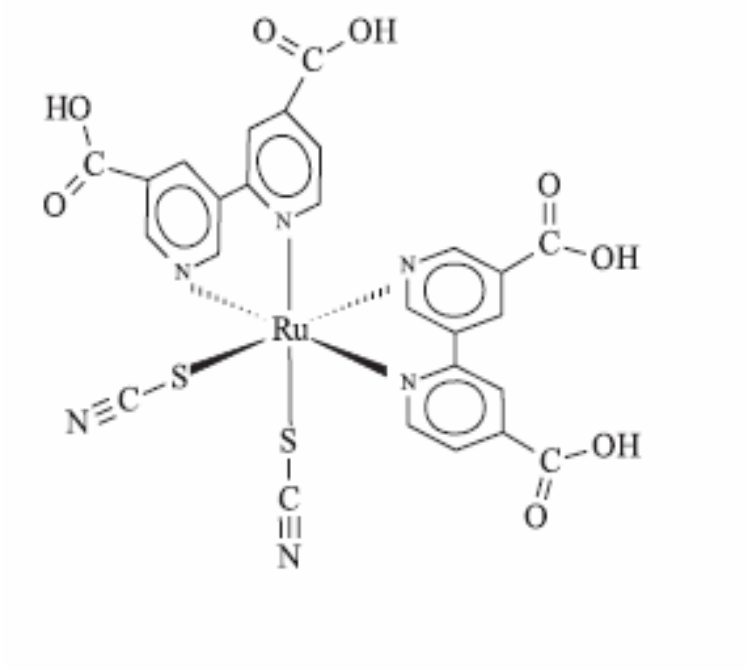

Figure 1.13 Chemical structure of a Ruthenium dye

The breakthrough in dye sensitization of semiconductor electrodes for solar cells was made by the use of metallo-organic ruthenium complexes along with nanostructured TiO_2 electrodes. The dyes having the general structure of $ML_2(X)_2$, where L stands for 2,2'-bipyridyl-4-4'-dicarboxylic acid, M for ruthenium or osmium and X for halide, cyanide, thiocynate, or water have been found promising [47,58,59]. Among these the *cis*-$RuL_2(NCS)_2$, also called N3 dye has shown superior performance and has been the top choice for dye sensitized solar cells.

The excitation of Ru complexes via photon absorption is of metal to ligand charge transfer (MLCT) type. This means that the highest occupied molecular orbital (HOMO) of the dye is localized near the metal atom, Ru in this case, whereas the lowest unoccupied molecular orbital (LUMO) is localized at the ligand species, in this case at the bipyridyl rings. At the excitation, an electron is lifted from the HOMO level to the LUMO level. Furthermore, the LUMO level, extending even to the COOH anchoring groups [47], is spatially close to the TiO_2 surface, which means that there is significant overlap between electron wavefunctions of the LUMO level of the dye and the conduction band of TiO_2. This directionality of the excitation is proposed as one of the reasons for the fast electron transfer process at the dye-TiO_2 interface [47].

1.3.2 Solid State Dye Sensitized Solar Cells

The all solid state dye sensitized solar cells have been a subject of intensive research over the last decade [60,61,62]. A solid state cell has a structure similar to the dye sensitized photoelectrochemical cells except for the replacement of electrolyte with a p-type semiconductor or organic hole conductor materials. It inherits the advantage of dye sensitized photoelectrochemical cells in terms of separating charge generation from charge transport. Therefore, the quality of the electrode material (purity and cristallinity) for either n-type or p-type semiconductors, is not as critical as that for classical photovoltaic cells, which have to provide good photoresponse as well as good charge mobility within the same compound. Moreover, being a kind of solid state device, it could be manufactured with simpler, less expensive technology than that for photoelectrochemical solar cells, since problems such as leakage, packing, and corrosion, which exist for liquid electrolytes, could be avoided [63].

Despite the advantages, the development of solid state devices has been less than satisfactory. The photoelectrochemical cell is in principle a molecular electronic device on the base of photochemical conversion on the molecular scale, while the solid state dye sensitized solar cell works like a p-n heterojunction, whose behavior should be described in terms of semiconductor physics [63].

1.3.2.1 Operation Principle of Solid State Dye Sensitized Solar Cells

A solid state dye sensitized solar cell is shown in figure 1.14. The mesoporous metal oxide electrode, commonly, TiO_2 is placed in contact with a solid state hole conductor. Attached to the surface of nanocrystalline electrode film is a monolayer of a charge transfer dye. Photoexcitation of the dye results in the injection of electrons into the conduction band of metal oxide electrode. The original state of the dye is restored by electron donation from the hole conductor. The regeneration of the sensitizer by the hole conductor intercepts the recapture of the conduction band electron by the oxidized dye. The hole conductor is regenerated in turn at the counter electrode, and the circuit is completed via electron migration through the external load [64]. The main difference between the photoelectrochemical and solid state cells relies on the kind of transport between the electrodes. In the cell using hole transporting material, the transport is typically electronic whereas in the DSSC using liquid or polymer electrolyte, ionic transport play a role. The following equations show the most important reactions involved in a DSSC using a hole transporting material. In the solid state DSSC version, the charge transfer reactions at the dye sensitized nanocrystalline TiO_2- hole transporting material (HTM) interface play a key role in determining the overall solar cell efficiency [45].

$$S^{*} \rightarrow S^{+} + e^{-}(TiO_2) \quad (1)$$

$$S^{+} + HTM \rightarrow S + HTM^{+} \quad (2)$$

$$HTM^{+} + e^{-}(\text{Al or Au}) \rightarrow HTM \quad (3)$$

$$S^{+} + e^{-}(TiO_2) \rightarrow S \quad (4)$$

$$e^{-}(TiO_2) + HTM^{+} \rightarrow HTM \quad (5)$$

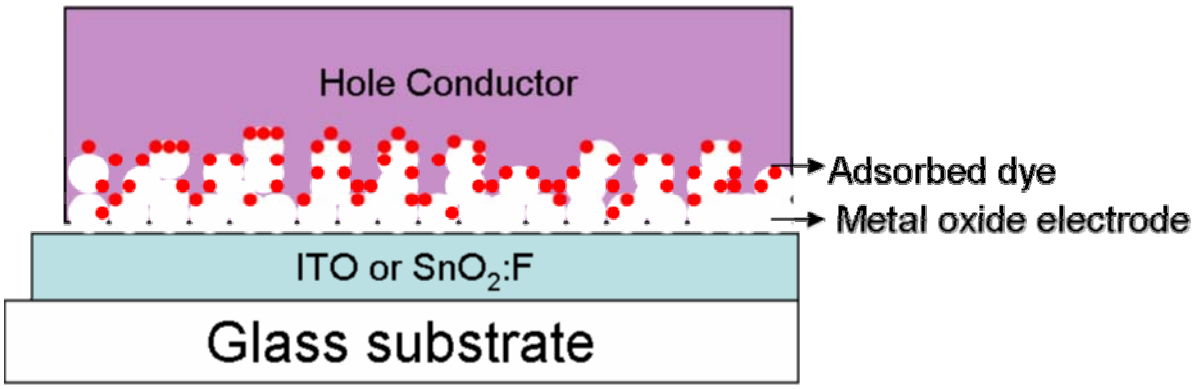

Figure 1.14 Schematic description of a solid state dye sensitized solar cell

The hole conductors employed in solid state dye sensitized solar cells can be classified as p-type semiconductors

1.3.2.2 P-type Semiconductors

The most common approach to fabricate a solid state DSSCs is by using p type semiconductors. Several aspects are essential for any p-type semiconductor in a dye sensitized solar cell (DSSC) [11,12,64].

1. It must be able to transfer holes from the sensitizing dye after the dye has injected electrons into the TiO_2; that is, the upper edge of the valence band of p-type semiconductors must be located above the ground state level of the dye (see figure 1.15).

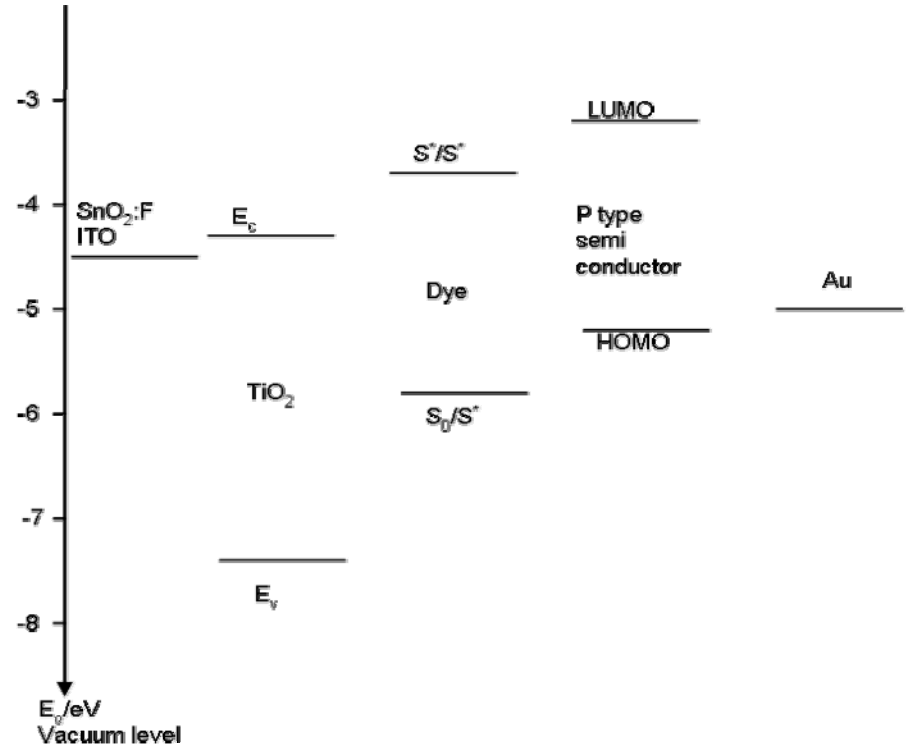

Figure 1.15 Energy diagram for an efficient charge transfer between solid state dye sensitized solar cell components

2. It must be able to be deposited within the porous nanocrystalline layer.

3. A method must be available for depositing without degrading or dissolving the monolayer of dye on TiO_2 nanocrystallites.

4. It must be transparent in the visible spectrum, or, if it absorbs light, it must be as efficient in electron injection as the dye.

5. It must penetrate into the pores of the nanoparticles.

Many inorganic p type semiconductors fulfill the requirements mentioned above; however, large band gap p type semiconductors such as SiC or GaN are not suitable for DSSC applications since deposition of those require high temperatures which would lead to the degradation of dye. P type semiconductors such as CuI, CuBr or CuSCN were found to be the successful canditates to replace the liquid electrolyte [61,65,66,67].

Tennakone et al reported on a solid state hybrid solar cell using CuI as hole transporter and cyanidin (a pigment extracted from flowers) as a sensitizer. The fully solid state solar cell of nanoporous n-TiO_2/cyanidin/p-CuI gave a short circuit current I_{sc} of 2.5 mA/cm^2 and a open

circuit voltage V_{oc} of 375 mV under 80 mW/cm^2 simulated sunlight [65]. The energy conversion efficiency was found to be 1 %. Tennakone et al [60] improved the efficiency of the solid state device further employing CuI as hole transporter and ruthenium bipyridyl dye complex as a sensitizer. The cells based on this structure produced V_{oc} of 600 mV and an I_{sc} of 1 mA/cm^2 under simulated 50 mW/cm^2 and the maximum power conversion efficiency 6% corresponds to a fill factor of about 45 %. When light intensities were higher than 100 mW/cm^2 the efficiency reduced to about 4.5 %.

Photodegradation of dye sensitized solid state TiO_2/dye/CuI cells was reported by Sirimanne et al in 2003 [68] where they investigated the stability of the CuI/dye/TiO_2 cells by using space resolved photocurrent imaging technique. They found that the formation of different morphologies depending on the CuI coating solution and unfilled TiO_2 pores could be responsible for the observed inhomogeneous photocurrent generation in the cells. Moreover, they concluded that the observed degradation was clearly due to the photoeffect. The excess iodine in the CuI film also decreased the photocurrent and degradation was explained as the modification of the interface of TiO_2/CuI due to the release of iodine and formation of trace amount of Cu_2O and/or CuO for the degradation of cell. A better stability was observed by covering the TiO_2 electrode by a thin MgO layer [69]. But degradation wasn`t compeletely stopped.

Previously, it was mentioned that depending on the CuI solution different morphologies are formed and TiO_2 pores are not completely filled due to inefficient penetration of CuI into the pores of TiO_2. Kumara et al [70] reported use of crystal growth inhibitors for deposition of hole conductors which enables filling of the porous matrix, resulting in the formation of more complete and secure contacts of the hole collector and the dyed surface. The crystal growth inhibitor used should have the special property of not leaving a solid residue at the grain boundaries or other interfaces upon evaporation of the solvent. 1-methyl-3-ethylimidazoliumthiocyanate (MEISCN) which is a molten salt, satisfied this requirement [70]. It was found that the crystal growth inhibitory action of MEISCN was dependent on strong absorption of SCN^- and CuI. In a study reported by Kumara et al [71], scanning electron microscopy studies on CuI films in the presence and absence of triethylamine hydrocyanate (THT) has been demonstrated. They observed that the crystallite size decreases in the presence of triethylamine hydrocyanate. The cells fabricated using THT for controlling the crystal growth gave a power conversion efficiency of 3.75 % and a peak IPCE of 59 % [71].

Kumara et al [66] reported an alternative to replace CuI by using CuSCN. It has been observed that solid state DSSC based on CuSCN have more stable performance. Although CuSCN possess appropriate bandgap and band energy values, the main problem, using this material was a satisfactory method for deposition. Dye sensitized solar cells made with CuSCN deposited electrochemically showed only a feeble response [55,66,69] and moreover, electrolytic deposition tend to degrade the dye coated on TiO_2 film. The solar cells prepared by dissolving CuSCN in n-propyl sulphide. On pressing a gold plated conducting tin oxide glass plate to the CuSCN surface, the cell delivers I_{sc}, V_{oc} on the order of 10 μA, 450 mV, respectively (15 W Osram lamp at intensity 300 W/m^2 as the light source). This low photoresponse was explained as not fully covering of CuSCN surface over the dye covered TiO_2 surface increasing the internal resistance of the cell. When graphite was painted on the CuSCN surface the I_{sc} increased to 1.5-2 mA/cm^2. Under AM 1.5 illumination the cell delivered I_{sc}, V_{oc} of 3.52 mA/cm^2, 616 mV, respectively giving an efficiency of 1.25 % [66]. Later, 2% efficiency was reported by O`Reagan et al [72] on another solid state DSSC with CuSCN as a hole conductor, where CuSCN was deposited into the pores of the dye sensitized nanocrystalline TiO_2 film from a dilute solution in propylsulfide. They concluded that 100 % of the CuSCN penetrates into the pores of the TiO_2. The cells showed energy conversion efficiencies of 2 % at 1 sun and also initial tests on stability showed promise.

Compared with inorganic p-type semiconductors, organic p-type semiconductors (see figure 1.16 [64]) possess the advantages of easy film formation and low cost.

In a study of solid state dye sensitized mesoporous TiO_2 solar cells with high photon to electron conversion efficiencies, Bach et al [62] reported a dye sensitized heterojunction if TiO_2 with the amorphous organic hole transport material 2,2',7,7'-tetranis(N,N-di-p-methoxyphenyl-amine) 9,9`-spirobifluorene(OMETAD). Photoinduced charge carrier generation at the heterojunction was found to be very efficient and the solar cells based on OMETAD converted the photons to electric current with a high yield of 33 % and the I_{sc} was 0.32 mA/cm^2, V_{oc} was 342 mV and the fill factor was 62 % corresponding to an overall efficiency of 0.74 %. In 2001, the performance of solid state dye sensitized solar cells based on spiro-OMETAD was further increased by Krüger et al [73]. Combining the results with a previous study of Krüger et al. they found out that molecules like 4-tert-butyl pyridine (tBP) prevents the problem of surface recombination by modifying the surface states. By blending the hole conductor matrix with a combination of 4-tert-butylpyridine(tBP) and $Li[CF_3SO_2]_2N$, a V_{oc} of 900 mV and an I_{sc} of 5.1 mA/cm^2 were obtained yielding an

efficiency of 2.56 % at AM 1.5 illumination. It is reported that the V_{oc} increases with the tBP concentration in the hole conductor film. With constant tBP concentration, an increase in lithium ion concentration resulted in an increase of short circuit current density. In 2002, Krüger et al. [74] improved the efficiency of solid state dye sensitized solar cell devices up o 3.2% by performing the dye adsorption in the presence of silver ions in the dye solution. In 2005, L.Mende et al reported [75] on TiO_2 pore filling and its effect on the efficiency of solid state dye sensitized solar cells. They were able to demonstrate 4% efficiency and also showed that wetting and pore filling of the nanoporous TiO_2 layer by the hole transporter appears to play a critical role for improving the efficiency of the solar cells and they concluded that the serial resistance in a cell increases if the pores of nanoporous TiO_2 are not completely filled and this leads to lower current densities and poorer performance of the cell under sunlight.

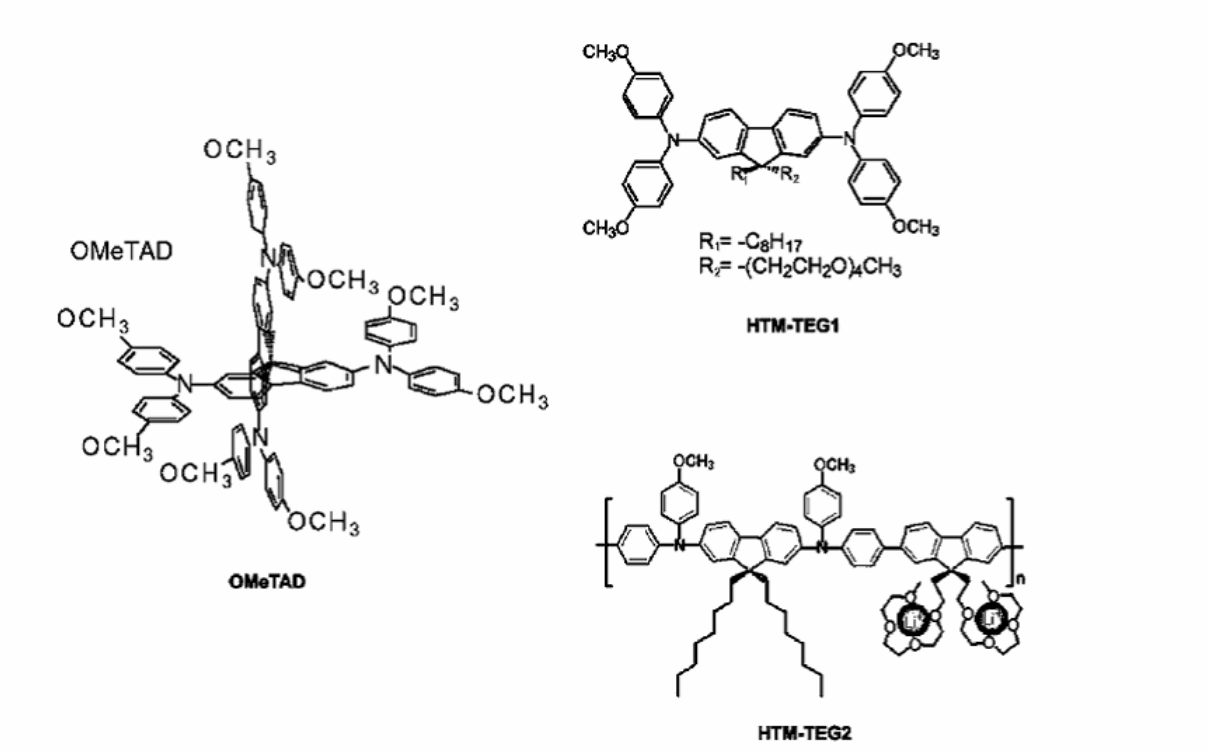

Figure 1.16 Several p type semiconductors utilized in solid state solar cells

Several other organic hole transport materials were used in solid state dye sensitized solar cells. Conducting polymers are well known as good hole transporting materials. Thus, these materials became potential candidates to be used as hole transporting material. The discovery of semiconducting, conjugated polymers and the ability to dope these polymers over the full range from insulator to metal has resulted in the design of a class of new materials that combines the electronic and optical properties of semiconductors and metals with the

attractive mechanical properties and processing advantages of polymers [18]. One of the requirements for a conducting polymer to act as hole transporting material in a dye sensitized solar cell is its wetability. Polymers cast from solution, should be able to penetrate into the pores of the nanoparticles. As a consequence, polymer molar mass is also crucial in order to achieve efficient pore filling [45].

Sicot et al reported on dye sensitized polythiophene solar cells using a poly(3-butylthiophene) with and without using a dye as a sensitizer. However, the efficiencies were extremely low. [13]. Gebeyehu et al have applied polythiophene derivatives as hole transporting material in DSSCs. Solid state devices using poly(3-octylthiophene) as hole transporting materials produced an open circuit voltage V_{oc} of 650 mV and a short circuit current of 0.45 mA/cm^2 under 80 mW/cm^2 [12,14]. In 2003, Smestad et al reported on polythiophene solid state dye sensitized TiO_2 solar cells. They achieved a V_{oc} of 0.8 V and an I_{sc} of 80-90 μA/cm^2 with a fill factor of 0.4 [11].

However, the conversion efficiencies of most solid state DSSCs employing organic p type semiconductors are relatively low particularly under high light irridiation.

The reasons for the low energy conversion can be summarized as following: [45]

1. The high charge recombination rate at the TiO_2-HTM interface between the electrons in the conduction band/trap states and the oxidized HTM.

2. The low conductivity of the hole conductor itself. Conducting polymers exhibit low hole mobility in comparison to inorganic materials. This is assigned to disorder characteristics of these materials giving rise to a broad distribution of trap states in the materials.

3. Low connectivity between the hole conductor and the hole collector electrode.

1.3.2.3 Solid State Electrolytes as “quasi solid state” DSSC

1.3.2.4 Gel Electrolytes

A polymeric gel is defined as a system that consists of a polymer network swollen with a solvent [45,76,77]. Gels combine the cohesive properties of the solids with the diffusive transport properties of liquids. When compared with pure polymer electrolytes, polymer gel electrolytes possess a high ambient ionic conductivity but poor mechanical properties [45].

Gel electrolytes are usually obtained by incorporating a large amount of a liquid plasticizer and/or solvent (containing the desired ionic salts) into a polymer matrix, giving rise to a stable gel with a polymer host structure. When gelation occurs, a dilute or more viscous polymer solution is converted into a system of high viscosity, a gel [45]. The polymer or oligomer that form this stable network is often named as a "gelator", because it solidifies the liquid phase. In order to improve the mechanical properties of the gel, components can be cross linked and/or thermoset may also be incorporated into the gel electrolyte formulation. Thus, gels can be obtained as a result of either a chemical or physical crosslinking process. Covalent crosslinking leads to the irreversible formation of gels. By contrast, the gel network formed via physical crosslinking is called an "entanglement network" [45]. There are several polymer matrices used to obtain polymer gels; the most investigated being poly(ethylene oxide), poly(acrylonitrile), poly(vinyl pyrrolidinine), poly(vinyl chloride), poly(vinyl carbonate), poly (vinylidene fluoride) and poly(methyl methacrylate) [45].

Among the various quasi solid state dye sensitized solar cell studies one of the very first studies was by Cao et al. Cao et al reported a quasi solid state dye sensitized solar cell using a mixture of NaI, ethylene carbonate, propylene carbonate and polyacrylonitrile [78]. However, the energy conversion efficiency was lower compared to the liquid dye sensitized solar cells which was attributed to the low penetration of the polymer network into the TiO_2 film.

Another important result on quasi solid state dye sensitized solar cell was reported by Wang et al [79] where they fabricated quasi solid state electrolyte based solar cells in which poly (vinylidenefluoride-co-hexafluoropropylene (PVDF-HFP) was used to solidfy a 3-methoxypropionitrile (MPN). When used in combination with an amphiphilic polypyridyl ruthenium dye, the device reached a conversion efficiency under full sunlight of over 6 %, showed high stabilities under both thermal stress at 80 ^{0}C and prolonged soaking with light.

Although high conversion efficiencies are reported, quasi solid state dye sensitized solar cells still can not reach the efficiencies of the conventional liquid electrolyte cells. Since the gel systems are thermodynamically unstable, this effect causes another problem [45]. Long storage might affect the solvent leakage, especially under ambient conditions decreasing their ionic conductivity and as a consequence the cell efficiency. High temperature conditions also have an effect on cell performance because a solvent with a high vapor pressure can affect the sealing conditions [45].

1.3.2.5 Polymer electrolytes

Polymer electrolytes are composed of alkaline salts dissolved in a high molecular mass polyether host or polypropylene oxide host [45,80]. In polymer electrolytes, the polymer matrix should be an efficient solvent for the salt, capable of dissociating it and minimizing the formation of ion pairs. The solubility of the salt relies on the ability of the electron donor atoms in the polymer chain to coordinate the cation through a Lewis type acid-base interaction [45]. This interaction also depends on the lattice energy of the salt and the structure of the host polymer. The mechanism for ionic motion in polymer electrolytes results from a solvation-desolvation process along the chains that occurs predominantly in the amorphous polymer phase [45].

Nogueira et al reported solid state dye sensitized solar cells by employing a copolymer, poly(epichlorohydrin-co-ethylene oxide), Epichlomer-16 . The electrolyte Epichlomer-16 was used without additional polymeric agent or plasticizer. The initial efficiency of 0,22 [81] was further improved to 2.6 % [82]. Another high efficiency was reported by Haque et al [83]. They reported a flexible solid state dye sensitized solar cells using Al_2O_3 coated TiO_2 electrodes and an I_2/NaI-doped solid state Epichlomer-16 electrolyte with an efficiency of 5.3 %. Kaneko et al reported efficiency of 7 % with a solid state dye sensitized solar cell incorporating polysaccharide solid involving redox electrolytes and an organic medium [84].

1.4 Nanoparticle-Quantum Dot Sensitized Solar Cells

Using the solid state dye sensitized solar cell concept, nanoparticle sensitized solar cells can be prepared by replacing the dye with inorganic nanoparticles or quantum dots. They can be adsorbed from a colloidal quantum dot solution [85] or produced in situ [15,86,87]. Quantum dots are class of semiconductor particles ranging in size from 2-10 nm in diameter. At these small sizes materials behave differently, proving unique optical and electronic properties.

The use of inorganic nanocrystals instead of organic dyes implies several advantages: the bandgap and thereby the absorption range are easily adjustable by the size of the crystals, bandedge type of absorption behaviour is the most favorable for effective light harvesting, and the surface properties of the particles can be modified in order to increase the photostability of the electrodes [15]. Nanocrystals have large extinction coefficients due to quantum confinement and intrinsic dipole moments, leading to rapid charge separation. In addition, semiconductor nanocrystals have a robust inorganic nature [88].

One of the first utilizations of the properties of these quantum sized particles for typical semiconductor applications was to embed the particles into porous TiO_2 films and to use those modified layers as light converting electrodes [89]. The incorporated nanoparticles shall be much smaller than the pore sizes of the nanoporous TiO_2 electrodes.

1.5 Extremely Thin Absorber (ETA) Solar Cells

Extremely thin absorber (ETA) solar cells are conceptually close to the solid state dye sensitized solar cells [90]. In the ETA solar cell, an extremely thin layer of a semiconductor such as $CuInS_2$ or CdTe replaces the dye in dye sensitized solar cells to cover the n type semiconductor film which is generally TiO_2. CuSCN has been the choice for the p type semiconductor [91]. The structure of the ETA solar cell has the advantage of enhanced light harvesting due to the surface enlargement and multiple scattering. Because photoinduced charge separation occurs on a limited length scale, higher levels of defects and impurities can be tolerated than in flat thin film devices, where the minority carriers are required to diffuse several micrometers. Same as the solid state dye sensitized solar cells the operation of the ETA solar cell is also based on a heterojunction with an exteremely large interface [92].

One of the exciting studies in this field was reported by Nanu et al [92]. They fabricated $TiO_2/CuInS_2$ ETA solar cell using atomic layer chemical vapour deposition technique. A 2 nm, thick Al_2O_3 tunnel barrier and a 10 nm thick In_2S_3 buffer layer were inserted between TiO_2 and $CuInS_2$ to overcome the interfacial recombination problem. This kind of cell produced an I_{sc} of 18 mA/cm^2 and a V_{oc} of 0.49 V and a fill factor of 0.44 corresponding to an energy conversion efficiency of 4 %. In the absence of Al_2O_3 and In_2S_3 buffer layers the cells showed moderate photoresponse proving the importance of the interfacial blocking layer.

1.6 Hybrid Solar Cells Based on Bulk Heterojunction Concept

An effective strategy for hybrid solar cell fabrication is to use blends of nanocrystals with semiconductive polymers as a photovoltaic layer. The basis of this is the bulk heterojunction concept [8,93,94,95]. The bulk heterojunction concept for organic solar cells has been previuosly described (see page 23). Bulk heterojunction concept in hybrid solar cells is similar to that used in organic solar cells. Excitons created upon photoexcitation have to be separated into free charge carriers. Exciton dissociation is known to occur very efficiently at interfaces between two semiconductors in a composite thin film such as a conjugated polymer

and fullerene mixtures [2]. Electrons will then be accepted by the material with the higher electron affinity (electron acceptor, usually fullerene or a derivative), and the hole by the material with the lower ionization potential, which also acts as electron donor.

In hybrid solar cells, one of the two organic components is replaced by inorganic semiconductor material. The solubility of the n-type and p-type components in the same solvent is an important paramater of the construction of hybrid solar cells. Hybrid solar cells can be formed by blending inorganic nanoparticles with semiconducting polymers [94]. Charge transfer junctions with high interfacial area are formed by blending semiconductor nanocrystals into conjugated polymers. Operation of such solar cells due to photocurrent generation at the interface of nanocrystal/polymer composite materials has been demonstrated in various blends containing CdSe [4,88,93], $CuInS_2$ [8,94], CdS [95] or PbS [96] nanocrystals.

The usage of inorganic semiconductor nanoparticles embedded into semiconducting polymer blends are promising for several reasons [94]:

1. Inorganic semiconductor materials can have high absorption coefficients and photoconductivity as many organic semiconductor materials.

2. The n- or p- type doping level of the nanocrystalline materials can easily be varied by synthetic routes so that charge transfer in composites of n- or p- type organic semiconducting materials with corresponding inorganic counterparts can be studied.

3. Band gap tuning in inorganic nanoparticles with different nanoparticle sizes can be used for realization of device architectures, such as tandem solar cells in which the different bandgaps can be obtained by modifying only one chemical compound [1,97].

If the inorganic nanoparticles become smaller than the size of the exciton in the bulk semiconductor (typically about 10 nm), their electronic structure changes. The electronic structure of such small particles are more like those of a giant molecule than an extended solid. The electronic and optical properties of such small particles depend not only on the material, of which they are composed but also on their size [9,88,98,99,100].

Blends of polymer and nanocrystals have yielded promising results as photovoltaic devices. A substantial interfacial area for charge separation is provided by nanocrystals, which have high surface area to volume ratios [4].

To enhance electron collection, it is desirable to form a defined pathway to the appropriate electrode for the charge which has been generated at a nanocrystal/polymer interface. In 1999, W. Huynh et al [4] reported on the construction of photovoltaic devices from a composite of 8x13 nm, elongated CdSe nanocrystals and regioregular poly(3-hexylthiophene) (P3HT). Elongated, rod shaped CdSe nanocrystals have a tendency to form directed chains, in which the particles stack along their axis. Devices constructed from thin films of 8x13 nm CdSe/P3HT composite displayed a photovoltaic effect with the current-voltage curves under monochromatic illumination at 514 nm for a device with 80% CdSe under 4.8 W/m^2 irridiation, the device had an I_{sc} of 0.031 mA/cm^2 and a V_{oc} of 0.57 V. The corresponding external quantum efficiency was 16% and the fill factor was 0.49. For a similar device constructed from 4x7 nm CdSe nanoparticles, the external quantum efficiency was 4% and the fill factor was 0.45. They found out that the rectification characteristics and V_{oc} don`t change with size. The difference in quantum efficiency by a factor of 4 resulting from a change in nanocrystal size was attributed to differences in aggregation of nanocrystals within the polymer. In a complementary work by Huynh et al [93], they fabricated an efficient organic/inorganic hybrid solar cell by blending CdSe (90 %) with P3HT. They achieved a power conversion efficiency of 1.7 % under simulated AM 1.5 illumination with CdSe nanocrystals of 7x60 nm size. The nanocrystal/polymer blend devices had a broad photocurrent spectrum extending from 300 to 720 nm.

Hybrid solar cells based on nanoparticles of $CuInS_2$ in organic matrices was reported by Elif Arici et al [8,94]. They reported on solution processed hybrid solar cells consisting of nanocrystalline inorganic semiconductor $CuInS_2$, and organic materials. Nanocrystalline $CuInS_2$ was used with fullerene derivatives to form interpenetrating interface donor-acceptor heterojunction solar cells. They investigated also bulk heterojunctions by replacing the $CuInS_2$ single layer by a blend of $CuInS_2$ and a p type polymer (PEDOT:PSS; poly(3,4-ethylenedioxythiophene:poly(styrene sulfonic acid) in the same cell configuration. Bulk heterojunction solar cells showed better photovoltaic response with external quantum efficiencies up to 20% [8].

Besides using quantized nanocrystals in hybrid devices, P. Van Hal et al [101] reported on hybrid devices based on blends of TiO_2 with MDMO-PPV. They investigated photoinduced electron transfer and photovoltaic response of MDMO-PPV:TiO_2 bulk heterojunctions. To prepare bulk heterojunctions they blended MDMO-PPV with titanium(iv)isopropoxide, a precursor of TiO_2. Subsequent conversion of titanium(iv)isopropoxide precursor via

hydrolysis in air in the dark resulted in the formation of a TiO_2 phase in the polymer film. Such a device exhibited an I_{sc} of 0.6 mA/cm^2 and a V_{oc} of 520 mV with a fill factor of 0.42. An external quantum efficiency up to 11% has been achieved.

In 2005, I. Gur et al [102] reported air stable all-inorganic nanocrystal solar cells processed from solution. Although the investigated cells completely consisted of inorganic nanoparticles the study was interesting since the solution processed bilayers on inorganic nanoparticles was also investigated. They fabricated planar donor acceptor heterojunctions by sequentially spincasting films of CdTe and CdSe and sintered the films at 200 ^{0}C to remove the solvent residues. The photoresponse of sintered CdTe/CdSe bilayer cells showed external quantum efficiency of 70%, I_{sc} of 11.6 mA/cm^2, V_{oc} of 0.4 V and a fillfactor of 0.45, resulting in 2.1% power conversion efficiency under simulated AM 1.5 illumination. By varying simple system parameters such as electrode material, also higher efficiencies were achieved in sintered nanocrystal cells. The cells employing a Ca top contact capped with Al had an AM1.5 power conversion efficiency of 2.9% with I_{sc} of 13.2 mA/cm^2, V_{oc} of 0.45 V and a fill factor of 0.49.

Recent efforts are focused on PbS nanoparticles. In a study reported by S. Zhang et al [103], they demonstrated hybrid solar cells from blends of MEH-PPV and PbS nanocrystals. They investigated the effect of different surfactant on the photovoltaic performance of the hybrid devices using PbS nanoparticles. However, the efficiencies were extremely low. The devices exhibited 250 nA short circuit current and an open circuit voltage of 0.47 V.

In 2006, W. Beek et al [104] reported on hybrid solar cells from regioregular polythiophene and ZnO nanoparticles. They used blends of nanocrystalline zincoxide (nc-ZnO) and regiregular P3HT from solution to construct hybrid polymer metal oxide bulk heterojunction solar cells. Thermal annealing of the spincast films significantly improved the solar energy conversion efficiency of these hybrid polymer metal oxide bulk heterojunction solar cells to 0.9%. Under AM 1.5 illumination the devices showed I_{sc} of 2.38 mA/cm^2 and a V_{oc} of 685 mV. They found that efficiency is strongly dependent on thermal annealing treatment and the amount of ZnO in the blend. However, photoluminescence and photoinduced absorption spectroscopy demonstrated that the charge carrier generation wasn`t quantitative, because a fraction of P3HT appeared not to be in contact with or close proximity to ZnO. The coarse morphology of the films also limited the device performance.

Chapter 2

2. Experimental

2.1 Substrate Preparation

As substrates, glass sheets of 1.5x 1.5 cm^2 covered with ITO, from Merck KG Darmstadt, were used with an ITO thickness of about 120 nm and sheet sheet resistance < 15 Ωcm^{-2}.

The ITO was patterned by etching with an acid mixture of HCl_{konz}:HNO_{3konz}:H_2O (4.6:0.4:5) for ~ 30 min. The part of the substrate which forms the contact is covered with a scotch tape preventing the etching. The scotch tape was removed after etching and the substrate was then cleaned by using acetone in an ultrasonic bath and finally with iso-propanol.

2.2 Device Preparation

2.2. 1 Device Preparation for Solid State Dye Sensitized Solar Cells

Figure 2.1 shows a scheme of a solid state dye sensitized solar cell.

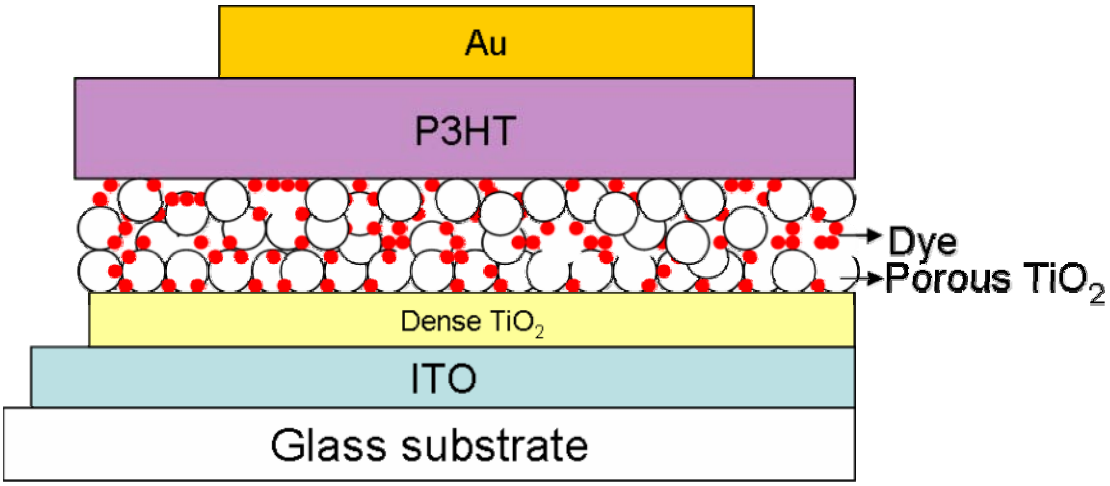

Figure 2.1 Schematic description of the investigated solid state dye sensitized solar cell

Compact TiO_2 layers were prepared according to ref [105] and were spincast under ambient conditions on top of the cleaned and patterned ITO substrates by using 8000 rpm resulting in approximately 100 nm thick films. After spin coating, the substrates were placed in an oven and sintered at 450 ^oC for 30 minutes yielding insoluble compact layers. A porous TiO_2 layer was deposited by doctorblading commercially available TiO_2 paste on top of the compact TiO_2 films. Then, the substrates were sintered once more at 450 ^oC for 30 minutes.

Ruthenium dye complex of $RuL_2(NCS)_2/2TBA$ (where L= 2,2′-bipyridyl-4,4′-dicarboxylic acid; TBA= tetrabutylammonium) was bought from Solaronix Switzerland. A Ru dye solution was prepared by dissolving 15 mg Ruthenium dye in 50 ml ethanol by using an ultrasonic bath. The TiO_2 electrodes were then immersed into the Ruthenium dye solution for 12 hours.

P3HT with an average molecular weight of 58,000 (American Dye Source) was used as received. 10 mg P3HT was dissolved in 1 ml chlorobenzene. A P3HT film was covered on top of the Ruthenium coated TiO_2 electrodes. Finally, 100 nm gold electrodes were thermally evaporated.

2.2.2 Materials used for Solid State Dye Sensitized Solar Cells

2.2.2.1 P3HT

Figure 2.2 shows the chemical structure of the frequently used organic semiconductor poly(3-hexylthiophene) (P3HT) for photovoltaic applications. Regioregular P3HT has been used in this work. P3HT is highly soluble in common organic solvents and has a broad absorption spectra with a maximum around 550 nm.

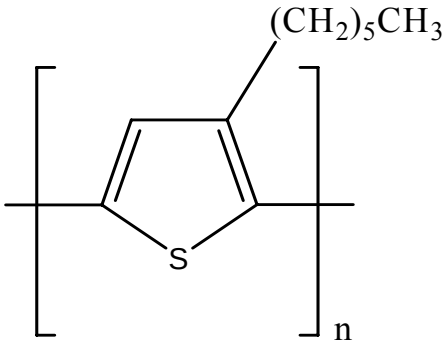

Figure 2.2 Chemical structure of P3HT

2.2.2.2 Ruthenium Dye

Ruthenium dye complex is one of the most promising dyes in dye sensitized solar cells. Ru-bis TBA dye is used as a sensitizer for TiO_2 electrodes. The chemical structure of Ru bis TBA is shown in figure 2.3.

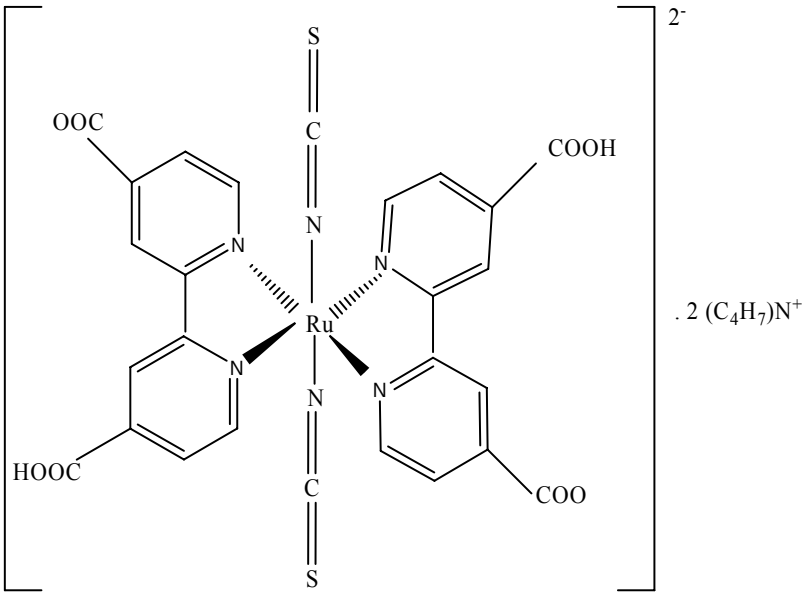

Figure 2.3 Chemical structure of $RuL_2(NCS)_2$/2TBA (where L= 2,2′-bipyridyl-4,4′-dicarboxylic acid; TBA= tetrabutylammonium)

The ruthenium dye complex is known to adsorb on TiO_2 nanoparticles. This dye exhibits three different absorption maxima due to metal ligand charge transfer [47].

2.2.3 Device Preparation for Hybrid Devices Using HgTe Nanocrystals and Nanoporous TiO_2 Electrodes

ITO substrates were etched and cleaned in an identical manner as described above. Compact TiO_2 layers were also prepared and sintered as described above. Porous TiO_2 layers were doctorbladed by using TiO_2 paste diluted with ethanol with 1:10 ratio and then sintered at 450 ^{o}C for 30 minutes.

Two types of water soluble and organic solvent soluble HgTe nanocrystals were employed in this thesis. Both types of HgTe nanocrystals were received from Prof. Wolfgang Heiss`s group (Semiconductor and Solid State Physics Department, JKU Linz). The particles were synthesized by DI Maksym Kovalenko following the route described in [106]. Water soluble

HgTe nanocrystals will be denoted as HgTe-AS whereas organic solvent soluble HgTe naocrystals will be denoted as HgTe-OS.

Water-soluble HgTe nanocrystals were obtained by precipitation reaction of Hg^{2+} and Te^{2-} in the presence of thioglycerol as surface capping hydrophilic ligand, similarly to the procedure described in ref [106].

The HgTe-OS nanocrystals were obtained by a ligand exchange procedure [106], making use of HgTe-AS nanocrystals.

The electrodes consisting of compact TiO_2 and a nanoporous TiO_2 layer are denoted as NP-TiO_2 electrodes. The nanocrystal sensitization was done by treating NP-TiO_2 electrodes with HgTe-AS nanocrystals for 12 hours. As hole conducting conjugated polymer poly-(3-hexyl-thiophene) (P3HT) was used by dissolving in chlorobenzene with a 1% weight concentration. The blend of nanocrystal/polymer was prepared by mixing HgTe-OS and P3HT with a weight ratio of 2.2/1, respectively. This is the experimentally optimized ratio. The active layers of all cells were deposited by dropcasting method. Device ASOS was prepared by treating NP-TiO_2 electrodes with HgTe-AS nanocrystals for 12 hours and dropcasting the HgTe-OS/P3HT blend on the treated electrodes. Reference OS consisted of HgTe-OS/P3HT blend on top of a bare NP-TiO_2 electrode. Reference AS was prepared by treating the NP-TiO_2 electrodes with HgTe-AS nanocrystals and dropcasting P3HT. Reference NO cell was prepared without any HgTe nanocrystals and consisted of bare NP-TiO_2 electrodes and P3HT. In all device configurations gold was chosen as the top electrode material (160 nm, thermally evaporated) because its workfunction is close to the highest molecular orbital (HOMO) of the hole conductor P3HT. Thus, hole injection from the polymeric organic material into the metal electrode is energetically possible.

2.2.4 Device Preparation for Hybrid Devices Using $CuInS_2$ as Nanoporous Electrodes

The synthesis of $CuInS_2$ (CIS) nanoparticles was performed by a colloidal route as presented in [107]. CIS particles were shielded by the organic surfactant triphenyl phosphate (TPP) to prevent partly further growth. After the synthesis, $CuInS_2$ nanoparticles were further treated with methanol. Methanol treatment leads to the precipitation of the nanoparticles since the surfactant TPP is removed by addition of methanol. Then, the nanoparticles were suspended again in pyridine forming a stable dispersion.

Devices were fabricated as shown in figure 2.4

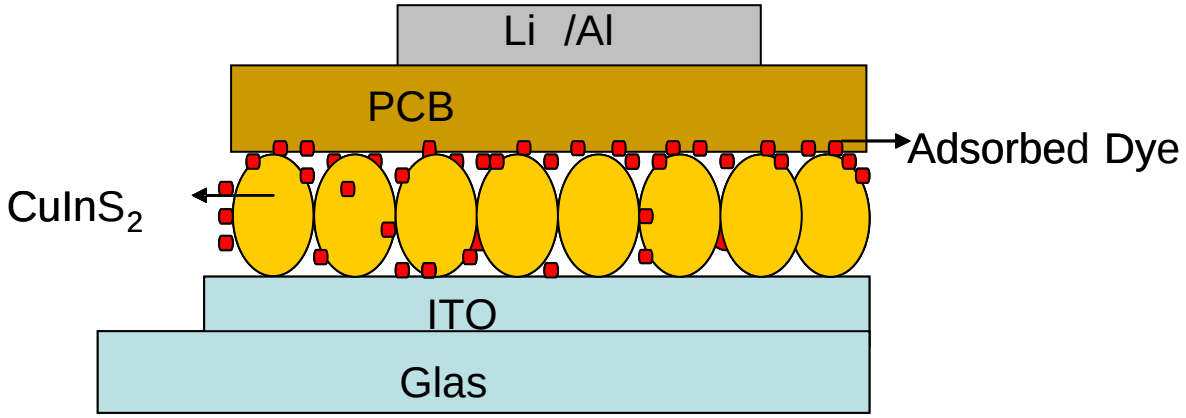

Figure 2.4 Schematic description of a hybrid device using $CuInS_2$ nanoparticles and PCBM.

ITO substrates were etched and cleaned as described above. Nanoporous films of CIS were prepared by doctor blading the CIS suspension onto indium tin oxide (ITO) glass. The films were annealed at 200 ^{O}C in air for 15 minutes. The nanomorphology of the films was measured by using Digital Instrument 3100 atomic force microscope (AFM). 15 mg of $RuL_2(NCS)_2$/2TBA (where L= 2,2′-bipyridyl-4,4′-dicarboxylic acid; TBA= tetrabutylammonium) dye was dissolved in 50 ml ethanol. 1-(3-methoxycarbonyl)-propyl-1-phenyl-[6,6]-C_{61} (PCBM) solution was prepared by dissolving 30 mg of PCBM in 1 ml chlorobenzene solution. The cells consisting of $CuInS_2$ and PCBM bilayers were characterized with and without using the dye complex on the surface. Dye coating was done by immersing the $CuInS_2$ films into dye solution for 12 hours. PCBM was dropcast on $CuInS_2$ films. 0.6 nm lithium fluoride (LiF) and 100 nm aluminium were thermally evaporated.

2.2.5 Device Preparation for Hybrid Devices Using PbS Nanoparticles and P3HT

PbS nanocrystals were received from Prof. Gregory Schole`s group (University of Toronto). Karolina Fritz synthesized the PbS nanoparticles by a method as described in ref [108]. The particles were coated with oleic acid as surfactant and dissolved in chloroform.

The scheme of the device using PbS nanoparticles and P3HT is shown in figure 2.5.

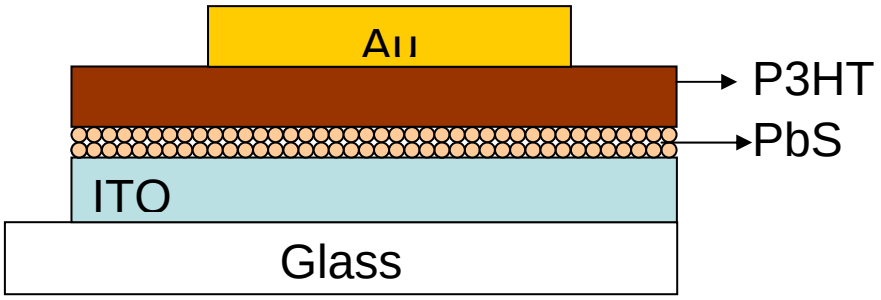

Figure 2.5 Schematic description of the hybrid device using PbS nanoparticles

The ITO substrates were etched and cleaned in the same way as described above. PbS nanoparticle solution was mixed with ethylacetate solution with 1:1 volume ratio and the mixed solution was ultrasonicated. This mixture was spincast at 700 rpm and sintered at 200 ^{0}C in a vacuum oven. P3HT was used as a hole transporter and finally 160 nm gold was thermally evaporated.

2.3 Device Characterization

The electrical characterization was carried out under inert argon environment inside a glove box system (MB 200 from MBraun). For solar cell characterization , a Keithley 236 sourcemeter was used.

For the characterization of the devices under light, a solar simulator (K. H. Steuernagel Lichttechnik GmbH) was used under AM 1.5 conditions. Devices were illuminated through the ITO coated glass.

Solar cell efficiencies were calculated according to formula 2.1:

$$\eta = \frac{I_{sc} * V_{oc} * FF}{P_{in}} \qquad (2.1)$$

where I_{sc} is the short circuit current density, V_{oc} is the open circuit voltage, FF is the fill factor and P_{in} is the incident light intensity.

The surface morphology measurements were carried out under ambient conditions with a Digital Instruments Dimension 3100 atomic force microscope in the tapping mode.

Cross-section scanning electron microscopy (SEM) analysis was done by using a LEO Supra 35 scanning electron microscope.

For measuring the IPCE response between 300 and 900 nm the samples were illuminated under argon atmosphere inside a glovebox with light from a Xenon lamp passing a monochromator (FWHM ~4 nm, illumination intensity ranging between ~ 50 μW cm^{-2} and ~200 μW cm^{-2}) and chopped with a frequency of 273 Hz. Using an EG&G Instruments 7260 lock-in amplifier the photocurrent of the solar cell was related to the photon flux, determined with a calibrated Si detector. The IR response for the cells containing HgTe nanocrystals was characterized by the use of a 15 cm grating spectrometer and an InSb detector. To eliminate quantification inconsistencies between the UV-Vis and the IR measurement setup, the y axis of the IPCE [%] curve was scaled to the same value as obtained with the silicon reference diode at 900 nm. IPCE was calculated using the following formula:

$$\text{IPCE}(\%) = \frac{1240 * I_{sc}}{\lambda * P_{in}} \qquad (2.2)$$

Where I_{sc} is the short circuit current density (μA/cm^2), λ is the incident photon wavelength (nm), P_{in} is the monochromatic light incidence (W/m^2).

Chapter 3

3. Results

3.1 Results on Solid State Dye Sensitized Solar Cells Using Poly (3-hexylthiophene) as Hole Conductor

The concept of solid state dye sensitized solar cells has been introduced in chapter 1. In 3.1 solid state dye sensitized solar cells have been fabricated using TiO_2 electrodes, ruthenium-bis TBA dye and poly(3-hexylthiophene). Previously, solid state devices based on polythiophenes as hole transporters have been demonstrated [11,12,13,14]. The efficiencies of such solar cells were still lower than that of photoelectrochemical solar cells. Several reasons can be considered for these low efficiencies such as the imperfect filling of the TiO_2 pores by polymeric hole conductor together with the adhesion of the polymer on the TiO_2 or on the dye. Besides that, another important problem is given by charge losses related to back reactions due to a direct contact between the dye regeneration system and the transparent conducting oxide (indium tin oxide (ITO) or fluorine doped tin oxide (SnO_2:F)). A compact TiO_2 with no pores between the conducting oxide and the nanoporous TiO_2 layer, acting as a blocking layer, has been introduced to prevent these back reactions [62].

In this section the effect of compact TiO_2 layers on polythiophene based solid state dye sensitized solar cells is demonstrated. Such compact layers improve the efficiencies from 0.08 % reported in literature for polythiophene based solid state dye sensitized solar cells to 0.3 %.

3.1.1 Morphology of TiO_2 electrodes

Two kinds of TiO_2 electrodes were used in this study: (i) compact TiO_2 electrodes with no pores between the particles (ii) nanoporous TiO_2 electrodes. The morphologies of both compact and porous TiO_2 layers were characterized by atomic force microscopy (AFM) as shown in Figure 3.1 (a) and (b), respectively [109]. Both types of electrodes were sintered at 450 ^{0}C for 30 minutes individually to insure the electrical contact between the particles and also to evaporate the solvent residues remaining between the particles. The AFM images were

taken after the sintering procedure. As can be seen from the AFM images the compact TiO_2 film was rather smooth with a surface roughness of 25 nm whereas the porous TiO_2 film has a rough surface with a surface roughness of 100 nm.

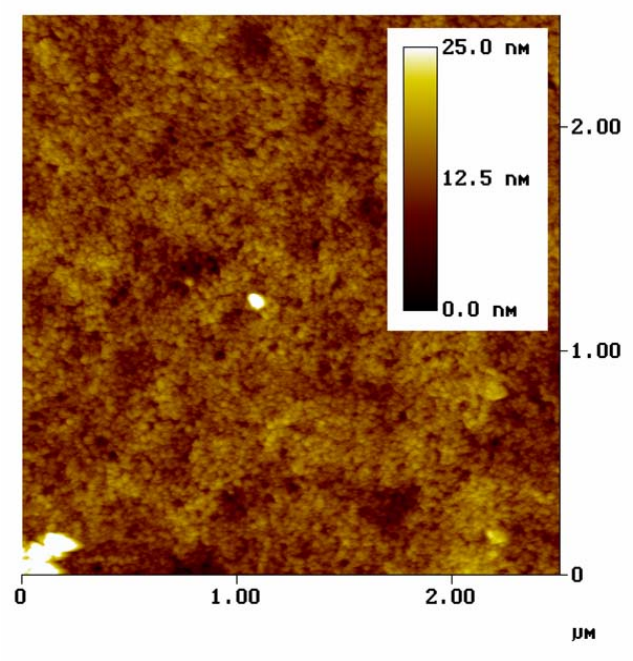

(a)

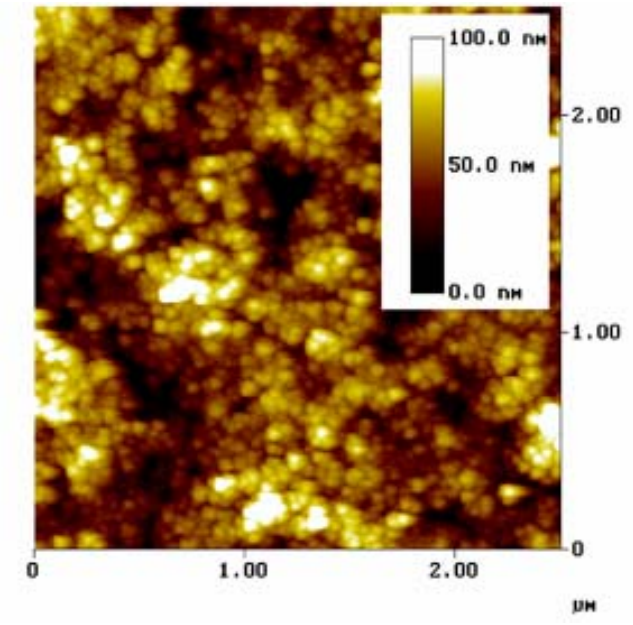

(b)

Figure 3.1 Atomic Force Microscopy (AFM) image of (a) compact TiO_2 (b) porous TiO_2 layer.

3.1.2 Dye Sensitization

On photoexcitation dye molecules adsorbed at the surface of an n-type (p-type) semiconductor on photoexcitation can inject electrons (holes) into the conduction (valence) band forming a dye cation (anion) [62]. This phenomenon is known as dye sensitization. In Figure 3.2 [109] the absorption spectra of TiO_2 electrodes with and without dye adsorption is shown. As can be seen from the figure in the dye coated TiO_2 spectrum new absorption appears compared with that of bare TiO_2 electrodes which is a consequence of adsorption of dye molecules on the TiO_2 surface.

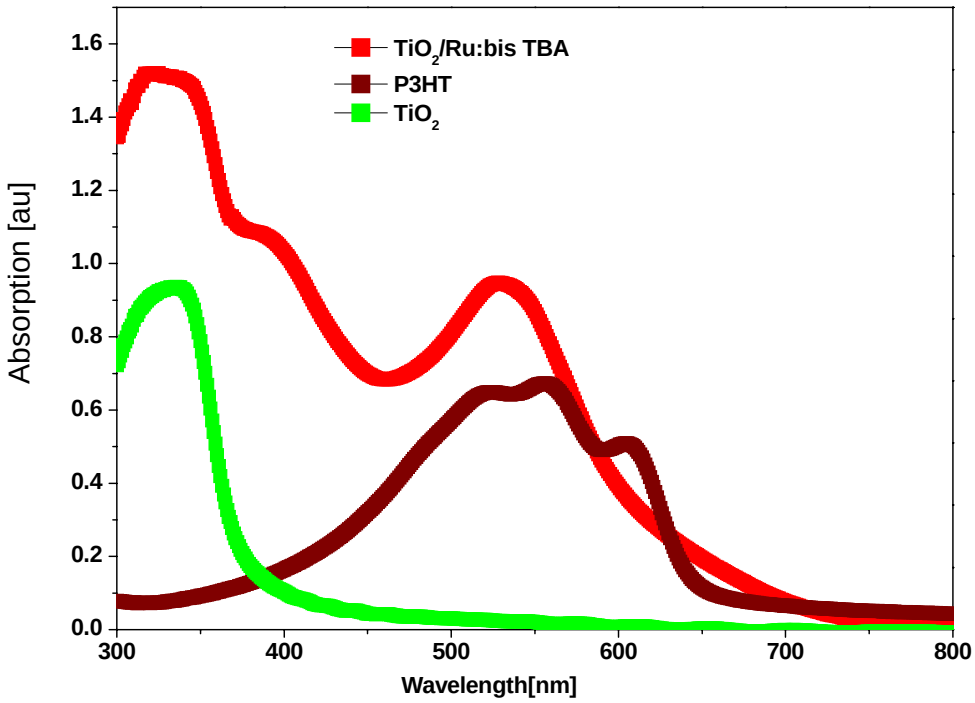

Figure 3.2 Absorption spectra of the individual components of the investigated solid state dye sensitized solar cell

3.1.3 Effect of Film Coating Techniques on the Morphology of the Solar Cells

In all solar cell configurations gold was chosen as a top electrode because its workfunction is close to the highest molecular orbital (HOMO) of the hole conductor P3HT. Thus, hole injection from the polymeric organic material into the metal electrode is energetically possible [12]. However, gold is known to diffuse through the organic materials if the organic layer

thickness is not sufficient. Therefore, the film preparation technique of the polythiophene layer was optimized. Several techniques such as spincoating, doctorblading and dropcasting were employed. Figures 3.3 (a), (b), (c) [109] show how employments of different film coating technique affect the morphology. As can be seen, neither by spincoating nor by doctorblading P3HT, the pores of the TiO_2 layer are closed, opening pathway for the diffusion of gold causing short circuits in the device. It can be seen from figure 3.3 (b) that by dropcasting, the surface of TiO_2 is fully covered with the polymer layer. For the photovoltaic characterization dropcasting method was used.

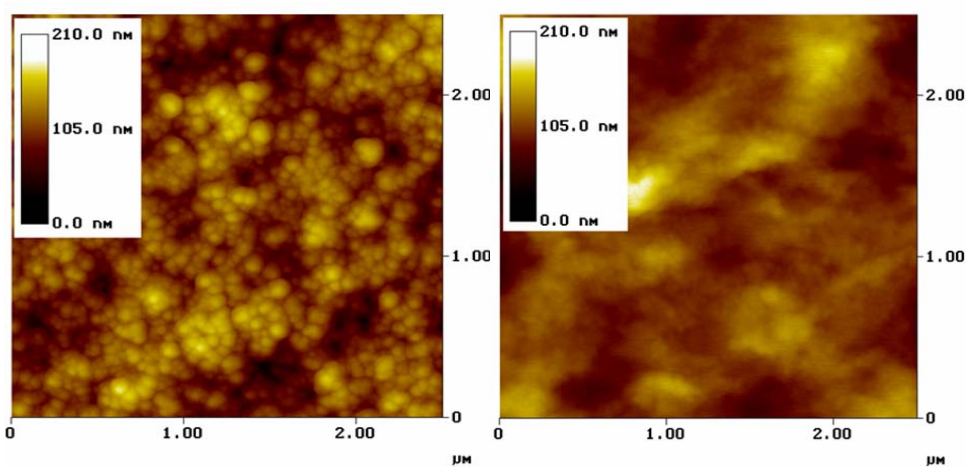

(a) (b)

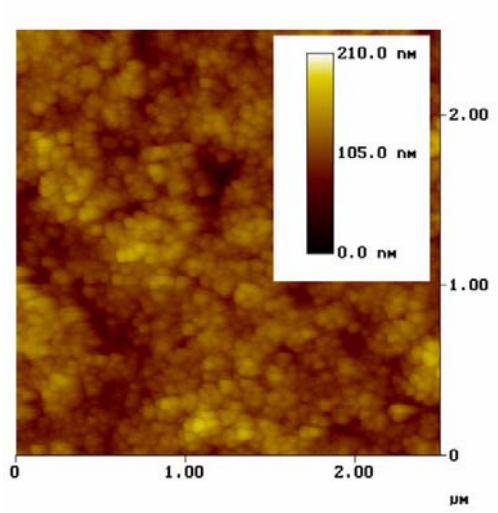

(c)

Figure 3.3 AFM images of P3HT films prepared by (a) spincoating (b) dropcasting (c) doctorblading onto the porous TiO_2

3.1.4 Current-Voltage Characteristics

Prevously, it was mentioned that a compact TiO_2 layer, acting as a blocking layer, prevents the charge losses related to back reactions [62,110]. The effect of compact TiO_2 layers on the device performance of the solid state hybrid solar cells have been investigated with and without employing the compact layers in the solar cell configuration. Figure 3.4 (a) and (b) [109] show the current voltage (I-V) characteristics of the solid state TiO_2/P3HT device without using a compact TiO_2 layer in linear and semilogarithmic scales, respectively. This kind of cell produced a short circuit current density (I_{sc}) of 0.06 mA/cm^2 and an open circuit voltage (V_{oc}) of 300 mV and a fill factor of 0.43. Figure 3.5 (a) and (b) show the I-V characteristics of a TiO_2/P3HT device with a compact TiO_2 layer. Such a cell produced a V_{oc} of 500 mV, I_{sc} of 0.4 mA/cm^2 and a fill factor of 0.5. The comparison of the results on photovoltaic performance with or without compact TiO_2 layers clearly indicated that in the former case short circuit current density was improved at least by one order of magnitude.

Next, the effect of a dye interlayer was investigated by inserting ruthenium dye between nanoporous TiO_2 and P3HT. For comparison, two kinds of cells (i) with dye interlayer but without a compact TiO_2 layer (ii) with compact TiO_2 and dye interlayer were fabricated. Figure 3.6 [109] shows that the cell (i) produced an I_{sc} of 0.09 mA/cm^2 and a V_{oc} of 550 mV and a fill factor of 0.3. Inserting a dye interlayer increased the short circuit current for both cells with or without compact TiO_2 layers. Figure 3.7 [109] shows the I-V characteristics of cell (ii). Inserting the dye interlayer increased the short circuit current to 2 mA/cm^2(see Fig. 3.7 [109]). V_{oc} was found to be 450 mV and fill factor was 0.3.

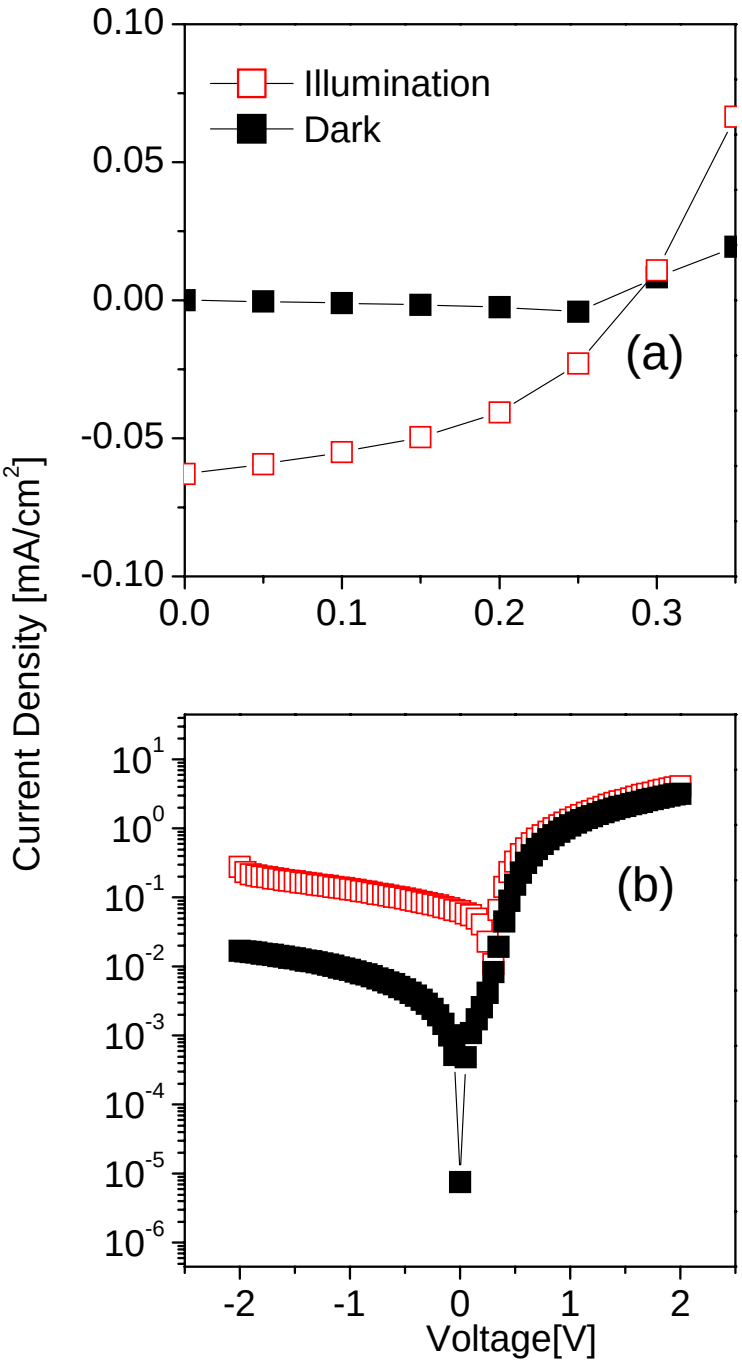

Figure 3.4 I-V Characteristics of solid state hybrid solar cell without a compact TiO_2 layer (a) linear (b) semilogarithmic scale

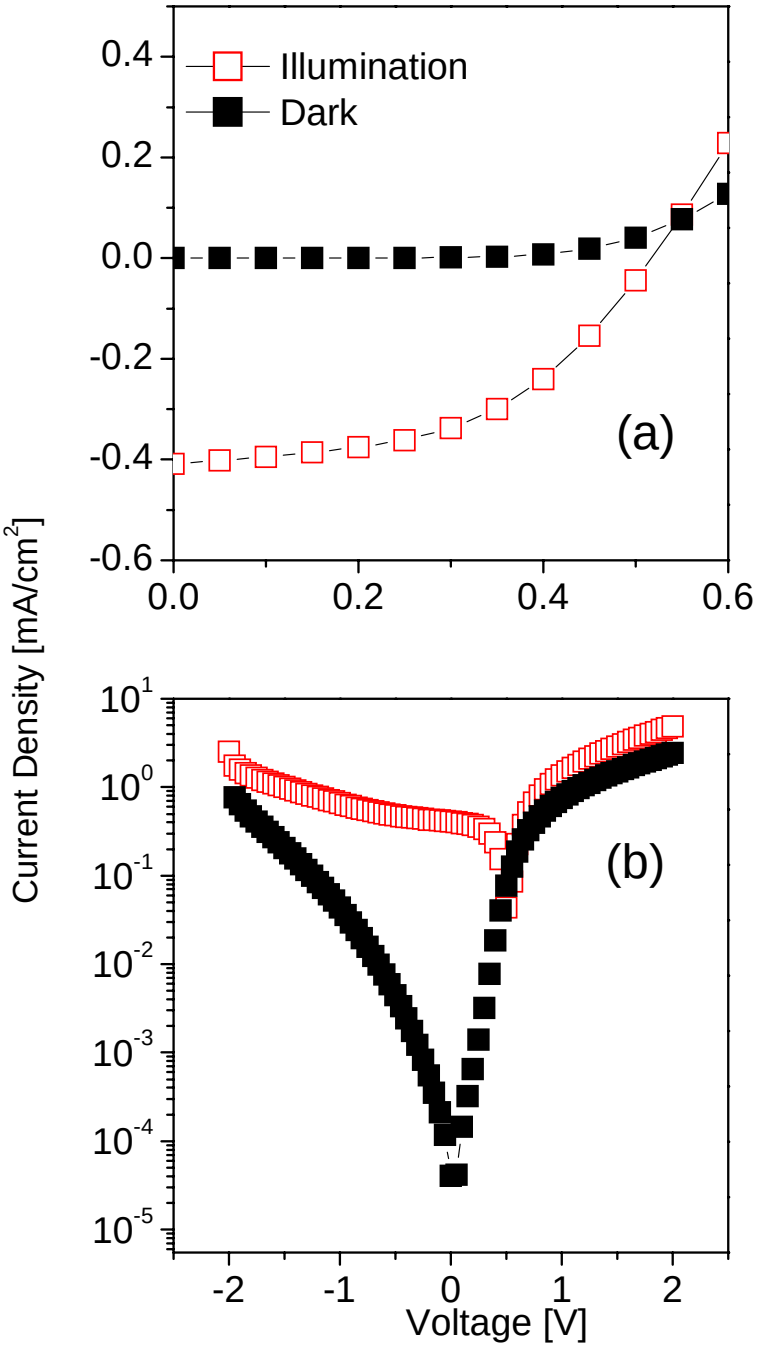

Figure 3.5 I-V Characteristics of solid state hybrid solar cell with compact TiO_2 layer (a) linear scale (b) semilogarithmic scale

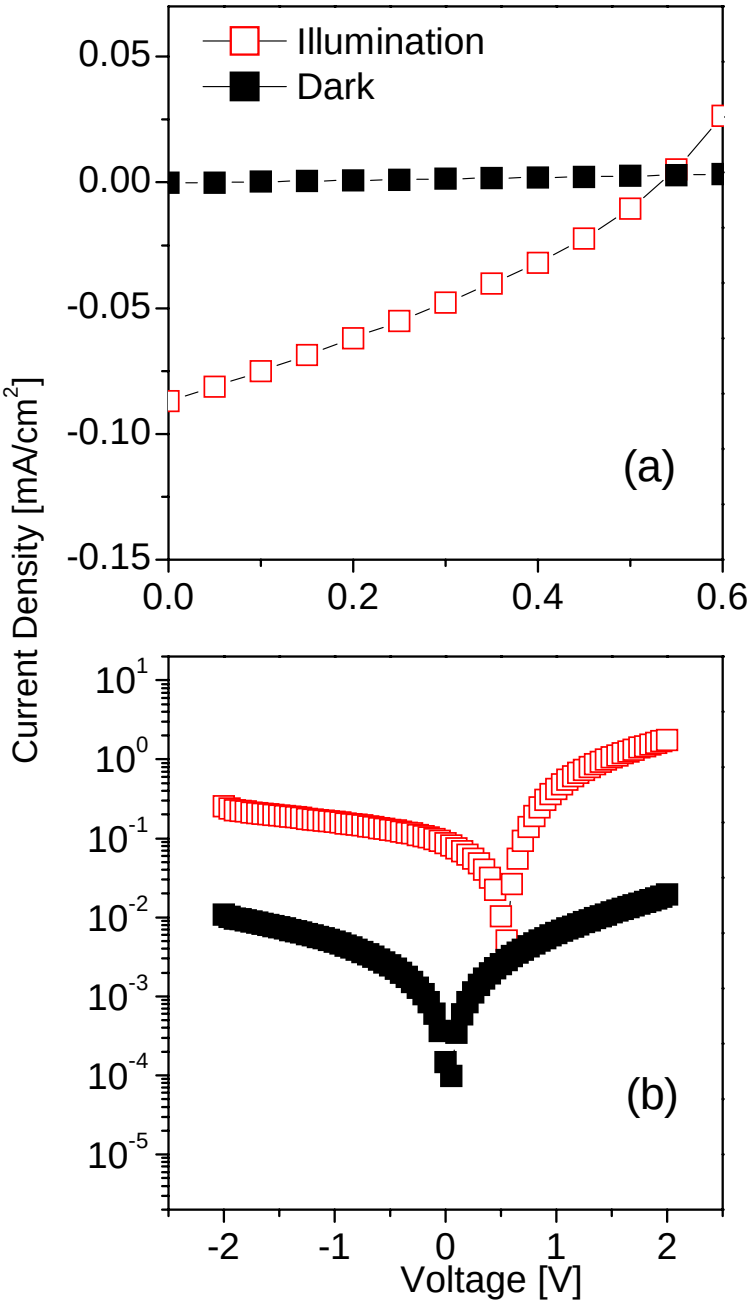

Figure 3.6 I-V Characteristics of solid state hybrid solar cells with a dye interlayer but without a compact TiO_2 layer (a) linear (b) semilogarithmic scale

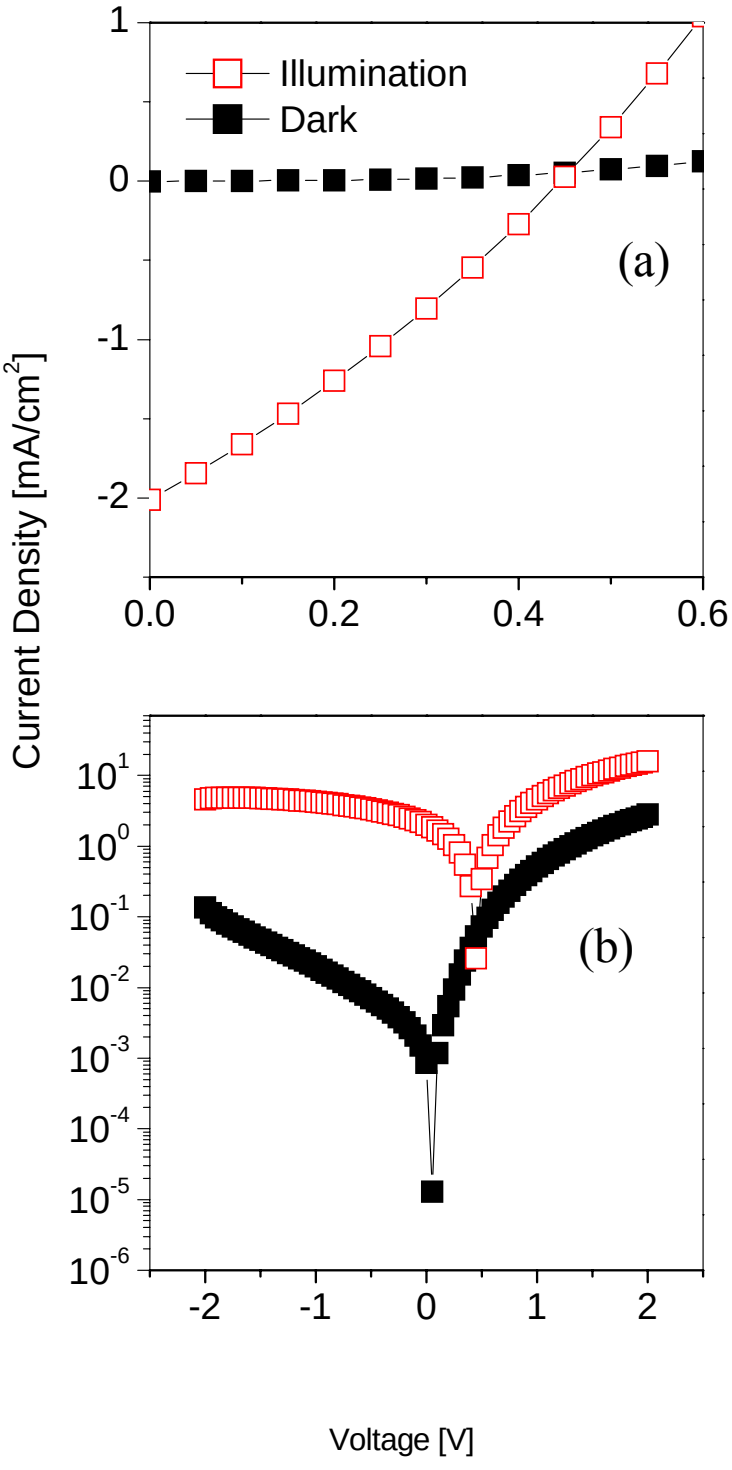

Figure 3.7 I-V Characteristics of solid state hybrid solar cells using a dye interlayer and a compact TiO_2 layer (a) linear (b) semilogarithmic scale

3.1.5 Incident Photon To Current Efficiency (IPCE)

The % IPCE relates the number of electrons to the number of incident photons measured under short circuit conditions. Information on the number of incident photons of different energy that contribute to the charge carrier generation is obtained [31]. By comparing the spectral response with the optical absorption spectra one can obtain information on the charge carrier generation mechanism. The comparison of the optical absorption spectra of the solar cell components with the IPCE as shown in figure 3.8 [109] shows that both P3HT and Ru dye contribute to the charge carrier generation. The cells without a compact TiO_2 layer had an IPCE response below 0.1 % (not shown). The cell with compact TiO_2 layers, but without dye, showed IPCE response of 1.6 % at 550 nm whereas the cell consisting of a dye interlayer between TiO_2 and P3HT showed IPCE response of 8 % at 550 nm. The enhancement in the IPCE upon insertion of a ruthenium dye layer is attributed to the additional absorption offered by the ruthenium dye.

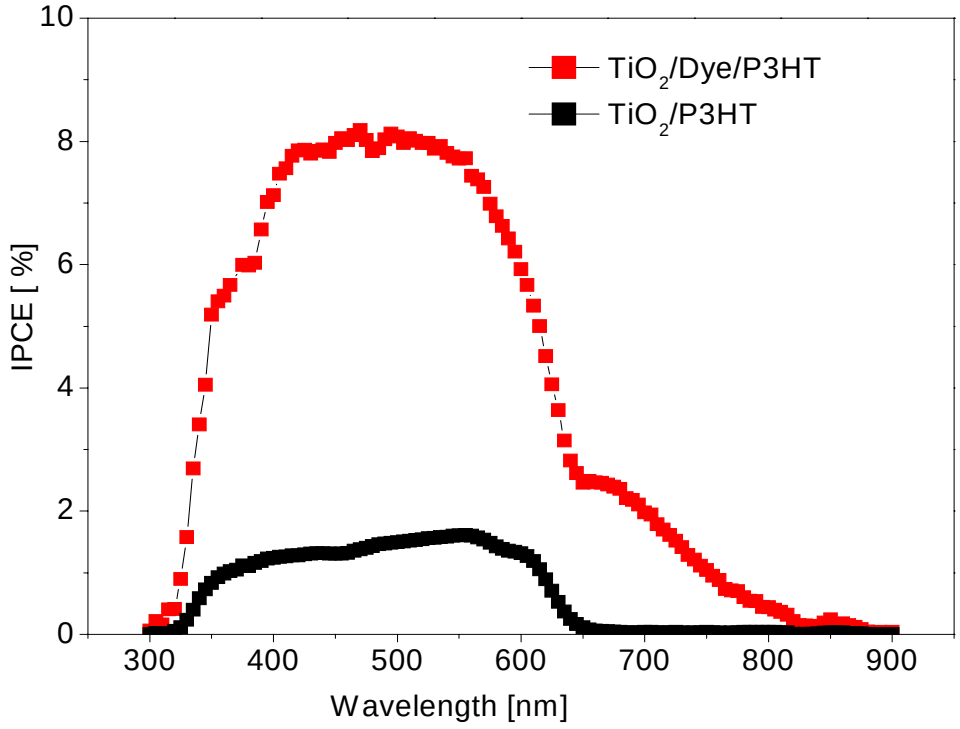

Figure 3.8 IPCE spectra of the investigated solid state hybrid solar cells

3.1.6 Conclusions

The influence of a compact TiO_2 layer on the photovoltaic performance of these solid state dye sensitized solar cells was investigated.

The compact TiO_2 layer between the transparent ITO electrode and the nanocrystalline TiO_2 layer increased the current by an order of magnitude. Further improvement was achieved by introducing a dye interlayer between nanoporous TiO_2 and P3HT. The results were comparatively higher than reported in the literature[11,12,13,14] on solid state devices using polythiophenes.

The information obtained from this section such as the importance of a compact TiO_2 layer and appropriate film coating technique helped for the development of the devices described in the following section.

3.2 Results on Hybrid Solar Cells Using HgTe Nanocrystals and Nanoporous TiO2 Electrodes: Solid State Quantum Dot Sensitized Solar Cells

In chapter 1, it was explained that nanocrystal sensitized solar cells can be prepared by replacing the dye with inorganic nanoparticles or quantum dots. The use of inorganic nanocrystals instead of organic dyes implies several advantages such as the bandgap tunability [15]. As a result of strong quantum confinement in nanocrystals they exhibit photoluminescence with high quantum efficiencies, and the emission peak as well as the absorption onset are strongly size-tunable [111] Therefore, nanocrystals have been used to improve the performance of organic light emitting diodes, [112,113] to obtain single photon sources operating at room temperature [114], and for the development of optically pumped laser devices [115,116,117]. In addition to applications in light emitters, semiconductor nanocrystals have been used in hybrid solar cells [4,8,86,91].

In this section solar cells were fabricated both using HgTe nanocrystals deposited on nanoporous TiO_2 electrodes as well as blending them into a hole transporting polymer. Thus, the solid state nanocrystal sensitized solar cell concept and the polymer/nanocrystal blended solar cell concept were combined, a combination which was never demonstrated before. The combination of these two solar cell concepts results in: (a) a higher photovoltaic response than the use of each concept individually with the same polymers and the same nanocrystals and (b) a shift of the photovoltaic response to longer wavelengths. The fabrication of such solar cells requires two types of nanocrystals, one must be miscible with the polymer and thus has to be soluble in organic solvents (referred hereafter as type OS). The second type, which is deposited on the TiO_2 electrode should not be miscible with the polymer to avoid redissolving during deposition of the polymer/nanocrystal blend on the nanocrystal sensitized electrode. Thus for the second type aqueous soluble nanocrystals (hereafter referred as type AS) were used. For both types colloidal HgTe nanocrystals were used, however stabilized by different organic ligands on their surface. While bulk HgTe is a zero-gap semiconductor, the band gap of chemically synthesized nanocrystals from this material offers a broad tunable bandgap range depending on the particle size [118]. Due to absorption related with this small band gap, HgTe nanocrystals offer the advantage that a larger portion of the solar spectrum can be used for photovoltaics compared with the nanocrystals usually used in hybrid solar cells. One

exception is a recent work, where PbS nanocrystals were used to extend the spectral response of a hybrid solar cell up to a wavelength of 1600 nm [96]. In comparison to the PbS based bulk heterojunction solar cells, however, the devices in this study show a significant higher photovoltaic response.

3.2.1 Morphology

The device presented here as a combination of a nanocrystal/polymer blended solar cell and a solid state nanocrystal sensitized solar cell concepts, denoted as "Device ASOS", contain both types of nanocrystals, HgTe-AS and HgTe-OS. "ASOS" refers to the usage of both, aqueous soluble HgTe-AS nanocrystals coated onto nanoporous TiO_2 (NP-TiO_2) electrode and organic solvent soluble HgTe-OS in poly(3-hexylthiophene) (P3HT) matrix as shown in Fig. 3.9 [119]. The semiconductor electrodes, denoted as NP-TiO_2 electrodes, are a combination of a thin compact TiO_2 film prepared as described in the reference [105] and a nanoporous TiO_2 layer with a thickness of 800 nm. To study the photovoltaic response of the ASOS devices systematically, various reference cells were prepared for comparison. "Reference AS" is identical to ASOS device but only with HgTe-AS nanocrystals on NP-TiO_2 electrode but without HgTe-OS in P3HT. "Reference OS" is with HgTe-OS nanocrystals in the polymer layer (nanocrystal/polymer blend) but without HgTe-AS nanocrystals on the NP-TiO_2 surface and the "Reference-NO" solar cell was prepared without any nanocrystals.

The size distribution of the HgTe nanocrystals was 3 to 6 nm, as determined from section analysis of atomic force microscopy measurements, performed on nanocrystals films on glass substrates, which is in good agreement with the results of transmission electron microscopy for HgTe nanocrystals emitting in the same wavelength region used in this work [106].

By analyzing the SEM cross sections, the thicknesses of the individual layers were controlled and the penetration of the polymer/nanocrystals into the underlying porous layers was studied, as exemplified in Fig. 3.9 [119] (a) for the ASOS device. As shown, the drop casting of the polymer results in a film thickness of approximately 300 nm. The polymer/TiO_2 interface is strongly corrugated, whereby near their interface all holes in the NP-TiO_2 layer are completely filled by the nanocrystal/polymer blend. The covering of the NP-TiO_2 surface with HgTe-AS is shown in more detail by the plan views in Fig 3.10 [119]. Fig. 3.10(a) [119] shows that the bare NP-TiO_2 electrode has two kinds of pores: Pores with lateral dimension in the order of 100 nm and much smaller pores between the TiO_2 grains which are smaller than the grain size of 50 nm. After immersion in the aqueous HgTe-AS solution for 12 hours, at

least the smaller pores at the interface are completely filled with nanocrystals (see Fig. 3.10(b)) [119].

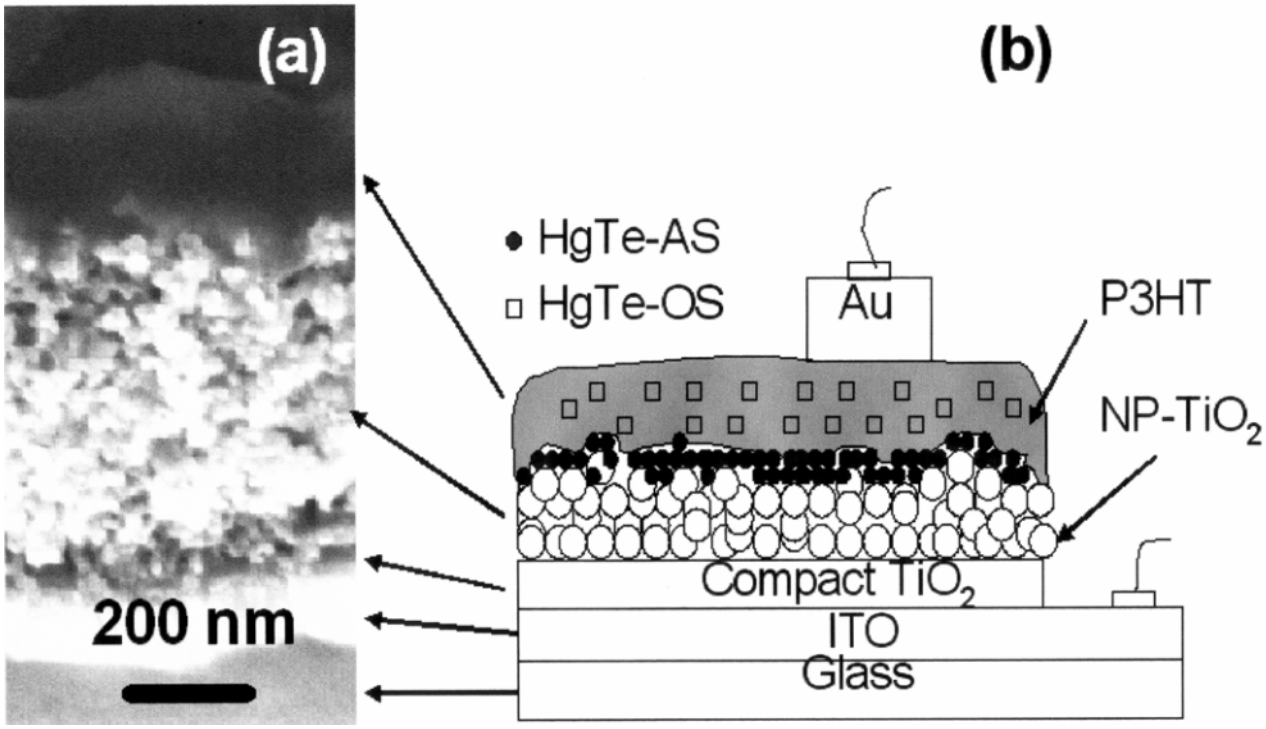

Figure 3.9 (a) Cross section SEM image (b) sketch of sample ASOS, the combination of a solid-state nanocrystal sensitized solar cell and a nanocrystal/polymer blended solar cell concepts

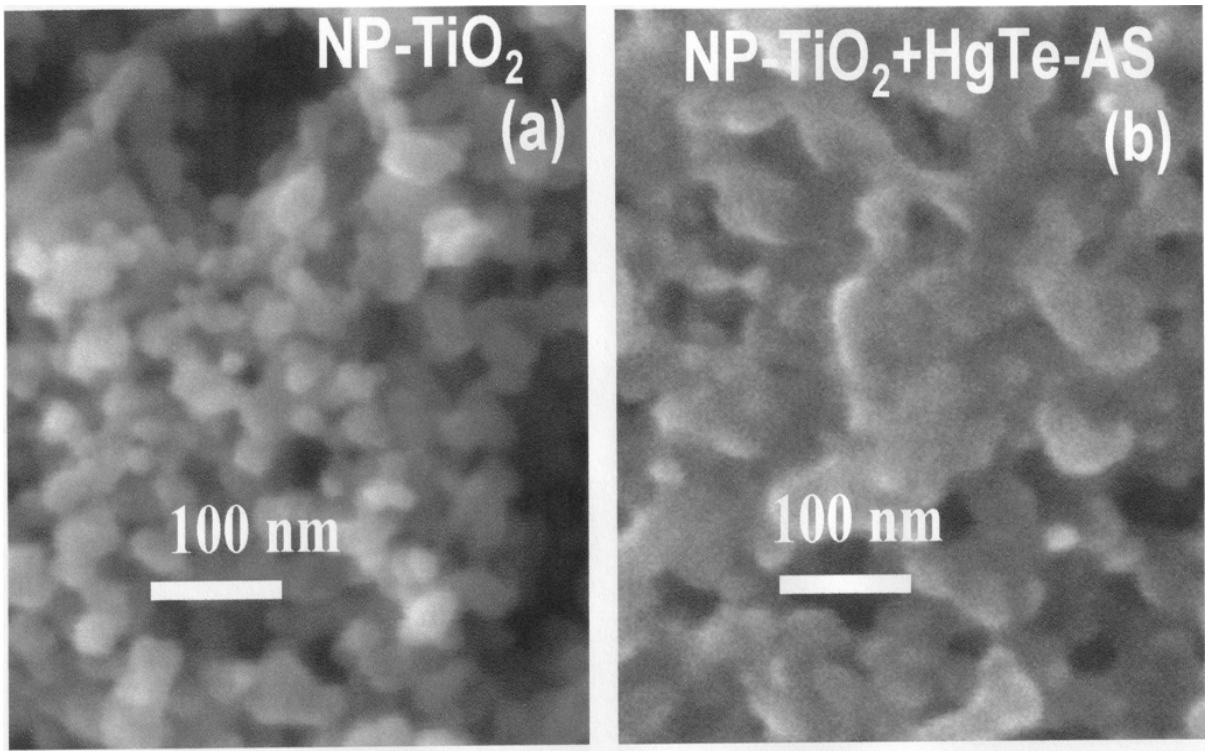

Figure 3.10 Plan views of (a) a bare NP-TiO_2 electrode and (b) of a NP- TiO_2 electrode treated with an aqueous solution of HgTe (AS) nanocrystals

3.2.2 Photovoltaic Response

The photovoltaic properties of the solar cells were characterized by measuring current–voltage (I-V) curves in the dark and under white light illumination (simulated AM 1.5, 100 mW/cm^2) through the ITO side. Without illumination all devices show diode like I-V curves as shown in Figs. 3.11, 3.12, 3.13 and 3.14 (a) and (b) [119] in linear and semilogarithmic scales, respectively. The reference NO cell without HgTe nanocrystals exhibits V_{oc}= 500 mV and a I_{sc}=0.4 mA/cm^2 (fill factor of 0.5). As a remarkable result, it was found that the incorporation of the HgTe nanocrystals improves the rectification of the diodes, since under reverse bias, the dark currents of device ASOS, and the reference cells AS and OS are much smaller than that of the reference without nanocrystals. Under illumination and reverse bias, the current is increased by several orders of magnitude. The characteristic parameters of the solar cells are deduced from the I-V curves on linear scales, as shown in Figs. 3.11, 3.12, 3.13 and 3.14. For device ASOS an open circuit voltage (V_{oc}) of 400 mV, a short circuit current density (I_{sc}) of around 2 mA/cm^2 and a fill factor of 0.5 were achieved. The power conversion efficiency was calculated to be 0.4 % under simulated AM 1.5 illumination. Device ASOS also gave a better photovoltaic performance than references AS and OS with nanocrystals on NP-TiO_2 surface or in the polymer only, respectively. For reference AS V_{oc}= 350 mV, I_{sc}=

0.8 mA/cm^2 and a fill factor of 0.4 were achieved whereas for reference OS V_{oc}= 400 mV, I_{sc}= 1.4 mA/cm^2 and a fill factor of 0.36 were obtained. The results show that the photovoltaic performance increase related with the incorporation of HgTe nanocystals is mainly due to the increase of the short circuit current.

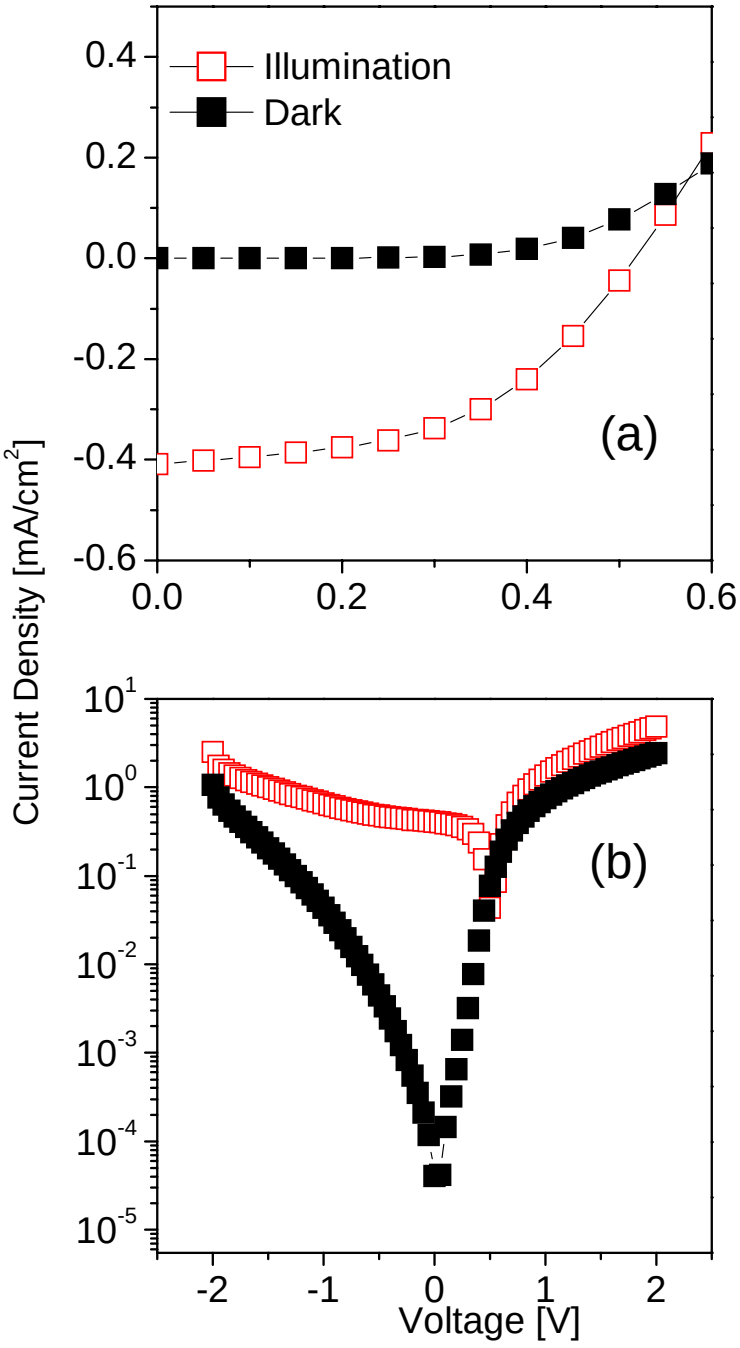

Figure 3.11 I-V characteristics of the reference NO cell without any HgTe nanocrystals (a) linear (b) semilogarithmic scale

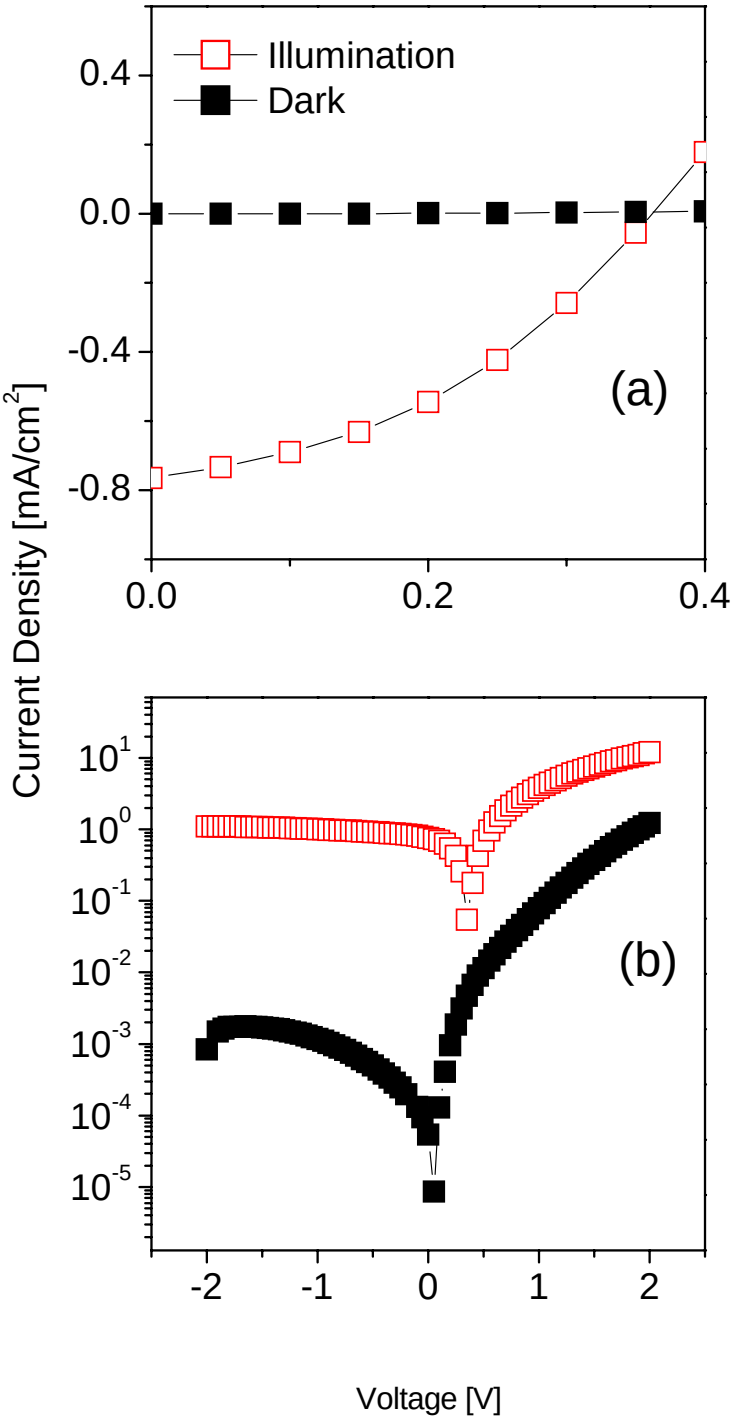

Figure 3.12 I-V characteristics of the reference AS cell with nanocrystals at NP-TiO_2 surface (a) linear (b) semilogarithmic scale

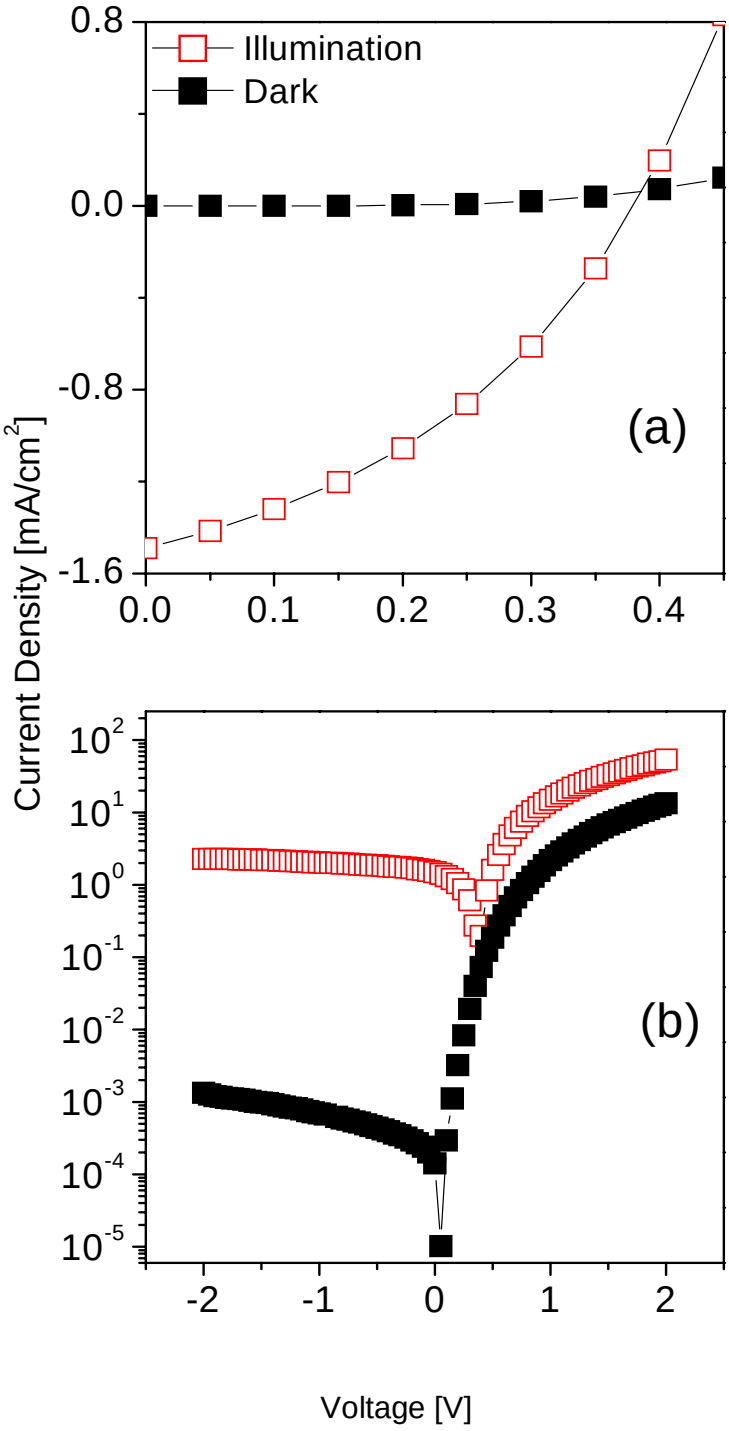

Figure 3.13 I-V characteristics of reference OS cell with nanocrystals embedded in the polymer (a) linear (b) semilogarithmic scale

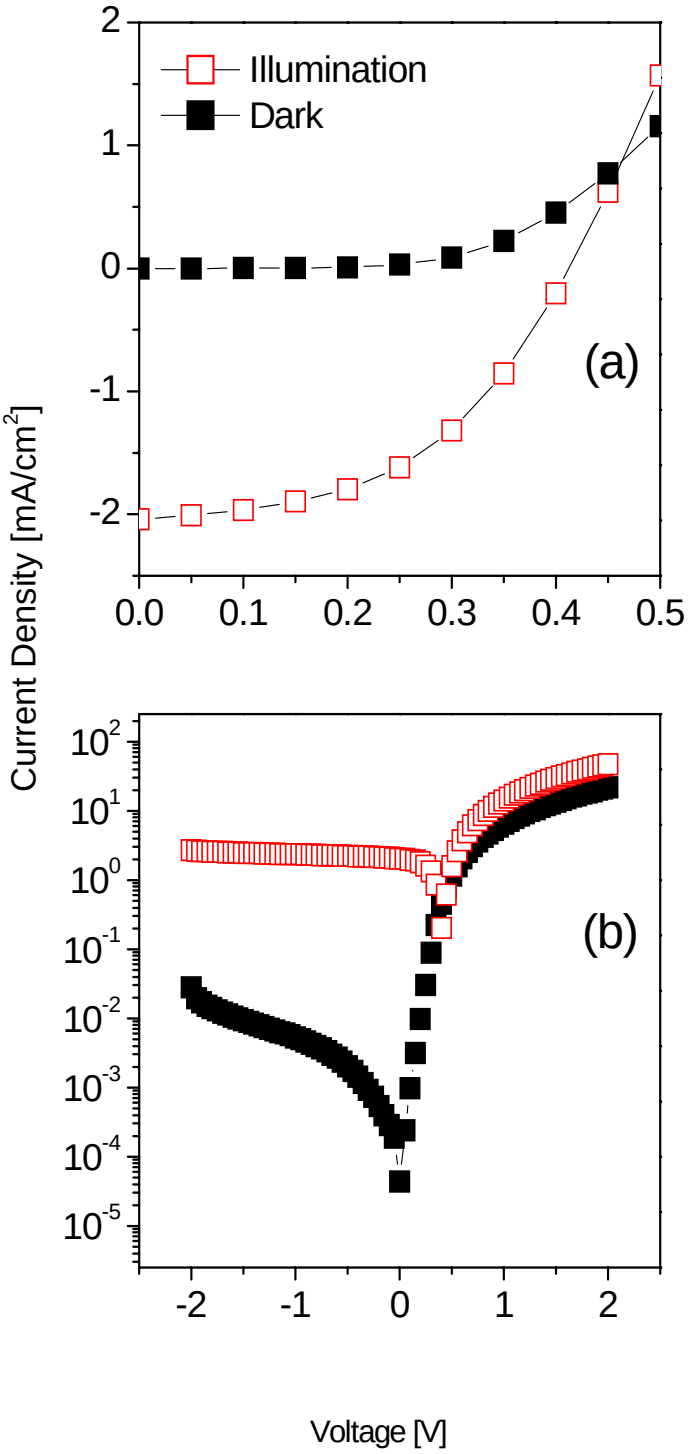

Figure 3.14 I-V characteristics of device ASOS where nanocrystal sensitized and nanocrystal/polymer blended concepts are combined (a) linear (b) semilogarithmic scale

3.2.3 Absorption Characteristics

The glass substrates, the ITO contact layer as well as the nanoporous TiO_2 were found to be sufficiently transparent in the whole spectral operation range of our devices, from 370 nm to 1500 nm. P3HT shows a broad absorption peak with a maximum at 553 nm and is almost transparent for wavelengths longer than 670 nm, as shown in Figs. 3.15 (a) and (b) [119]. The HgTe nanocrystals show a weak absorption peak at long wavelength close to 1400 nm, as measured for HgTe-OS nanocrystals (Fig. 3.15 (b)). This absorption corresponds to the fundamental optical transition across the band gap of the nanocrystals with sizes in the range of 3-6 nm. At shorter wavelengths absorption is observed due to transitions into excited nanocrystal states.

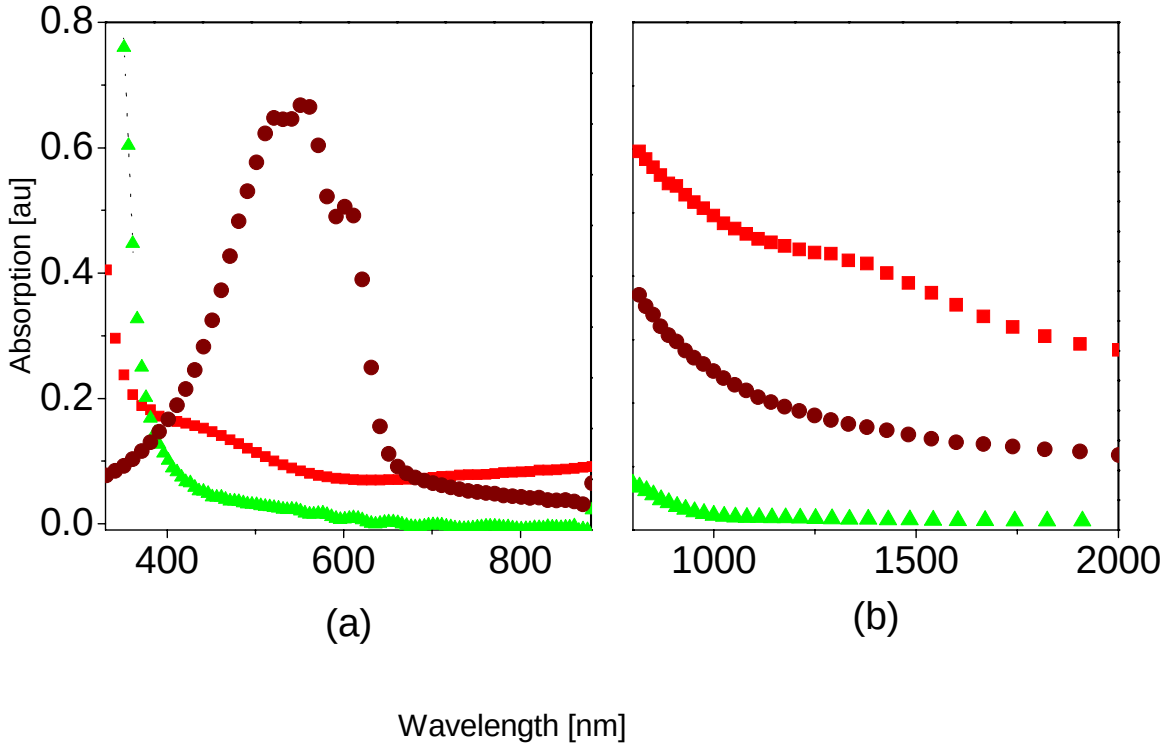

Figure 3.15 Absorption spectra of TiO_2 (▲), HgTe-OS(■) and P3HT(●). The different wavelength regions shown in (a) and (b) are measured by using different experimental setups.

3.2.4 Incident Photon to Current Efficiencies (IPCE)

The photoresponse of the reference devices NO, AS, OS and ASOS device is compared by their spectral dependence of the incident photon to current efficiency (IPCE) in Fig. 3.16 [119]. The reference sample without nanocrystals (reference NO) shows a photoresponse only at wavelengths shorter than 650 nm and with a maximum IPCE of 1.6 %. Incorporating the nanocrystals in the P3HT (reference-OS) increases the photoresponse in the visible spectral range and sensitizes the spectral region at wavelengths longer than 650 nm. By the additional nanocrystals at the NP-TiO_2/P3HT interface (device ASOS) the photoresponse is further increased, resulting in a maximum IPCE of 10 %, at wavelengths around 550 nm. For reference AS the maximum response is 2.5%. For the response of the solar cells at wavelengths shorter than 670 nm the broad IPCE feature with a maximum around 550 nm is related with both, the P3HT absorption (see figure 3.15(a)) and the additional absorption offered by the HgTe nanocrystals due to transitions into nanocrystal excited states, which improves the IPCE. For the HgTe containing devices, the photoresponse is extended to wavelengths in the infrared up to 1500 nm. The response of the cells at these long wavelengths is attributed to the HgTe nanocrystals only, since the reference NO cell with no nanocrystals does not show any response at wavelengths longer than 670 nm (see fig. 3.16) [119]. The onset of the IPCE curve around 1500 nm corresponds to the band gap of the HgTe nanocrystals. The results show, that the HgTe nanocrystals are optically active both in the P3HT layer (type OS) as well as at the NP-TiO_2/P3HT interface (type AS).

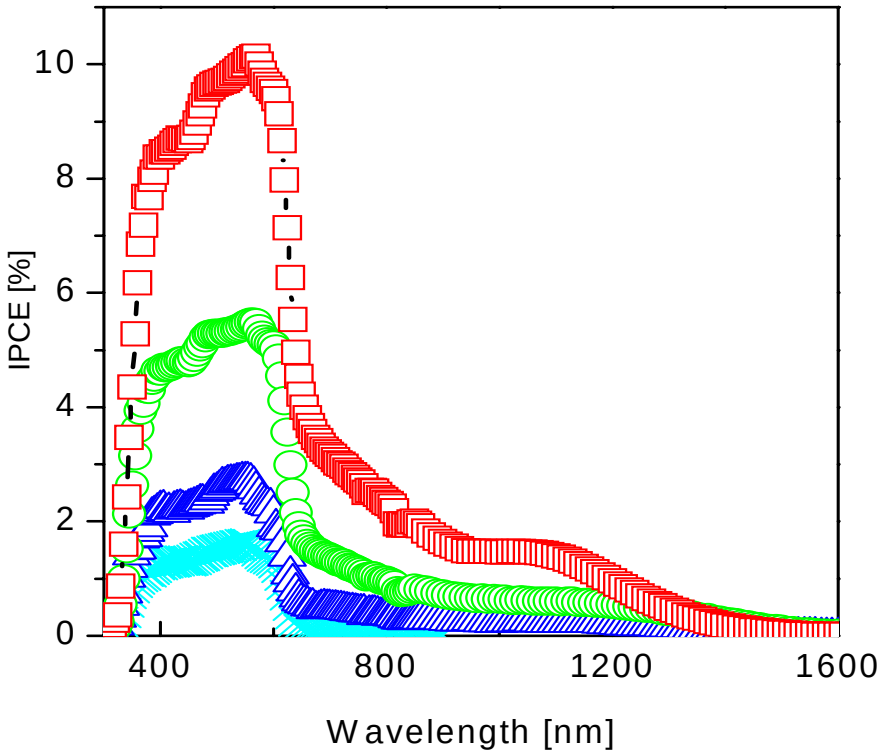

Figure 3.16 Incident photon to current efficiency (IPCE) of devices ASOS(□), references OS(○), AS (Δ) and of the reference NO(X).

For an efficient charge transfer the lowest unoccupied molecular orbital (LUMO) of the electron donor should be energetically above the conduction band of TiO_2 as electron acceptor. It is difficult to determine the energy levels of HgTe nanoparticles. The electroctrochemical methods lead to incorrect and tedious results in this case. Therefore, the exact energetic mechanism for the obtained improvement of charge generation by adding nanocrystals is still under discussion. However, some additional effects should be taken into account for improving the efficiency: In the spectral range where P3HT absorbs there is an additional absorption offered by HgTe nanocrystals which contribute to the charge carrier generation. Also the extension of the spectral range of the devices in the infrared arises due to the absorption offered by HgTe, since the devices with no nanocrystals don`t show any response in the infrared. In addition, HgTe-AS nanocrystals may help to reduce the interfacial charge carrier recombination at the NP-TiO_2 interface making the combination of both solar

cell concepts more efficient than the individual concepts with a power conversion efficiency of 0.4% under simulated AM 1.5 conditions

3.2.5 Conclusion

A novel concept for nanocrystal based hybrid solar cell, where HgTe nanocrystals were used to improve the photovoltaic performance of the cells as well as to extend the spectral region of operation up to 1500 nm. HgTe nanocrystals offer the possibility to push the wavelength operation limit of hybrid solar cells to even longer wavelengths, which are not accessible by conventional dyes or most conjugated polymers, making such hybrid devices interesting not only for solar cells but also for infrared sensitive hybrid photodetectors.

3.3 Results on Nanoporous $CuInS_2$ Electrodes For Hybrid Solar Cells

The concept of solid state dye sensitized solar cell using TiO_2 electrodes was described in chapter 1. TiO_2 is one of the most common n-type semiconductors which is used as an electron transporting layer in these kinds of devices. TiO_2 absorbs in the UV region with a maximum around 370 nm. Therefore, a dye is required to sensitize these electrodes. This was also explained previously. The surface modification of TiO_2 with inorganic nanoparticles [15,89] or replacement of TiO_2 electrodes with Nb_2O_5 or ZnO electrodes have already been demonstrated. However, devices made from nanoporous electrodes prepared from size quantized nanoparticles haven`t been demonstrated before. In this section, solar cells consisting of nanoporous electrodes prepared by using size quantized nanoparticles are demonstrated. Solar cells were fabricated using $CuInS_2$ nanoparticles which were prepared by a colloidal synthesis route. A hybrid solar cell consisting of $CuInS_2$ as a p-type nanostructured electrode was fabricated [120]. Bilayers of nanoporous $CuInS_2$ and PCBM 1-(3-methoxycarbonyl)-propyl-1-1-phenyl-[6,6]-C_{61} with or without using a dye complex of $RuL_2(NCS)/TBA(2:2)$ (where L= 2,2′-bipyridyl-4,4′-dicarboxylic acid; TBA= tetrabutylammonium) were realized and investigated (see figure 3.16).

3.3.1 Morphology of $CuInS_2$ Electrodes

The morphology of the $CuInS_2$ layers after treatment is shown in figure 3.17. The surface of $CuInS_2$ layer is porous with a maximum roughness of 300 nm. Formation of $CuInS_2$ aggregates in layers might be explained by the replacement of the highly viscose surfactant TPP with a boiling point above 360°C by the organic solvent pyridine with a lower boiling point of 115°. Surface modification of $CuInS_2$ nanoparticles might lead to a preferred aggregation after drying the layers with a broad absorbance range in the visible range comparable to the absorbance of macroscopic $CuInS_2$.

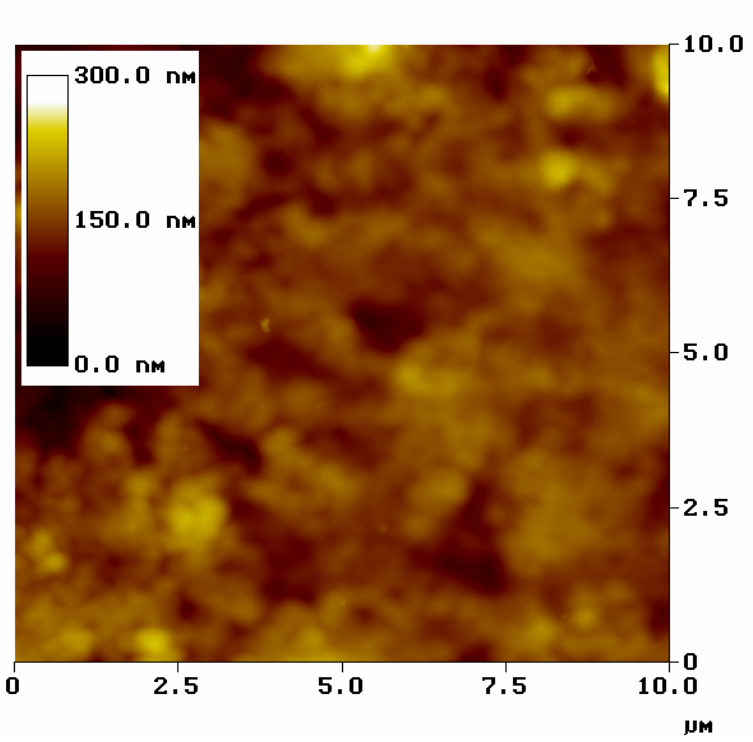

Figure 3.17 AFM image of nanoporous $CuInS_2$ Electrodes

3.3.2 Photovoltaic Characterization

The photovoltaic properties of the solar cells were characterized by measuring current–voltage (I-V) curves in dark and under white light illumination (AM1.5, 100 mW/cm^2) conditions. Typically, $CuInS_2$/PCBM bilayer devices in dark show diode like I-V curves with a rectification ratio (RR=+/- 2V) 5 (bottom curve semilogarithmic plot in Fig. 3.18 [120], upper curve linear plot). Under illumination, the $CuInS_2$ cells produced an open circuit voltage (V_{oc}) of 0.25 V and a short circuit current (I_{sc}) of 0.2 mA/cm^2 with a fill factor of 0.3.

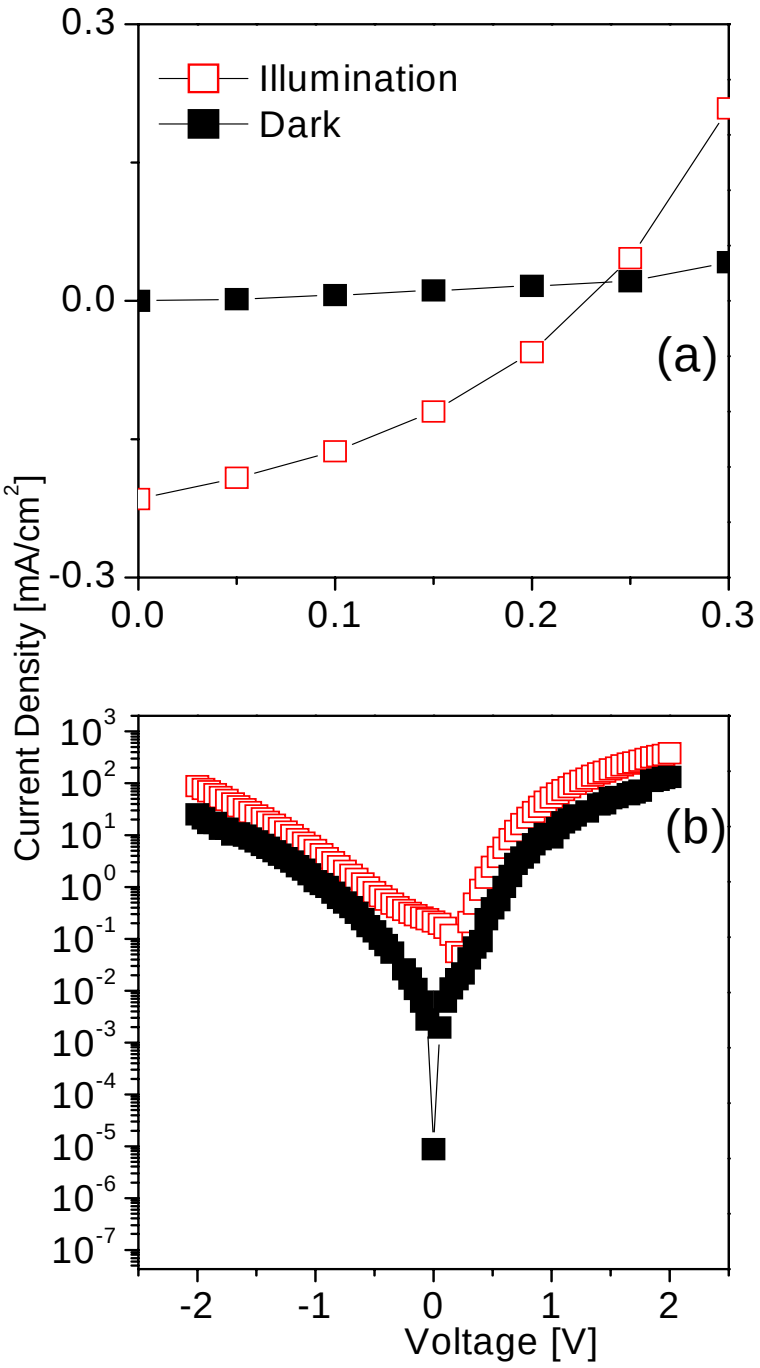

Figure 3.18 I-V characteristics of ITO/$CuInS_2$/PCBM/LiF/Al solar cells (a) linear (b) semilogarithmic scale

Next, a thin dye interlayer between $CuInS_2$ and PCBM layers was inserted to increase the light absorbance within the cell. For these devices, we achieved typically a V_{oc} of 0.5 V and an I_{sc} of 0.6 mA/cm^2 with a fill factor of 0.5 (see Fig. 3.19) [120].

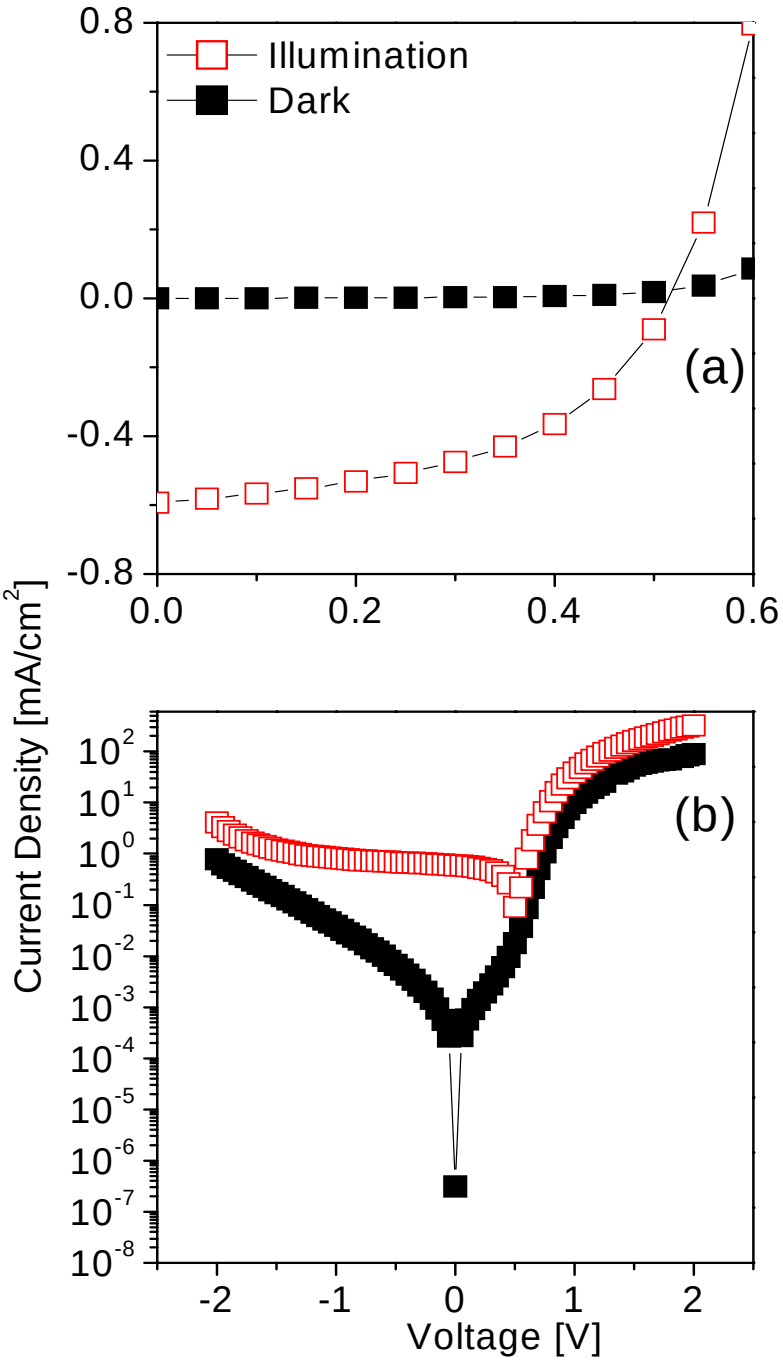

Figure 3.19 I-V characteristics of ITO/$CuInS_2$/Ru-Dye/PCBM/LiF/Al solar cells (a) linear (b) semilogarithmic scale

3.3.3 Absorption Characteristics

The absorption spectra of the individual components of the fabricated solar cells are shown in figure 3.20 [120].

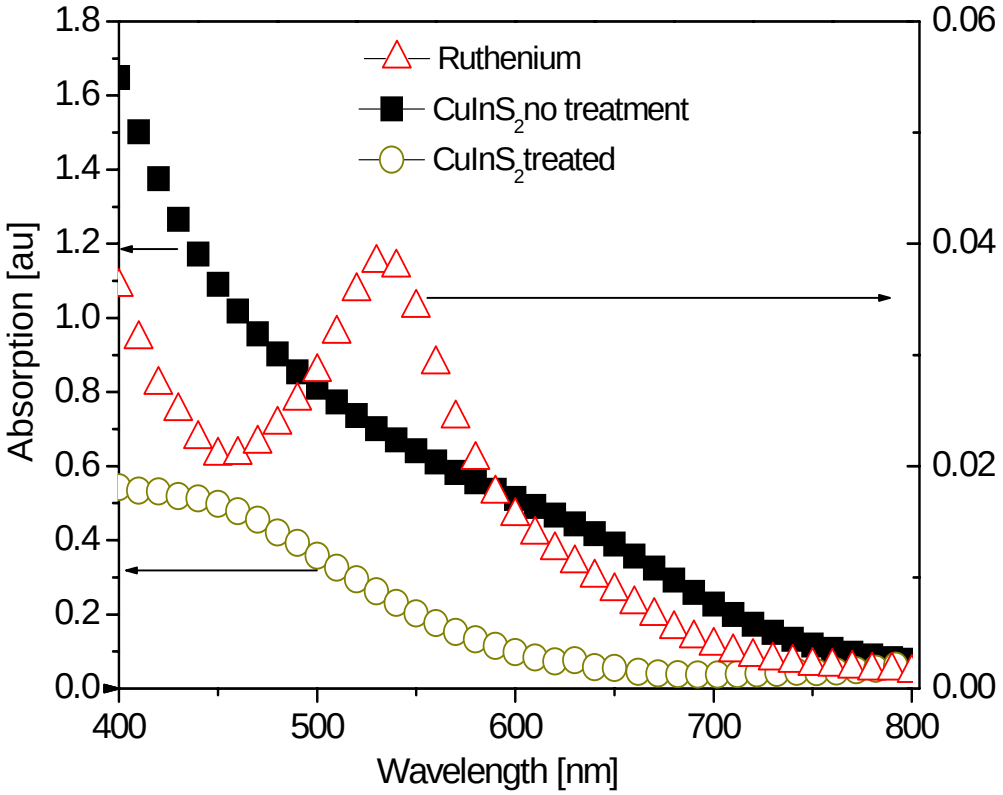

Figure 3.20 Absorption characteristics of individual components employed in the solar cell configurations

Because of the weak interactions between TPP and inorganic surface, TPP is expected to exchange by pyridine as described in the experimental part. On the other hand, the aggregation of $CuInS_2$ nanoparticles to bigger aggregates can not also be avoided during this surface modification. After treatment of the particles with methanol and pyridine, the bigger aggregates were precipitated as a powder and removed from the dispersion by filtering. For the $CuInS_2$ nanoparticles, an absorption edge starting at 580 nm was measured. The Ru- dye has a broad absorbance peak with a maximum at 550 nm.

3.3.4 Incident Photon to Current Efficiency(IPCE)

The photo responses of the devices with and without dye complex were shown by the spectral dependence of the incident photon to current efficiency (IPCE) curves in figure 3.21 [120]. A broad photo response for $CuInS_2$/PCBM bilayers was observed, which is in agreement with the absorbance behaviour of $CuInS_2$ nanoparticles. Inserting a thin layer of the Ru-dye, the overall IPCE values increase by a factor of 2.5. Additionally, a maximum at around 500 nm occurs, indicating the superposition of the photo currents from the Ru-dye as well as from the $CuInS_2$ electrode.

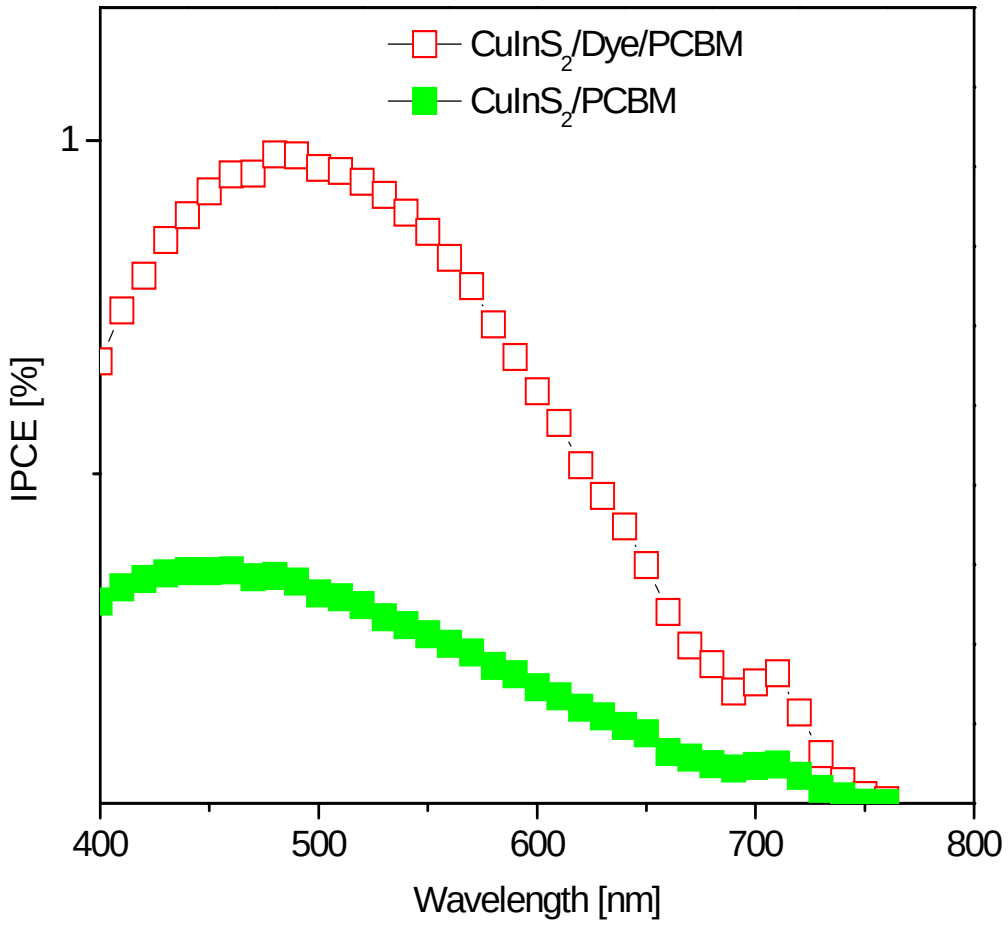

Figure 3.21 Incident photon to current efficiency (IPCE) of the solar cells ITO/$CuInS_2$/PCBM/LiF/Al and ITO/$CuInS_2$/Ru-Dye/PCBM/LiF/Al

Because of the general increase of the IPCE values of the cells having a dye interlayer, the changes can not be attributed only to the additional dye absorption. By considering the electrically insulating dye as a buffer layer, decreasing the probability of recombination losses at the $CuInS_2$/ PCBM interface [51] may be the reason for the better device performance.

3.3.5 Conclusion

A solid state hybrid solar cell with a thin Ru-dye layer inserted between a p-type semiconducting $CuInS_2$ as an absorbing nanoporous electrode and a PCBM as an electron accepting and transport layer. This configuration offers new possibilities in the further development of solid state hybrid solar cells. From a technological point of view the low temperature sintering is advantageous since flexible plastic foils can be used instead of glass as a substrate. All active components in this new solar cell configuration are solution processable, therefore allowing a large-area fabrication. A potential advantage of $CuInS_2$ as photo active electrode might be the construction of thinner devices compared to the TiO_x-based dye sensitized solar cells. Further improvement is also desirable by replacing the $CuInS_2$ to lower band gap semiconductors such as $CuInSe_2$ or InAs for a better light harvesting.

3.4 Results on Solution Processable Bilayer Heterojunction Hybrid Solar Cells Using PbS Nanoparticles

Preparation of bilayer heterojunction solar cells is simple as compared with the bulk heterojunction solar cells. In bulk heterojunction solar cells there are several parameters such as miscibility of the two materials in the blend, solvent etc. which are difficult to control. In bilayer heterojunction solar cells, two or more layers of different materials are sequentially cast over another.

In section 3.4 a method for preparing solution processed bilayer heterojunction solar cells has been realized and the effect of temperature annealing on the morphology and photovoltaic performance of the hybrid devices have been investigated.

3.4.1 Morphology of PbS Films

The morphology of PbS films was characterized by atomic force microscopy (AFM). Figure 3.22 (a) and (b) show the AFM image of PbS films prepared without mixing with ethylacetate before and after annealing, respectively. The PbS nanoparticles seem to form agglomerates before annealing. After annealing the surface of PbS films is smoothened. However, the resulting films were soluble. Since in bilayer heterojunction configuration, the layers are sequentially cast, it is important that the over layer shouldn`t dissolve the under layer.

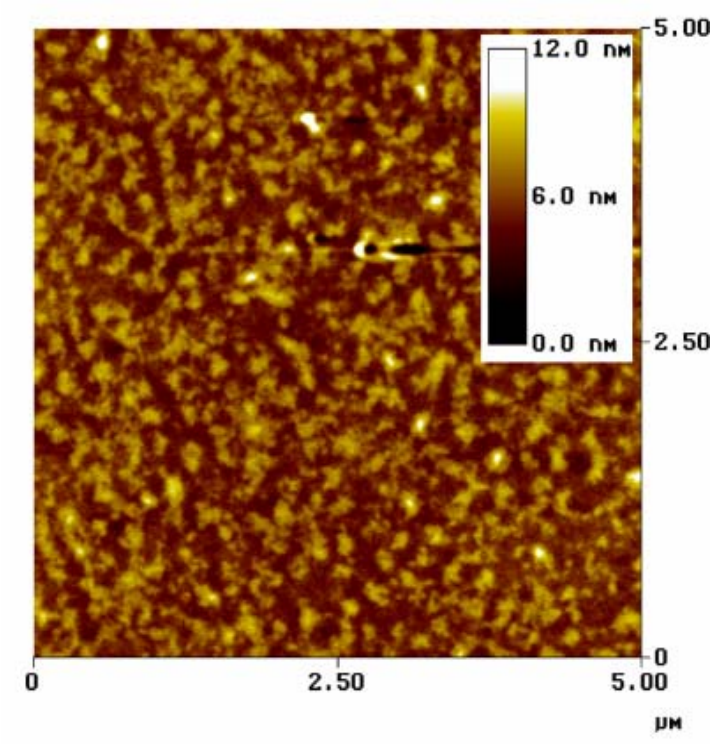

(a)

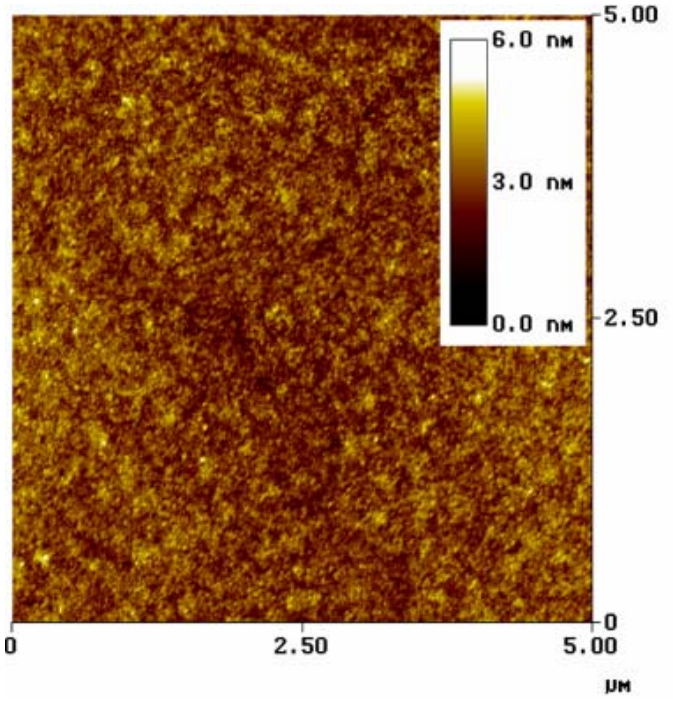

Figure 3.22 AFM image of PbS film (a) before (b) after annealing

It was realized that addition of ethylacetate into the PbS solution led to insoluble PbS films. The effect of this mixing on the morphology is shown in figure 3.23 (a) and (b) before and after annealing, respectively. In both cases, the PbS films have smooth surfaces. However,

after annealing the films seem to have a compact structure with no pores and also becomes insoluble.

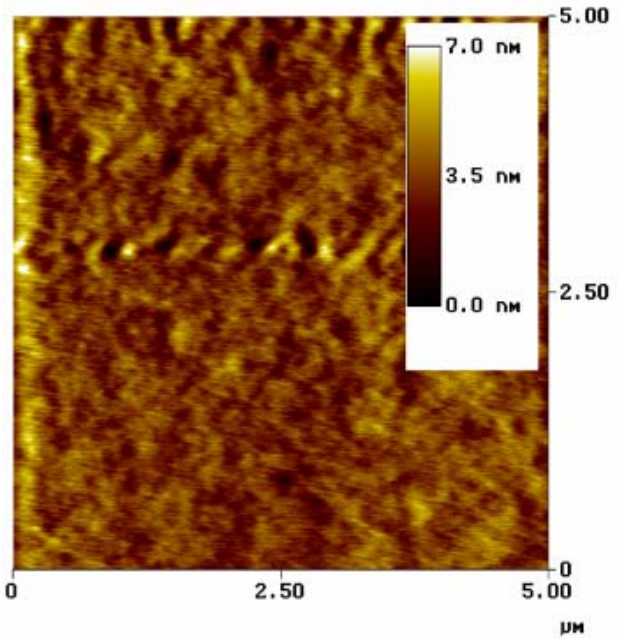

(a)

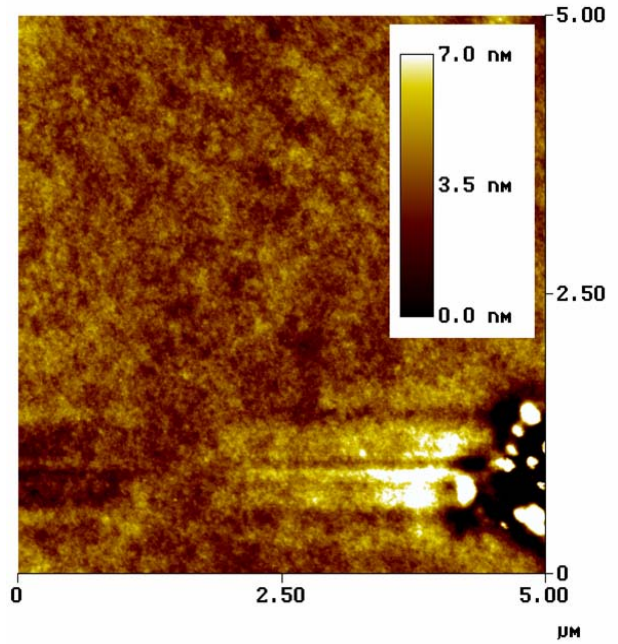

(b)

Figure 3.23 AFM image of PbS film prepared after mixing the nanoparticles with ethylacetate (a) before and (b) after annealing

3.4.2 Current-Voltage Characterization

The photovoltaic properties of the solar cells were characterized by measuring current–voltage (I-V) curves in the dark and under white light illumination (simulated AM 1.5, 100 mW/cm^2) through the ITO side. Without illumination the device shows diode like I-V curves as shown in figure 3.24. Under illumination and reverse bias, the current is increased by several orders of magnitude, proving a high photo-sensitivity of the solar cells. The characteristic parameters of the solar cells are deduced from the I-V curves on linear scales. This device exhibited an I_{sc} of 0.3 mA/cm^2 and a V_{oc} of 350 mV with a fill factor of 0.35.

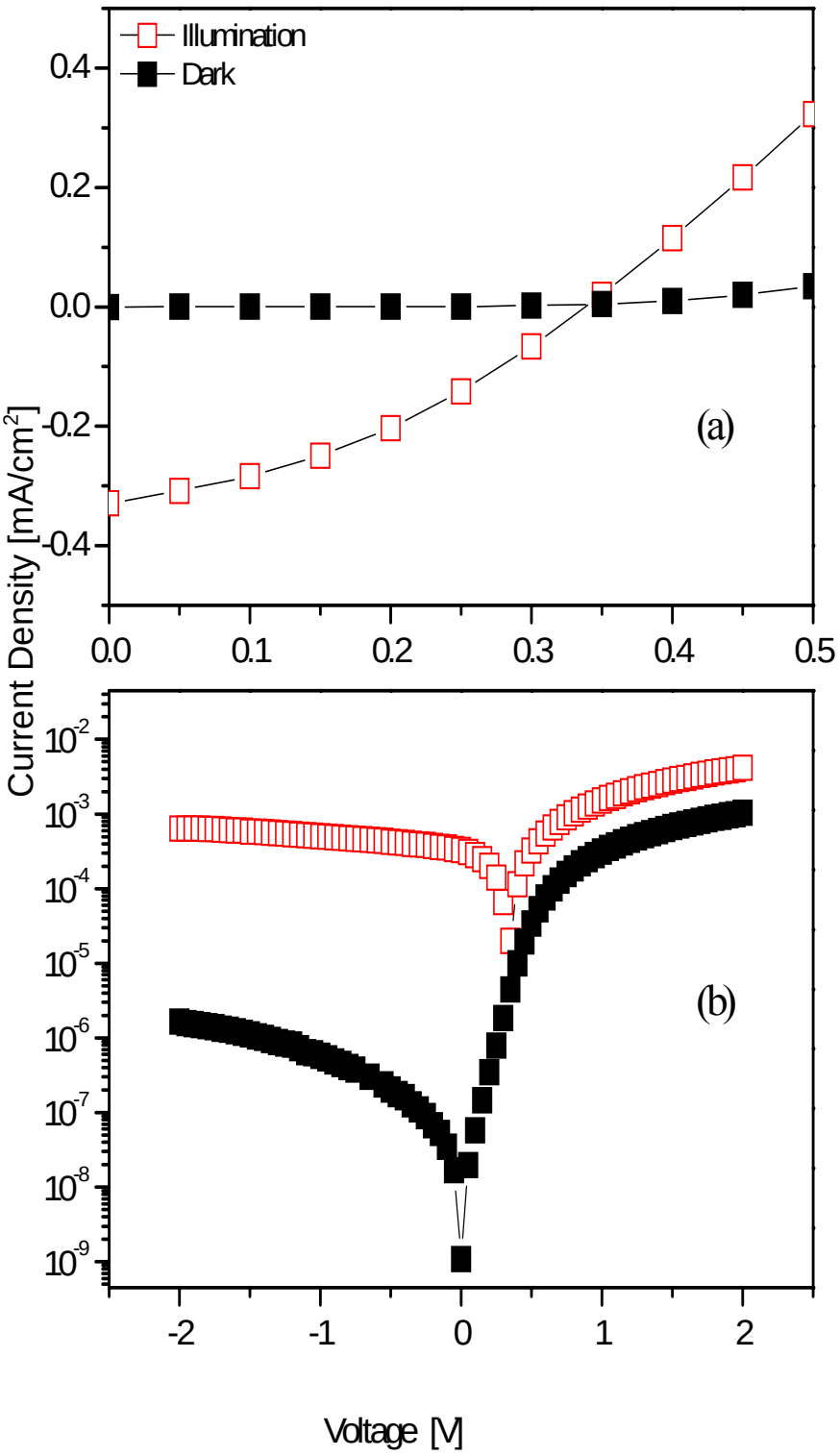

Figure 3.24 I-V characteristics of ITO/PbS/P3HT/Au hybrid device

3.4.3 Absorption Characteristics and Incident Photon to Current Efficiency(IPCE)

Figure 3.25 shows the comparison of spectral response of the hybrid device with the absorption spectra. As can be seen from the figure both PbS and P3HT contribute to the charge carrier generation. The response at wavelengths longer than 650 nm is attributed to the PbS absorption.

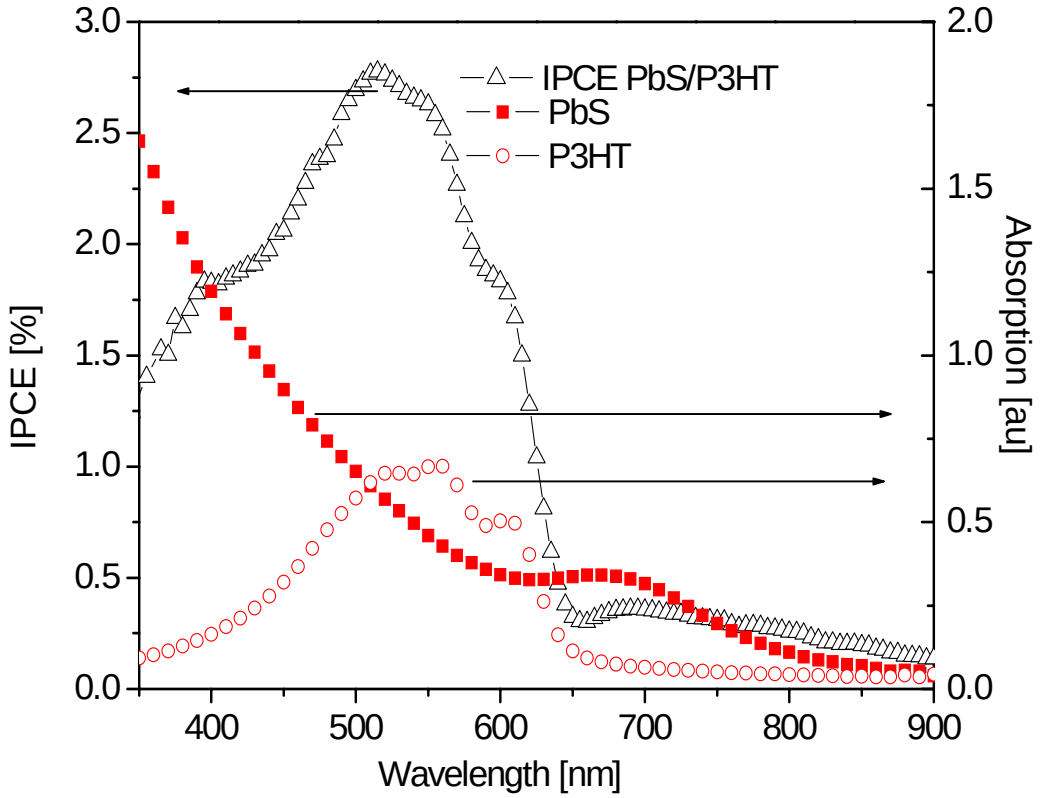

Figure 3.25 Comparison of IPCE with the absorption spectra of individual components

3.4.4 Conclusions

Solution processed bilayer heterojunction hybrid solar cells using PbS nanoparticles and P3HT have been realized. PbS was used as an electron transporting layer and P3HT was used as organic hole transporting material. Here, a mechanism for photovoltaic conversion based on donor-acceptor charge transfer is proposed. Photoexcitations at the PbS/P3HT junction experience an energetic driving force for the charge transfer, with holes in the P3HT and electrons in PbS. After absorption and charge transfer, majority holes in the P3HT are

transported to the gold and likewise, electrons can be transported to the ITO. The difference of electrode`s work functions form a field across the active materials and provides driving force for carrier extraction. Devices consisting of PbS-only and P3HT-only devices were also fabricated. The comparison of the device performances shows a significant enhancement in the creation and extraction of carriers due to the presence of a charge transfer interface within the device. Cells with only PbS or only P3HT layers showed no significant rectification. The observed photovoltaic effect in the bilayer is not a result of Schottky contacts but rather is due to the intended heterojunction.

4. Summary and Outlook

4.1 Summary

In this thesis, four types of solid state hybrid solar cells were fabricated and characterized. Initially, solid state hybrid solar cells using TiO_2 electrodes as electron transporting layer and P3HT as a hole transporter were investigated. Devices with and without using compact TiO_2 layers. Devices without compact TiO_2 layers produced an I_{sc} of 0.06 mA/cm^2 and a V_{oc} of 300 mV and a fill factor of 0.43. Solid state devices employing a compact TiO_2 layer exhibited an I_{sc} of 0.4 mA/cm^2 and a V_{oc} of 500 mV with a fill factor of 0.5. The further improvement was achieved by introducing a dye interlayer between transparent conducting oxide (ITO) and nanoporous TiO_2 electrodes. The dye interlayer raises the I_{sc} to 2 mA/cm^2 and the V_{oc} to 450 mV with a fill factor of 0.3. The overall efficiency of the devices with a compact TiO_2 layer and a dye interlayer was 0.3 %. Further possible enhancement can be achieved by focusing on efficient pore filling of TiO_2 by P3HT.

Secondly, hybrid solar cells, combining two solar cell concepts, a solid-state nanocrystal-sensitized solar cell and a nanocrystal/polymer blended solar cell concepts are described. HgTe nanocrystals are demonstrated to increase the photon harvesting efficiency of hybrid solar cells over a broad spectral region between 350 nm and 1500 nm. These devices give incident photon to current efficiencies up to 10% at around 550 nm monochromatic irradiation and short circuit current densities of 2 mA/cm^2 under simulated AM 1.5 (100 mW/cm^2) illumination. The improvement of the cell is attributed to the HgTe nanocrystals since in the spectral range where P3HT absorbs there is an additional absorption offered by HgTe nanocrystals which contributes to the charge carrier generation. Also the extension of the spectral range of the devices in the infrared arises due to the absorption offered by HgTe nanocrystals. Such hybrid devices are interesting not only for solar cells but also for infrared sensitive hybrid photodetectors.

Also, hybrid devices using nanoporous $CuInS_2$ electrodes have been demonstrated. A ligand exchange has been performed on $CuInS_2$ nanoparticles. $CuInS_2$/PCBM bilayers were

characterized with and without a dye interlayer. The dye interlayer improved the device performance.

Finally, solution processed bilayer heterojunction hybrid devices were prepared by using PbS nanoparticles and P3HT.

4.2 Outlook

One of the drawback for the technological utilization of the hybrid solar cells is their low efficiency. However, hybrid solar cell research has attracted much attention due to the simple processability and low costs. The development and improvement of the hybrid solar cells gained very much speed, however, their efficiencies are still low compared with the conventional inorganic solar cells. Further optimization is required for different types of devices. For the improvement of solid state dye sensitized solar cells, the following points should be considered:

I Optimization of the TiO_2 nanomorphology by controlling the pore size distribution.

II Optimization of the dyes. The stability of the dye and adsorption of the dye are very important parameters.

III Development of low molecular and low bandgap, high mobility hole transporters.

The development of hybrid solar cells based on inorganic semiconductor nanoparticles depends on the improvement of the nanoparticle synthesis routes. The main problem of the synthesis is the reproducibility problem, that is, the properties of the nanoparticles change from batch to batch. The surfactant which prevents the particles from further growth and also from the oxidation is an insulating layer. Therefore, the surfactant hinders the charge transfer. For the future development of hybrid solar cells nanoparticles should be tailored considering the photovoltaic requirements.

Despite the low efficiencies, the concept of hybrid devices is very interesting and there is no reason not to catch up the efficiencies of organic or inorganic solar cells if the above problems are considered.

Curriculum Vitae

Serap Günes

Personal Details

Name:	Serap Günes
Date of Birth:	26.05.1976
Place of Birth:	Istanbul, Turkey
Nationality:	Turkish
Marital Status:	Married
Personal Address:	Julius Raab Strasse, 5/7, 2318, A-4040, Linz
Cell Phone:	+43 676 697 49 19
Professional Address:	Linz Institute of Organic Solar Cells (LIOS), Johannes Kepler University Linz, www.lios.at
Phone:	+43 732 2468 8767
Email:	serap.guenes@jku.at

Education

September 2002- July 2006:	PhD studies at Linz Institute of Organic Solar Cells(LIOS),Johannes Kepler University Linz PhD topic: NANOSTRUCTURED ELECTRODES FROM INORGANIC MATERIALS FOR HYBRID SOLAR CELLS Supervisor: o.Prof. Dr. Mag. Niyazi Serdar Sariciftci
September 1999-July 2001:	Master Degree in Physics, Yildiz Technical University, Arts and Science Faculty, Physics Department, Istanbul/Turkey Supervisor: Prof. Dr. Savval Mamedov
June 1998:	Bachelor Degree in Physics, Yildiz Technical University, Arts and Science Faculty, Physics Department, Istanbul/Turkey Supervisor: Prof. Dr. Idris Gümüs

Work Experience:

1999- recent	Research assistant at Physics Department, Yildiz Technical University, Science and Art Faculty, Istanbul/Turkey

Awards:

1997-1998	Top student of Physics Department of Yildiz Technical University, Science and Art Faculty, Istanbul/Turkey
1997-1998	Second best student of Faculty of Arts and Science Yildiz Technical University, Istanbul/Turkey
2002-2006	National Scholarship of Council of Higher Education(YÖK) Turkey

Projects Attended:

European FP6 Project "Molecular Orientation, Low Band Gap and New Hybrid Device Concepts for the Improvement of Flexible Organic Cells (Mollycell)"

Skills:
Experience in
Design, fabrication and characterization of organic and hybrid solar cells
Nanoscience and technology (Physical characterization of inorganic semiconductor nanoparticles)
Surface characterization by means of atomic force microscopy (AFM) and scanning near field optical microscopy (SNOM).

Languages:

Turkish: Mother Tongue
English: Fluent
German: Middle level

PUBLICATIONS:

1. S. Günes, H. Neugebauer, N. S. Sariciftci, J. Roither, M. Kovalenko, W. Heiss, *A Novel Concept for Hybrid Solar Cells Using HgTe Nanocrystals and TiO_2 Electrodes,* Advanced Functional Materials, 16, (2006), 1095
2. Th. Singh, S. Günes, N. Marjanovic, N.S. Sariciftci, R. Menon, *Correlation between morphology and ambipolar transport in organic field-effect transistors,* Journal of Applied Physics 97 (2005), 114508-1
3. Th. Singh, N. Marjanovic, P. Stadler, M. Auinger, G. Matt, S. Günes, N.S. Sariciftci, R. Schwoediauer, S. Bauer, *Fabrication and characterization of solution-processed methanofullerene-based organic field-effect transistors*, Journal of Applied Physics 97 (2005), 083714-1
4. Th. Singh, N. Marjanovic, G. Matt, S. Günes, N.S. Sariciftci, A. Montaigne, A. Andreev, H. Sitter, R. Schwoediauer, S. Bauer, *High-mobility n-channel organic field-effect transistors based on epitaxially grown C_{60} films,* Organic Electronics 6 (2005), 105-110
5. Th. Singh, F. Meghdadi, S. Günes, N. Marjanovic, G. Horowitz, P. Lang, S. Bauer, N.S. Sariciftci, *High-Performance ambipolar pentacene organic field-effect transistors on poly(vinylalcohol) organic gate dielectric*, Advanced Materials 17 (2005), 2315
6. L. Campos, A. Tontcheva, S. Günes, G. Sonmez, H. Neugebauer, N.S. Sariciftci, F. Wudl, *Extended Photocurrent Spectrum of a Low Band Gap Polymer in a Bulk Heterojunction Solar Cell,* Chemistry of Materials Vol 17 No. 16 (2005), 4031-4033
7. A. Montaigne Ramil, Th.B. Singh, N.T. Haber, N. Marjanović, S. Günes, A. Andreev, G.J. Matt, R. Resel, H. Sitter and S. Sariciftci, *Influence of film growth conditions on carrier mobility of hot wall epitaxially grown fullerene based transistors***,** Journal of Crystal Growth, accepted January 2006
8. N. Marjanovic, B. Singh, G. Dennler, H. Neugebauer, S. Günes, N. S. Sariciftci, S. Bauer, *Photoresponse of Organic Field Effect Transistors,* Organic Electronics, accepted January 2006
9. L. Nguyen, S. Günes, H. Neugebauer, N. S. Sariciftci, Fateme Banishoeib, Anja Henckens, Thomas Cleij, Laurence Lutsen, Dirk Vanderzande, *Precursor Route Poly(Thienylene*

Vinylene)for Organic Solar Cells: Photophysics and Photovoltaic Performance, Solar Energy Materials and Solar Cells, accepted March 2006
10.L. Campos, A.J. Mozer, S. Günes, C. Winder, H. Neugebauer, N. S. Sariciftci, B. Thompson, B. D. Reeves, C. R. G. Grenier, J. R. Reynolds, *Photovoltaic Activity of a PolyProdot Derivative in a Bulk Heterojunction Solar Cell*, accepted, Solar Energy Materials and Solar Cells
11. B. Singh, S. Günes, N. S. Sariciftci, S. Erten, C. Zafer, S. Icli, *Soluble Derivatives of Perylene and Naphtalene Diimides for n-channel Organic Field Effect Transistors*, Organic Electronics, in print, Organic Electronics, April 2006
12. S.Lu, R. Koeppe, S. Günes, N. S. Sariciftci, *High Efficiency Quasi Solid State Dye Sensitized Solar Cells with Cross Linked Cyano-Acrylate as Electrolyte Matrix*, submitted to Solar Energy Materials and Solar Cells
13. S. Günes, H. Neugebauer, N. S. Sariciftci, *Conjugated Polymer Based Organic Solar Cells and Photodetectors*, in preparation, invited review for Chemical Reviews
14. S. Günes, N. S. Sariciftci, *Hybrid Solar Cells using Organic/Inorganic Nanoclusters,* invited review for Nanoclusters and Nanostructured Surfaces, in preparation, edited by Ray Asok
15. S. Günes, N. S. Sariciftci, *Sensitization of TiOx Nanoelectrodes with other Nanoparticles in Hybrid Solar Cells*, in preparation, invited paper for Inorganic Chimica Acta.

Conference Proceedings:

1. Th. Singh, N. Marjanovic, G. Matt, S. Guenes, N.S. Sariciftci, A. Montaigne Ramil, A. Andreev, H. Sitter, R. Schwoediauer, S. Bauer, *Enhanced mobility of organic field-effect transistors with epitaxially grown C_{60} film by in-situ heat treatment of the organic dielectric*, Mater. Res. Soc. Symp. Proc. Vol 871E (2005), 14.9.1
2. N. Marjanovic, B. Singh, S. Günes, N. S. Sariciftci, S. Schwodibauer, S. Bauer, *Photoresponse of Organic Field-Effect Transistors based on soluble semiconductors and dielectrics*, Mater. Res. Soc. Symp. Proc. Vol 871E (2005)
3. N. Marjanovic, Th. B. Singh, G. Dennler, S. Günes, H. Neugebauer, N. S. Sariciftci R. Koeppe, S. Bauer, *Photo-induced phenomena in Organic Field-Effect Phototransistors based on Conjugated Polymer/Fullerene Blends and Organic Dielectric*, Proceedings of SPIE, Coden:PSISDG ISSN:0277-786X, AN 2006:494654, 2006
4. S. Günes, H. Neugebauer, E. Arici, N. S. Sariciftci, *Nanoporous $CuInS_2$ Electrodes for Hybrid Solar Cells*, Proceedings of SPIE, Coden:PSISDG ISSN:0277-786X, AN 2006:506615, 2006
5. L. Nguyen, S. Günes, H. Neugebauer, N. S. Sariciftci, Fateme Banishoeib, Anja Henckens, Thomas Cleij, Laurence Lutsen, Dirk Vanderzande, *Low Bandgap Poly(Thienylene Vinylene) for Organic Solar Cells: Photophysics and Photovoltaic Performance*, Proceedings for SPIE, Coden:PSISDG ISSN:0277-786X, AN 2006:494664, 2006
6. S. Günes, H. Neugebauer, N. S.Sariciftci, *Solid State Dye Sensitized Solar Cells using Poly(3-hexylthiophene) as Hole Transporting Material*, in preparation, ECS Transactions.
7. S. Bereznev, R. Koeppe, I. Konovalov, J. Kois, S. Günes, A. Öpik, E. Mellikov, N. S. Sariciftci, *Hybrid solar cells based on $CuInS_2$ and organic buffer-sensitizer layers*, submitted to EMRS.

Conference Attandence:

Oral Presentations

1. S. Günes, R. Koeppe, E. Arici, N. S. Sariciftci, "$CuInS_2$ Nanoparticles for Hybrid Solar Cells" Turkish Physical Society Meeting,14-17 September 2004, Bodrum, Turkey
2. S. Günes, S. Hofer, H. Neugebauer, N. S. Sariciftci, J. Roither, M. Kovalenko, G. Pillwein, W. Heiss, "Hybrid Solar Cells Using $CuInS_2$, TiO_2 and HgTe Nanocrystals", Nano- TR I, 25-27 May 2005, Ankara, Turkey
3. S. Günes, P. Senkarabacak, H. Neugebauer, N. S. Sariciftci, J. Roither, M. Kovalenko, G. Pillwein, W. Heiss "Sensitization of TiO_2 Electrodes with HgTe Nanocrystals", Material Research Society Meeting, 28 November-2 December 2005, Boston, USA
4. S. Günes, S. Hofer, H. Neugebauer, N. S. Sariciftci, "Hybrid Solar Cells with Incorporated Nanoparticles", SPIE Meeting, 3-7 April 2006, Strasbourg, France

Schools:

1. Summerschool on *"Basic Principles and New Concepts in Quantum Solar Energy Conversion"*, 14-19 September 2003, Hirschegg, Germany
2. Nanochannel Springschool on *"RTN Molecules in Nanochannels, Synthesis, Spectroscopy and Applications"*, 13-18 March 2005, Briegels, Switzerland

References

[1] M. Green, *Progress in Photovoltaics*, 9, 123, 2001.
[2] S.E. Shaheen, C. Brabec, N.S. Sariciftci, F. Padinger, T. Fromherz, and J.C. Hummelen, *App. Phys. Lett.*, 78, 841, 2001.
[3] E. Arici, D. Meissner, and N. S. Sariciftci, in *Encyc. Nanoscience and Nanotech.,* edited by H. S. Nalwa, 1, 2004.
[4] W. Huynh, X. Peng, and A. P. Alivisatos, *Adv. Mat.*, 11,11, 1999.
[5] M. Grätzel, *J. Photochem. and Photobio A*,164,3, 2004.
[6] G. Yu, J. Gao, J.C. Hummelen, F. Wudl, and A. J. Heeger, *Science*, 270, 1789, 1995.
[7] N.S.Sariciftci, L. Smilowitz, A.J.Heeger, and F.Wudl, *Science*, 258, 1474,1992.
[8] E. Arici, N. S. Sariciftci, and D. Meissner, *Adv. Func. Mat.*, 2, 13, 2003.
[9] H. Weller, *Ang. Chemie.Int. Eng. Ed.*, 32, 41, 1993.
[10] M. K. Nazeeruddin, A. Kay, I. Rodicio, R. Humphry-Baker, E. Müller, R. Liska, N. Vlachopoulos, and M. Graetzel, *J. Am. Chem. Soc.*, 115, 6382, 1993.
[11]G. Smestad, S. Spiekermann, J, Kowalik, C. D. Grant, A. M. Schwartzberg, J. Zhang, L. M. Tolbert, and E. Moons, *Sol. En. Mat. and Sol. Cells*, 76, 85, 2003.
[12]D.Gebeyehu, C. Brabec, N. S. Sariciftci, D. Vangeneugden, R. Kiebooms, D. Vanderzande, F. Kienberger, and H. Schindler, *Synth. Met.*, 125, 279, 2002.
[13]L. Sicot, C. Fiorini, A. Lorin, J.M. Nunzi, P. Raimond and C. Sentein, *Synth. Met.*, 102, 991, 1999.
[14]D. Gebeyehu, C.J. Brabec, F. Padinger, T. Fromherz, S. Spiekermann, N. Vlachopoulos, F.Kienberger, H. Schindler and N.S. Sariciftci, *Synth. Met*., 125, 279, 2002.
[15] R. Vogel and H. Weller, *J.Phys. Chem*., 98, 3183, 1994.
[16] N.S.Sariciftci, *Materials Today*, 1369, 36, 2004.
[17] J. Nelson, *Curr. Opin. İn Solid State Mat. Sci.*, 6, 87, 2002.
[18] *Handbook of Conducting Polymers*; Vol 1-2, edited by T. A. Skotheim, (Marcel Dekker Inc., NewYork, 1986).
[19] J. Singh, *Semiconductor Optoelectronics*, edited by S. W. Director, (McGraw Hill Inc, USA)
[20] H. Hoppe and N. S. Sariciftci, *J.Mat. Res. Soc*, 19, 7,2004.
[21] I.D. Parker, *J. Appl. Phys*. 75, 3, 1656, 2004.
[22] C. Winder, Diploma Thesis, Linz, 2001.
[23] H. Antoniadis, B. R. Hsich, M. A. Abkowitz, S. A. Jenehke, and M. Stolla, *Synt. Met.*, 62, 265, 2004.
[24] M. Sze, Pyhsics of Semiconductor Devices (John Wiley & Sons), New York, 1981.
[25] D. Wöhrle and D. Meissner, *Adv. Mat.*, 3, 129, 1991.
[26] D. Meissner, S. Siebentritt, and S. Günster, *Int. Symp. On Opt. Mat. Tech. Eff. And Sol. Energ. Conv. XI*, Toulouse, 1992.
[27] C.W. Tang and A.C. Albrecht, *J. Chem. Phys*. 62, 2139, 1975.
[28] P. Peumans, A. Yakimov, and S. R. Forrest, *App. Phys. Rev.*, 93, 3693, 2003.
[29] L.A.A. Pettersson, L. S. Roman, and O. Inganäs, *J. Appl. Phys*. 86, 487, 1999.
[30] C. W. Tang, *Appl. Phys. Lett.* 48, 183, 1986.
[31] J. Rostalski and D. Meissner, *Sol. Energ. Mat. Sol. Cells*, 63, 37, 2000.
[32] M. Murgia, F. Biscarini, M. Cavallini, C. Taliani, and G. Ruani, *Synth. Met.* 121, 1533, 2001.
[33] G. Ruani, C. Fontanini, M. Mugia, and C. Taliani, and S. B. Ross, *J. Chem. Phys.*, 116, 1713, 2002.
[34] T. Toccoli, A. Boschetti, C. Corradi, L. Guerini, M. Mazzola, and S. Iannotta, *Synth. Met.* 138, 3, 2003.
[35] V.I. Arkhipov, P. Heremans, and H. Bässler, *Appl. Phys. Lett.* 82, 4605, 2003.

[36] N.S. Sariciftci and A. J. Heeger, in *Handbook of Organic Conductive Molecules and Polymers*; Vol.1, edited by H.S. Nalwa (John Wiley&Sons Ltd., Chichester, 1997), 413.
[37] G. Zerza, C. J. Brabec, G. Cerullo, S. D. Silvestri, and N. S. Sariciftci, *Synt. Met*, 119, 637, 2001.
[38] A. F. Nogueira, I. Monzari, J. Nelson, J. R. Durrant, C. Winder, N. S. Sariciftci, and C. Brabec, *J. Phys. Chem B*, 107, 1567, 2003.
[39] N. S. Sariciftci, D. Braun, C. Zhang, V. I. Srdanov, A. J. Heeger, G. Stucky, and F. Wudl, *Appl. Phys. Lett,* 62, 585. 1994.
[40] Harald Hoppe, PhD Thesis, Linz, 2004.
[41] M. Granström, K. Petritsch, A. C. Arias, A. Lux, M. R. Andersson, and R.H. Friend, *Nature*, 395, 257, 1998.
[42]L. Chen, D. Godovsky, O. Inganäs, J. C. Hummelen, R. A.J. Jannsen, M. Svennson, and M. R. Andersson, *Adv. Mat.*, 12, 1367, 2000.
[43]C. Brabec, A. Cravino, D. Meissner, N. S. Sariciftci, M. T. Rispens, L. Sanchez, J.C. Hummelen, and T. Fromherz, *Thin Solid Films*, 403-404, 368, 2002.
[44] M. Drees, K. Premaratne, W. Graupner, J.R. Heflin, R.M. Davis, D. Marciu and M. Miller, Appl. Phys. Lett. 81, 1, 2002.
[45] A.F.Nogueira, C. Longo, and M.A. De Paoli, *Coord. Chem. Rew*. 248, 1455, 2004.
[46] M. Grätzel, *Inorganic Chem.*,44, 20, 2005.
[47] H. Halme, PhD Thesis, Espoo (Finland), 2002.
[48] A.S. Polo, M.K. Itokazu, and N. Y. M. Iha, *Coord. Chem. Rev.*, 248, 1343, 2004.
[49] K. Kalyanasundaram, N. Vlachopoulos, V. Krishnan, A. Monnier, and M. Grätzel, *J. Phys. Chem*, 91, 1987, 2342.
[50] H. Mao, H. Deng, H. Li, Y. Shen, Z. Lu, and H. Xu, *J. Photochem. Photobio. A. Chem*, 114, 209, 1998.
[51] A. Kay and M. Grätzel, *J. Phys. Chem*. 97, 6272, 1993.
[52] J. Fang, J. Wu, X. Lu, Y. Shen and Z. Lu, *Chem. Phys. Lett.* 270, 145, 1997.
[53] M. K. Nazeeruddin, R. Humphry Baker, M. Grätzel and B. A.Murrer, *Chem. Commun.* 719, 1998.
[54] M. K. Nazeeruddin, R. Humphry Baker, M. Grätzel, D. Wöhrle, G. Schneider, A. Hirth, and N. Trombach, *J. Porph, Phth*.,3, 230, 1999.
[55] K. Kalyanasundaram and M. Grätzel, *Coord. Chem. Rev.*, 177, 347, 1998.
[56] N. Murakami, C. G. Garcia, and C.A.Bignozzi, in Handbook of Photochemistry and Photobiology, edited by H.S. Nalwa, vol 1, 49, (American Scientific Publishers, Los Angeles).
[57] J. M. Rehm, G.L. McLendon, Y. Nagasawa, K. Yoshira, J. Moser, and M. Grätzel, *J. Phys.Chem.*, 100, 9577, 1996.
[58] A. Hagfeldt and M. Grätzel, *Acc. Chem. Res*., 33, 5, 269, 2000.
[59] G. Sauve', M. E. Cass, G. Coia, S. J. Doig, I. Lauermann, K. E. Pomykal, and N. S. Lewis, *J. Phys. Chem. B*, 104, 6821.
[60]K. Tennakone, G. R. R. Kumara, I.R.M. Kottegoda, K.G.U Wijayantha and V.P.S. Perrera, *J.Phys. D: Appl. Phys*. 31, 1998, 1492.
[61] B.Oreagan and D. T. Schwartz, *Chem. Mat.*, 10, 1501, 1998.
[62] U. Bach, D. Lupo, P. Comte, J.E. Moser, F. Weissortel, J. Salbeck, H. Spreitzer, and M. Grätzel, *Nature*, 395, 583, 1995.
[63]A. Fujishima and X.T. Zhang, *Proc. Jap. Acad. B*, 2, 33, 2005.
[64] B. Li, L. Wang, B. Kang and P. Wang, and Y. Qiu, *Sol. Energ. Mat. Solar Cells*, 90, 549, 2006.
[65] K. Tennakone, G.R.R.A Kumara, A. R. Kumarasinghe, K.G.U. Wijayantha, and P.M. Sirimanne, *Semicond. Sci. And Tech*. 10, 1689, 1995.

[66] G.R.R.A Kumara, A. Konno, G.K.R. Senadeera, P.V.V. Jayaweera, Dbra De Silva, and K. Tennakone, *Sol. En. Mat. Sol. Cells*, 69, 195, 2001.
[67] K. Tennakone, G.K.R. Senadeera, Dbra De Silva, and I.R.M. Kottegoda, *Appl. Phys. Lett.*, 77, 2367, 2000.
[68] P.M.Sirimanne, T. Jeranko, P.Bogdanoff, S. Fiechter, and H. Tributsch, *Semicond. Sci Tech.* 18, 708, 2003.
[69] K. Tennakone, J. Bandara, P.R.M Bandaranayeke, G.R.R.A Kumara, and A. Kono, *Japan. J. Appl. Phys.*, 7B, L732, 2001.
[70] G.R.A. Kumara, A. Konno, K. Shiratsuchi, J. Tsukahara, and K. Tennakone, *Chem. Mat.*, 14, 954, 2002.
[71] G.R.A. Kumara, S. Kaneko, M. Okuya, and K. Tennakone, *Langmuir*, 18, 10493, 2002.
[72] B. O`Reagan, F. Lenzmann, R. Muis, and J. Wienke, *Chem. Mat.*, 14, 5023, 2002.
[73] J. Krüger, R. Plass, L. Cevey, M. Piccirelli, M. Grätzel, and U. Bach, *Appl. Phys. Lett.*, 79, 2085, 2001.
[74] J. Krüger, R. Plass, M. Grätzel, and H. J. Matthiek, *App. Phys. Lett.*, 81, 367, 2002.
[75] L. Schmidt Mende and M. Grätzel, *Thin Solid Films*, 500, 296, 2006.
[76] S.B. Ross Murphy, in *Polymer Networks-Principles of Their Formation, Structure and Properties*, edited by R.F.T. Stepto, (Blackie Academic and Professional, London), 1998.
[77] S. Megahed and B. Scosati, *Interface*, 4, 34, 1995.
[78] F. Cao, G. Oskam, and P. Searson, *J. Phys. Chem.*, 99, 17071, 1995.
[79] P. Wang, S. M. Zakeeruddin, J. Moser, R. Humphry Baker, and M. Grätzel, *J. Am. Chem. Soc.*, 126, 7164, 2004.
[80] M. Armand, in *Polymer Electrolyte Reviews*, edited by J.R.Maccallum, C.A. Vincent,(Elsevier, London),1987.
[81] A.F. Nogueira and M.A. De Paoli, *Synth. Met*., 61, 135, 2000.
[82] A.F. Nogueira, J.R. Durrant, and M. A. De Paoli, *Adv. Mat.*, 13, 826, 2001.
[83] S. Haque, E. Palomores, H. M. Upadhyaya, L. Otley, R. J. Otter, A.B. Holmes, and J. R. Durrant, *Chem. Comm.*, 24, 3008, 2003.
[84] M. Kaneko and T. Hoshi, *Chem. Lett.*, 32, 872, 2003.
[85] A. Zaban, O.I. Micic, B.A. Gregg, and A.J. Nozik, *Langmuir*, 14, 3153, 1998.
[86] D. Liu and P.V. Kamat, *J. Phys. Chem.*, 97, 10769, 1993.
[87] P. Hoyer and R. Könenkamp, *Appl. Phys. Lett.*, 66, 349, 1995.
[88] A. P. Alivisatos, *Science*, 271, 933, 1996.
[89] Q. Shen, D. Arae, and T. Toyoda, *J. Photochem. and Photobio A*: Chem, 164, 75.
[90] I. Kaiser, K. Ernst, K. Fischer, R. Könenkamp, C. Rost., I. Sieber, and M. Ch. Lux Steiner, *Sol. En. Mat. Sol. Cells*, 67, 89, 2004.
[91] K. Ernst, A. Belaidi, and R. Könenkamp, *Semicond. Sci. Tech.*, 18, 475, 2004.
[92] M. Nanu, J. Schoonmann, and A. Goossens, *Adv. Func. Mat.*, 15, 95, 2005.
[93] W. Huynh, J. Dittmer, and A. P. Alivisatos, *Science*, 295, 2425, 2002.
[94] E. Arici, D. Meissner, F. Schäffler, and N.S. Sariciftci, *Int. Journ. Photoenergy*, 5, 199, 2003.
[95] N. C. Greenham, X. Peng, and A. P. Alivisatos, *Phys.Rev.B.*, 54, 17628, 1996.
[96] S. McDonald, G. Konstantatos, S. Zhang, P. W. Cyr, E. J. D. Klem, L. Levina, and H. Sargent, *Nature Mat.*, 4, 138, 2005.
[97] M. Green, *Physica E*, 14, 65, 2002.
[98] M. L. Steigerwald and L. Eisrus, *Acc. Chem. Res.*, 23, 283, 1990.
[99] S.A. Empedocles and M.G. Bawendi, *Acc. Chem. Res.*, 32, 389, 1999.
[100] C.J. Murphy and J. L. Coffer, Appl. Spectr., 56, 16, 2002.
[101] P.A.V Hal, M.M. Wienk, J.M. Kroon, W.J.H. Verhees, L.H. Sloff, W.J.H.V Gennip, P. Jonkhejm, and R. A. J. Janssen, *Adv. Mat.*, 15, 118, 2003.
[102] I. Gur, N.A. Fromer, M. L.Geier, and A.P.Alivisatos, *Science*, 310, 462.

[103] S.Zhang, P.W. Cyr, S. A. McDonald, G. Konstantatos, and E.H.Sargent, *App. Phys. Lett.*, 87, 233101, 2005.
[104] W. J. E. Beek, M. M. Wienk, and R. A. J. Janssen, *Adv. Func. Mat*.,
[105] L. Kavan and M. Graetzel, *Elect. Chimi. Acta*, 40, 643, 1995.
[106] N. Gaponik, D. V. Talapin, A.L. Rogach, A. Eychmüller, and A. H. Weller, *Nano Lett.*, 2, 80, 2002.
[107] C. Czekelius, M. Hilgendorff, L. Spanhel, I. Bedja, M. Lench, G. Müller, U. Bloeck, D. Su, and M. Giersig, *Adv. Mat.*, 11, 643, 1999.
[108] M. A. Hines and G. D. Scholes, *Adv. Mat.*, 15, 1844, 2003.
[109] S. Günes, H. Neugebauer, and N. S.Sariciftci, , *ECS Transactions*, submitted, 2006.
[110] U. Bach, PhD Thesis, EPFL, Lausanne.
[111] D. V. Talapin, A. L. Rogach, A. Kornowski, M. Haase, and H. Weller, *Nano Lett.,* 1, 207, 2001.
[112] V. L. Colvin, M.C. Schlamp and, A.P. Alivisatos, *Nature (London)*, 370, 354, 1994.
[113] N. Tessler, V. Medvedev, M. Kazes, S.H. Kan, and U. Banin, *Science*, 295, 1506, 2002.
[114] P. Michler, A. Imamoglu, M. D. Mason, P. J. Carson, G. F. Strouse, and S. K. Buratto, *Nature (London)*, 406, 968, 2000.
[115] V. I. Klimov, A. A. Mikhailovsky, A. V. Malko, J. A. Hollingsworth, C. A. Leatherdale, H. –J. Eisler, and M. G. Bawendi, *Science*, 290, 314.
[116] A. A. Mikhailovsky, A. V. Malko, J. A. Hollingsworth, M. G. Bawendi, and V. I. Klimov, *Appl. Phys. Lett.*, 80, 2380, 2002.
[117] A. V. Malko, A. A Mikhailovsky, M. A. Petruska, J. A. Hollingsworth, H. Htoon, M. G. Bawend, and V. I. Klimov, *Appl. Phys. Lett.*, 81, 1303, 2002.
[118] A. Rogach, S. Kershaw, M. Burt, M. Harrison, A. Kornovski, A. Eychmüller, and H. Weller, *Adv. Mat.*, 11, 552, 1999.
[119] S. Günes, H. Neugebauer, N. S. Sariciftci, J. Roither, M. Kovalenko, and W. Heiss, *Adv. Func. Mat.*, 16, 1095, 2006.
[120] S. Günes, H. Neugebauer, E. Arici, and N. S. Sariciftci, *Proceedings of SPIE*, Coden:PSISDG ISSN:0277-786X, AN 2006:506615, 2006.